



**Politecnico  
di Torino**

**Politecnico di Torino**

Corso di Laurea Magistrale in Ingegneria per l'Ambiente e il Territorio, Climate Change

Sessione di Laurea Marzo 2022

# **Future projections of temperature and precipitation extremes for the city of Beira, Mozambique**

*Part of the interdisciplinary Master Thesis lab: "After the storm.  
Designing post-cyclone strategies for the city of Beira, Mozambique"*

Supervisor:

Jost-Diedrich Graf Von Hardenberg

Co-supervisor:

Alberto Viglione

Candidate:

Andrea Vito Vacca (ID 278348)

A.a. 2021/2022

# Abstract

Due to its geographical location, geomorphology and socio-economic context, Beira (Mozambique) is one of the cities most threatened by climate change worldwide. The large-scale destruction wreaked by Cyclone Idai in March 2019 has turned the spotlight on the vulnerability of the city to extreme weather events. Correspondingly, Politecnico di Torino has launched an interdisciplinary master thesis laboratory to support Comunità di Sant'Egidio in developing a vision for the future of Beira, based on sustainability and resilience to climate change. In this context, the objective of the present work is to depict the future of the extreme climatic conditions that are likely to affect the area in the next decades.

To pursue this aim, a multi-model ensemble of climate simulations from CMIP6 (sixth phase of the Coupled Model Intercomparison Project) has been employed to analyse future projections under two alternative scenarios. Based on daily temperature and precipitation data, indices of moderate climate extremes are computed and analysed. The performance of models in simulating the indices in the study area is firstly assessed by comparing them with indices derived from the ERA5 reanalysis dataset. Subsequently, trend analysis and the temporal comparison of probability density functions are employed to assess the projected changes of the indices.

The results obtained for indices based on maximum and minimum daily temperature are consistent with global warming. An increase in the intensity and frequency of temperature extremes is projected along the 21st century for both future scenarios. On the other side, projections concerning precipitation indices are more uncertain, given that models often disagree on the sign of change. Nonetheless, the results suggest the increase in the drought conditions and of the intensity and variability of heavy rainfall under the high emission scenario. Besides, extreme precipitation events are expected to last longer, thus potentially increasing the risk of flooding.

Furthermore, a methodology has been proposed to extrapolate from the observed indices information about the critical precipitation events that have devastated the area in the past (e.g. cyclone Idai). This empirical approach has led, despite a certain degree of uncertainty, to correlate the values of internationally recognised indices with high-return period precipitation events and to predict an increase of their frequency according to future projections.

The output of this work is intended to be useful for data-based decision making regarding adaptation strategies and for future studies on the climate of the area.

# Acknowledgments

First of all, I would like to thank my supervisor, Jost-Diedrich Graf Von Hardenberg, for guiding me through this work, for pushing me to do my best and for introducing me to the fascinating and vibrant world of climate research. I would also like to thank Professor Alberto Viglione for his valuable suggestions and efforts in getting me into this project.

I am grateful to the interdisciplinary master thesis lab of the Politecnico di Torino, and in particular to the coordinator Prof. Francesca de Filippi, for the opportunity to work on such a relevant topic, which has allowed me to open my mind to a world (apparently) so far away from my own.

Finally, I would like to thank Luigi Cafiero, my travelling companion, with whom I have been in contact from the first to the last day of this work, to solve problems and share impressions.

# Contents

LIST OF FIGURES .....	5
LIST OF TABLES .....	9
1. INTRODUCTION.....	10
1.1 Beira after the storm .....	10
1.2 Climate extremes, how are they monitored?.....	15
2. DATA AND MODELS.....	19
2.1 Climate Models.....	19
2.2 Climate data .....	23
2.3 Pre-processing.....	26
2.3.1 Cut and Remap original data .....	26
2.3.2 Bias Correction .....	26
3. METHODOLOGY.....	29
3.1 Indices Definition and Calculation .....	30
3.2 Ability of models to simulate temperature and precipitation extremes ..	36
3.3 Future Projections .....	42
3.3.1 Trend Analysis.....	43
3.3.2 Probability Density Functions .....	45
3.4 Correlation between extreme indices and critical events in Beira .....	48
4. RESULTS.....	52
4.1 Future Projections .....	52
4.1.1 Intensity of Extreme Temperatures .....	53
4.1.2 Frequency of Temperature Extremes .....	56
4.1.3 Intensity of Precipitation Extremes .....	62
4.1.4 Frequency of Precipitation Extremes .....	67
4.1.5 Summary.....	71
4.2 Correlation between extreme indices and critical events in Beira .....	72
4.2.1 Indices cross-correlation.....	73
4.2.2 Identification of critical destructive events .....	75
4.2.3 Indices and Critical events.....	77
4.2.4 Future projections of critical events .....	81

5. DISCUSSION .....	85
5.1 Extreme Temperatures .....	85
5.2 Heavy Precipitation.....	87
5.3 Droughts.....	88
5.4 Extreme weather events .....	89
5.5 Impacts.....	90
5.5.1 Ecosystems.....	91
5.5.2 Water scarcity and food security.....	92
5.5.3 Human Health .....	93
5.5.4 Human settlements and infrastructures .....	94
6. CONCLUSIONS.....	95
7. BIBLIOGRAPHY .....	98
8. APPENDIX A: destructive past events for Beira.....	104
9. APPENDIX B: future projections .....	110

# LIST OF FIGURES

1. *Mozambique maps. Left: Population density of Mozambique, in thousands inhabitants. Right: Topography of Mozambique, colours represent the altitude in meters. Source: The World Bank, 2012..... 11*
2. *Left: Location of the Sofala province in Mozambique. In red, the area of the city of Beira. Source: Estatísticas do distrito cidade de Beira. Right: Satellite image of the city of Beira, washed by Pungwe and Buzi rivers. Source: Earthstar Geographics, webmap by ESRI; ..... 12*
3. *Flooding after the passage of TC IDAI in Mozambique, near Beira. Sources: left: <https://www.cesvi.eu/news/cyclone-idai-tragedy-mozambique/> right: National Institute of Disaster Management, Mozambique..... 13*
4. *Map illustrating the cumulative satellite detected surface waters in the Sofala province and its surroundings, as observed from the Sentinel-1 imagery acquired between 13 & 26 March. Source: UNITAR (<https://unitar.org/maps/countries/67>)..... 13*
5. *Representation of the Beira city with its main elements: the port, the coast, the social infrastructures. Source: <https://storymaps.arcgis.com/stories/2112d5d782004c9ea79069c2de881748>..... 15*
6. *Left: The effect of changes in temperature distribution on extremes. a) effects of a shift of the entire distribution toward a warmer climate; b) effects of an increased temperature variability; c) effects of a variation in the shape of the distribution, i.e. an increased asymmetry toward the hotter part of the distribution. Source: IPCC, 2012 Right: probability distribution of daily precipitation. The extremes are located at the right-tail of the distribution. Source: Zhang et al. (2011)..... 16*
7. *A representation of a General Circulation Model. The Earth is subdivided into boxes that are connected through fluxes of mass and energy. In each box, numerical equations representing physical and chemical processes are solved. .... 20*
8. *Scenarios matrix for CMIP6 simulations. Each cell is a combination of SSP and climate outcome based on a forcing outcome that IAM demonstrated to be feasible. Green cells represents the corresponding CMIP5 RCPs of each row, the socio-economic scenarios for the older generation of models. Dark blue cells indicate scenarios that will serve as the basis for climate model projections, which have the priority to be ran by the modelling groups. Source: O'Neill et al., 2016..... 22*
9. *Evolution of the CO2 emissions, concentrations, anthropogenic radiative forcing and global mean temperature for the scenarios defined in the context of the CMIP6. Grey areas represent scenarios variability. Source: Riahi et al., 2016..... 22*
10. *Representation of the bias correction applied to daily minimum temperature simulated by ACCESS-CM2. Up: PDFs of the observed and simulated Tn in the reanalysis period. The bias is the difference between the means. Bottom: The simulated time series is scaled readjusting the mean to the observed one. A 10-years moving average is applied to the time series to smooth them. .... 28*
11. *Diagram showing the methodology of the work. All the steps are performed using raw data derived from the two different socioeconomic scenarios (SSP1-2.6, SSP5-8.5)... 30*
12. *Rainfall amount over Mozambique in December, January and February, during the rainy season. The area of the city of Beira presents relatively high values of*

	<i>precipitation with respect to other parts of the country. Source: INAM, Instituto Nacional de Meteorologia (www.inam.gov.mz).....</i>	<i>33</i>
13.	<i>determination of IETD for defining independent extreme storms in the inR95p index. Different lines represent the different models. Changing the IETD value results in changing the number of detected annual independent extreme events in the rainfall time series. IETD =7 was chosen because the number of events does not change “significantly” after that.....</i>	<i>35</i>
14.	<i>Portrait Diagrams displaying the Performance Index (normalized bias between models' projections and reanalysis over the period 1979-2014) with a blue-red color scale. In this way, the performance of models is evaluated. The black dots indicate where the null hypothesis of the Kolmogorov-Smirnov test of the same underling cumulative distribution is not rejected. Up: Indices computed starting from data not-bias corrected. Bottom: Indices computed starting from bias-corrected data.....</i>	<i>38</i>
15.	<i>Comparison between ERA5 and models time series after the Bias Correction. The thick black line represents the Ensemble Mean, while the shading is the area between the 5th and 95th percentile.....</i>	<i>41</i>
16.	<i>PDFs of the maximum annual temperature (TXx) computed by binning values from all the models over the 30-years subperiods, through the Kernel Density Estimator. Histograms are plotted for comparison. The curve allows a better view of the distributions and their evolution over time, but it "abates" some probability peaks. ...</i>	<i>47</i>
17.	<i>Flow diagram showing the steps of the approach applied in order to infer about critical destructive precipitation events by the analysis of moderate climate extremes indices.</i>	<i>49</i>
18.	<i>Representation of the values of Rx1day computed starting from reanalysis data, for the year 2019 over the area of interest. This image demonstrates that the index of extreme rainfall contains information about the criticality of that year for Beira, given the high values reported (reddish areas). From this point, an empirical approach described in this paragraph was developed to construct a criterion whereby, starting from indices values, one year is defined as “critical” for Beira. ....</i>	<i>50</i>
19.	<i>Box plots representing the intermodal variability of the mean absolute anomalies in the near future (2026-2055) and far future (2071-2100) of Temperature Intensity indices compared to the baseline period (1981-2010), for both scenarios. ....</i>	<i>53</i>
20.	<i>Temporal evolution of maximum of daily maximum temperature (TXx) and minimum of daily minimum temperature (TNn). A moving average of 10 years is applied to the Ensemble Means (thick lines). The shadings represent the areas between the 75<sup>th</sup> and 25<sup>th</sup> percentiles. The black line represents the historical period simulation, the dashed line represents the observed values of the indices, and the red and blue lines are the future scenarios.....</i>	<i>54</i>
21.	<i>Temporal evolution over the three sub-periods of probability density functions of TXx (left) and TNn (right) in the scenario SSP5-8. ....</i>	<i>54</i>
22.	<i>Trend detected for the Daily Temperature Range over the scenario SSP5-8.5. Thick line is the Ensemble mean. The shading represents the area between the 95<sup>th</sup> and 5<sup>th</sup> percentile.....</i>	<i>55</i>
23.	<i>Box plots representing the intermodal variability of the mean absolute anomalies in the near future (2026-2055) and far future (2071-2100) of Temperature frequency indices compared to the baseline period (1981-2010), for both scenarios. ....</i>	<i>57</i>
24.	<i>Temporal evolution of warm nights (Tn90p) and warm days (Tx90p). A moving average of 10 years is applied to the Ensemble Means (thick lines). The shadings represent the</i>	

areas between the 75 <sup>th</sup> and 25 <sup>th</sup> percentiles. The black line represents the historical period simulation, the dashed line represents the observed values of the indices, and the red and blue lines are the future scenarios. ....	58
25. PDFs temporal evolution and comparison with ERA5, regarding Tn90p and Tx90p under SSP5-8.5 (up) and SSP1-2.6 (bottom).....	59
26. Temporal evolution of Tn10p and Tx10p with relative negative trends. The thick line is the ensemble mean while shading represents the area between the 5 <sup>th</sup> and 95 <sup>th</sup> percentile.....	60
27. Trend computed over sub-periods for Tn10p and Tx10p. Is evident the effect of trend "flattening" as a result of the obsolete threshold definition.....	60
28. Temporal evolution of warm spell duration index (wsdi) under the two future scenarios. A moving average of 10 years is applied to the Ensemble Means (thick lines). The shadings represent the areas between the 75 <sup>th</sup> and 25 <sup>th</sup> percentiles. The black line represents the historical period simulation, the dashed line represents the observed values of the indices, and the red and blue lines are the future scenarios. ....	61
29. Box plots representing the intermodal variability of the mean absolute anomalies in the near future (2026-2055) and far future (2071-2100) of Precipitation intensity indices compared to the baseline period (1981-2010), for both scenarios. ....	63
30. Positive trends detected for Rx1day and Rx5day under SSP5-8.5.....	64
31. PDFs evolution under SSP5-8.5 and the observed PDF in the baseline period (dashed line) .....	65
32. Trend (left) and PDF (right) evolution of PRCPTOT under SSP5-8.5.....	65
33. Box plots representing the intermodal variability of the mean absolute anomalies in the near future (2026-2055) and far future (2071-2100) of Precipitation frequency indices compared to the baseline period (1981-2010), for both scenarios. ....	67
34. Consecutive dry days. Up: time series and trends for both scenarios. Shading indicates the area between the 95 <sup>th</sup> and 5 <sup>th</sup> percentile. Bottom: evolution of the pdf over the three reference periods under the two scenarios. ....	68
35. Time series of Consecutive wet days and the detected trend. Shading indicates the area between the 95 <sup>th</sup> and 5 <sup>th</sup> percentile. Thick line represents the ensemble mean. ....	69
36. nR95p time series and trend under SSP5-8.5. Shading indicates the area between the 95 <sup>th</sup> and 5 <sup>th</sup> percentile (left). Thick line represents the ensemble mean. Evolution of the PDFs over the three reference periods under SSP5-8.5. ....	69
37. inR95p time series and trend under SSP5-8.5. Shading indicates the area between the 95 <sup>th</sup> and 5 <sup>th</sup> percentile (left). The thick line represents the ensemble mean. ....	70
38. cwd95 time series and trend under SSP5-8.5. Shading indicates the area between the 95 <sup>th</sup> and 5 <sup>th</sup> percentile (left). Evolution of the PDFs over the three reference periods under SSP5-8.5.....	70
39. Box plots of the 20 indices showing the standardised anomaly at the end of the century 2071-2100, compared to the baseline period 1981-2010. wsdi is represented in a different box because its values are out of scale compared to the others, due to the very large increasing at the end of the century, as described in 4.1.1.....	72
40. Correlation Tables. The colours scales with values of the non-dimensional Spearman's correlation coefficient (that varies between -1 and 1). Above, the correlation table of observed indices (ERA5). Below, the correlation table of simulated indices (mean value over the 18 models' correlations). ....	73



41. Bar diagram for the time series of selected indices. Red bars are located in correspondence to the years 1997, 2000,2001, 2007 and 2019, where relatively high values are recorded.....	77
42. Three-dimensional scatter plot of the indices chosen to correlate with the critical events. K-means clustering is used to divide the 30 years into 5 clusters. In red is the critical cluster, grouping the critical years for the city of Beira. ....	78
43. Timeseries of observed indices and relative thresholds used to define the n-dimensional Critical Zone .....	79
44. The concept of Critical Zone. Three-dimensional representation of the Critical Zone (red parallelepiped) within the 3D scatterplot of Rx1-Rx5-R95p. ....	80
45. Representation of the position of simulated years in 2D. Red lines are the boundaries of the Critical Zone. ....	81
46. Burning embers showing the increased risk due to climate change for selected key risks in Africa. The projected increase is assessed for global warming increasing above pre-industrial levels (1850–1900). At the actual level of global warming (about 1.1°C), all three risks are already classified to moderate risk (IPCC, 2022).....	91
47. During the flood, residents had to climb trees to save themselves, while waiting for rescue .....	105
48. Cyclone Eline-Leon. Right: Track of the cyclone approaching the area of Beira. Colours toward the violet indicate an increasing power of the tropical cyclone (category 4 TC). Source: <a href="http://www.meteofrance.re">http://www.meteofrance.re</a> Right: Cyclone Eline while making landfall close to Beira. The red line is the Mozambique boundary with the ocean. Source: RSMC ARCHIVES.....	105
49. Flooding of Mozambique before and after the cyclone and number of persons affected. Area of Sofala was heavily affected by the event. Source: Relifweb.....	105
50. Cyclone Favio while making landfall in the south of Beira. Source: RSMC ARCHIVES .....	106
51. Cyclone Favio track, area affected by it and by the previous floods. Source: US Agency for International Development.....	107
52. Cyclone Idai approaching Mozambique on 14 March 2019. Image acquired by Nasa's aqua satellite.....	108
53. Rainfall accumulation between 3 and 17 March 2019 and storm track of Idai cyclone. Image taken from Probst et al. (2019) .....	109

# LIST OF TABLES

1. Description of daily variables used in this study, output of the ensemble of simulations .....	24
2. Information about the CMIP6 models used in this study .....	25
3. Extreme Climate Indices used in this study. Percentiles are computed over the base period 1981-2010. * Non-ETCCDI .....	31
4. Model Performance Index before bias correction (left) and after bias correction (right). .....	39
5. Index Agreement before bias correction (left) and after bias correction (right). .....	40
6. Sum up of Trend Analysis results for Temperature Intensity indices. Yellow coloured cells in the Mean Trend column indicate a statistically significant trend. ....	56
7. Trend values for Tn10p and Tx10p under SSP5-8.5 and SSP1-2.6 considering only the baseline period, not affected by the "flattening effect" .....	60
8. Sum up of Trend Analysis results for Temperature frequency indices. Yellow coloured cells in the Mean Trend column indicate a statistically significant trend. ....	62
9. Sum up of Trend Analysis results for Precipitation intensity indices. Blue colored cells in the Mean Trend column indicate a statistically significant trend. ....	66
10. Sum up of Trend Analysis results for Precipitation frequency indices. Blue coloured cells in the Mean Trend column indicate a statistically significant trend. ....	71
11. Description of the most critical events for the city of Beira. Data about people affected and killed are estimations. Source: <a href="https://www.emdat.be">https://www.emdat.be</a> .....	76
12. Threshold values for each index. They are used to define a year as critical .....	80
13. Count of years falling in the Critical Zone on the three sub-periods averaged over the models. ....	82
14. Mean and standard deviation of the sampling distribution resulted from the bootstrapping procedure. Data are resampled using 9 out of 18 models 100 times, and the results about the frequency of critical events are each time recorded. ....	82
15. Threshold values for the subset of three indices used to define a year as critical. ....	83
16. Count of years falling in the newly defined Critical Zone on the three sub periods averaged over the models. ....	83
17. Mean and standard deviation of the sampling distribution resulted from the bootstrapping procedure. Data are resampled using 9 out of 18 models for 100 times. ....	83

# 1.INTRODUCTION

## 1.1 Beira after the storm

Climate change is affecting weather and climate patterns in every region of the globe. Extensive changes in the atmosphere, hydrosphere, cryosphere and biosphere have been attributed to the human influence on the climate system, and risk continuing at such a pace that societies might not be able to adapt.

Mozambique is one of the countries of Africa most threatened by climate change. The reason is the socio-economic vulnerability of the country and its exposure to climate hazards.

Mozambique is the ninth country with the lowest human development index (HDI) in the world<sup>1</sup>. After 15 years of violent civil war (from 1977 to 1992), Mozambique emerged as one of the most impoverished economies worldwide. Since then, the economy has undertaken sustained growth but is still characterized by strong inequalities<sup>2</sup>. Over 46% of Mozambicans live in chronic poverty, unable to satisfy basic food needs, without having access to basic services such as education and adequate housing. This percentage rises to 50% in the province of Sofala, which is the study area in this thesis (Trujillo, M., 2019).

Most Mozambicans live in rural areas (84% of the total population, often in informal settlements) and work in the agricultural sector, most of the time for their subsistence. Indeed, the economy of Mozambique is largely based on agricultural production (25% of the country's GDP), one activity that is being heavily affected by altered precipitation and drought patterns, especially in rain-fed fields (Jägermeyr et al., 2021). Expanding and promising sectors for the economy of Mozambique are liquefied natural gas production<sup>3</sup> and eco-tourism (Da Silva, Jose Juliao, 2019).

---

<sup>1</sup> <https://hdr.undp.org/en/content/human-development-index-hdi>

<sup>2</sup> <https://www.worldbank.org/en/news/infographic/2018/11/14/mozambique-poverty-assessment-strong-but-not-broadly-shared-growth>

<sup>3</sup> <https://www.bbc.co.uk/news/world-africa-22008933>

Mozambique is located in South-Eastern Africa, bordered by the Indian Ocean throughout 2300km of coastline, in front of Madagascar. The climate is tropical, characterized by two seasons: a wet season from October to March and a dry season from April to September. Its geographical location has some inconveniences, among which is to function as natural drainage of water from the Africa interior. Indeed, rivers flow in a West-East direction ending into the ocean, and the topography is characterized by a descending altitude towards the coast, a succession of mountains, plateaus and plains (Da Silva, Jose Juliao, 2019). During the rainy season, the coastal lowlands are often subjected to flooding due to overflowing rivers, coastal storms and tropical cyclones. These hazards are critical since about 40% of the population lives on the coasts, making it the most densely populated area in the country. Over the course of its history, Mozambique has had to deal with a succession of natural disasters with devastating impacts, including floods due to meteorological extreme events and prolonged droughts.

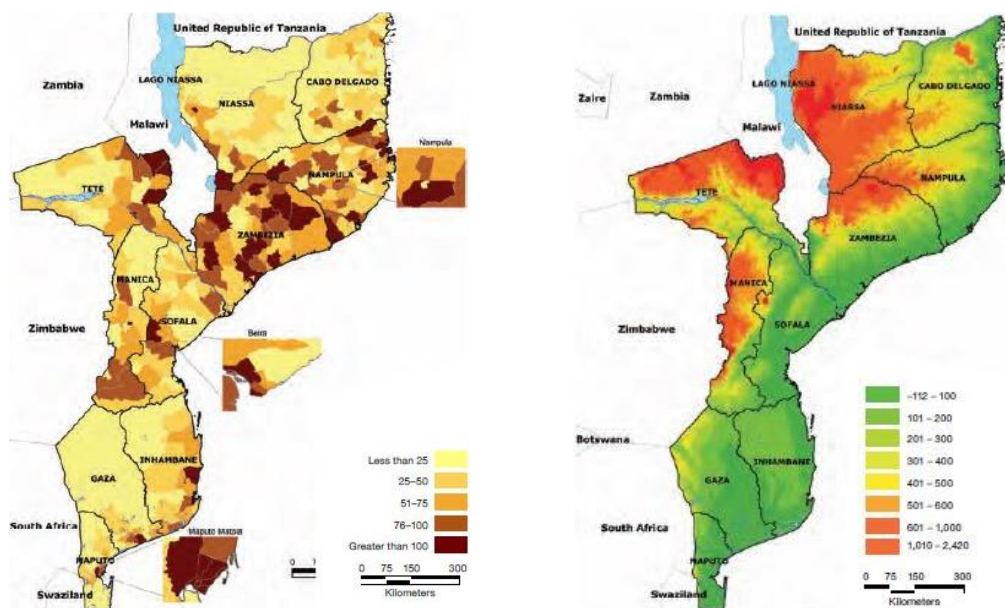


Figure 1: Mozambique maps. Left: Population density of Mozambique, in thousands inhabitants.  
 Right: Topography of Mozambique, colours represent the altitude in meters.  
 Source: The World Bank, 2012.

In this context, is important to address the role of climate change, to investigate how it affects the climate hazards that already in the past have caused widespread destruction (Appendix B). The intensification of the hydrological cycle and the sea level rise are

among the well-documented effects of climate change that pose a threat to the coastal communities of Mozambique. Mozambique ranked fifth worldwide by the value of the Global Climate Risk index between 2000 and 2019 and first considering only 2019 (Eckstein et al., 2021). The negative primacy in 2019 is a consequence of the large-scale destruction caused by Tropical Cyclone Idai, which hit the centre of the country causing thousands of fatalities and enormous damages. The area most impacted by the Cyclone was the Province of Sofala, in central Mozambique, with 53% of the inhabitants affected (Trujillo, M., 2019).

The capital of this province, the city of Beira, is the fourth largest city of Mozambique, home of approximately half a million inhabitants. It has a strategic relevance for the country because of its port, a gateway for trade. The settlements, mostly informal, are characterised by high population density, inadequate infrastructure and a high rate of poverty (Spekker et al., 2017). The city is situated in a wetland, at a point of convergence of the Buzi and Pungwe Rivers – two major water bodies of Mozambique and is largely located below the high tide level (Chemane et al., 1997).

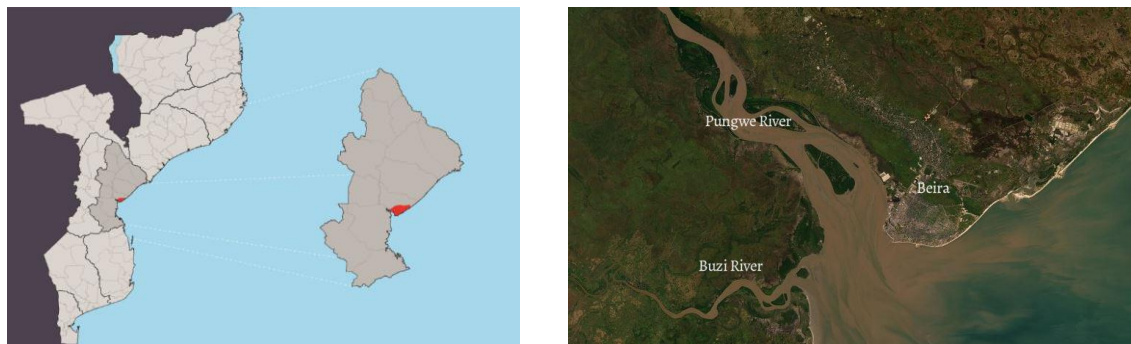


Figure 2: Left: Location of the Sofala province in Mozambique. In red, the area of the city of Beira. Source: Estatísticas do distrito cidade de Beira. Right: Satellite image of the city of Beira, washed by Pungwe and Buzi rivers. Source: Earthstar Geographics, webmap by ESRI;

According to the International Red Cross, Cyclone Idai destroyed 90% of the city of Beira<sup>4</sup>. The cyclone made landfall near the city on 14<sup>th</sup> March 2019 bringing a

<sup>4</sup> <https://www.africanews.com/2019/03/19/beira-the-mozambican-city-barred-beaten-battered-by-cyclone-idai/>

combination of strong winds (180-220 km/h), heavy rain (200mm in 24 hours) and storm surges (over 4 meters). An estimated 3,000 sq. km of land and 700.000 hectares of cultivated land were flooded and about 1.5 million people were heavily affected (Trujillo, M., 2019). An insight into Cyclone Idai is contained in Appendix B.



Figure 3: Flooding after the passage of TC IDAI in Mozambique, near Beira. Sources:  
left: <https://www.cesvi.eu/news/cyclone-idai-tragedy-mozambique/>  
right: National Institute of Disaster Management, Mozambique

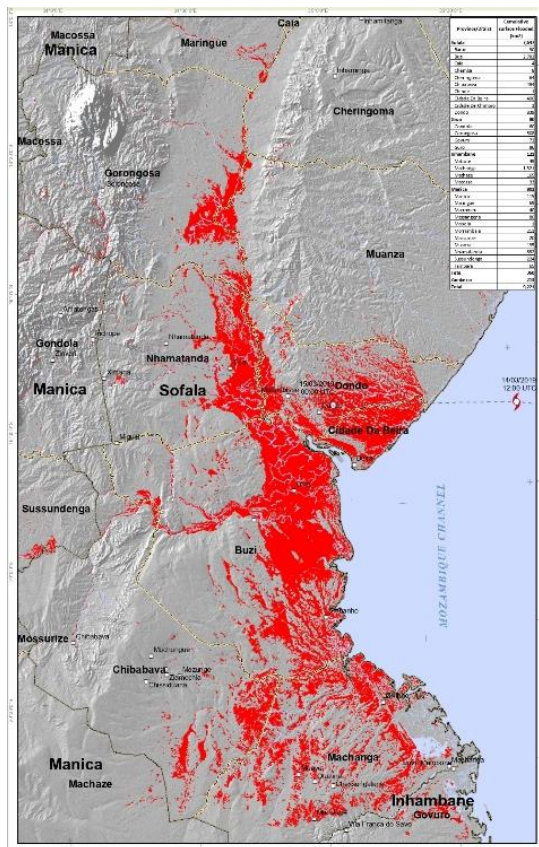


Figure 4: Map illustrating the cumulative satellite detected surface waters in the Sofala province and its surroundings, as observed from the Sentinel-1 imagery acquired between 13 & 26 March.

Source: UNITAR (<https://unitar.org/maps/countries/67>)



In the context of these tragic events, *Politecnico di Torino* launched the interdisciplinary master thesis laboratory: “*After the storm. Designing post-cyclone strategies for the city of Beira, Mozambique*”. The aim is to support the *Comunità di Sant’Egidio*, which operates on the territory, in developing a vision for the future of Beira, based on sustainability and resilience to climate change.

Indeed, extreme weather events of this magnitude could recur and potentially become more frequent or more intense due to current climate change. After Idai, Cyclone Eloise hit Beira on 23 January 2021, causing further damage to a city that has not yet fully recovered from the destruction of 2019. In the first few months of 2022 alone, five tropical storms formed in the Mozambique Channel, bringing torrential rain and strong winds to the coastal populations of Madagascar and Mozambique. Such a high number of storms in such a short time has not been repeated since 1975<sup>5</sup>.

The vulnerabilities of the city to extreme weather events pose a huge adaptation challenge. Beira must necessarily be ready and take the opportunity to rethink itself in a way that is safe for its inhabitants. The municipality of the city, together with external partners, has elaborated after the disaster of 2019 the Municipal Recovery and Resilience plan to ‘Built Beira Back better’<sup>6</sup>.

The present work intends to fit into this ambition. The objective is to analyse data from climate models concerning the future of climate extremes in the city area and understand how they are expected to change during the 21st century. In particular, **extremes of temperature and precipitation** will be studied according to established methodologies in the field of climatology, but also new approaches will be explored. Finally, the results will be discussed and related to climate change, and possible impacts to the community will be outlined. The output of this thesis is intended to be useful to support climate change adaptation strategies and actions, and for future studies on the climate of the area.

---

<sup>5</sup> <https://www.gdacs.org/>

<sup>6</sup> <https://www.slideshare.net/BasAgerbeek/beira-municipal-recovery-and-resilience-plan-volume-1-main-report>

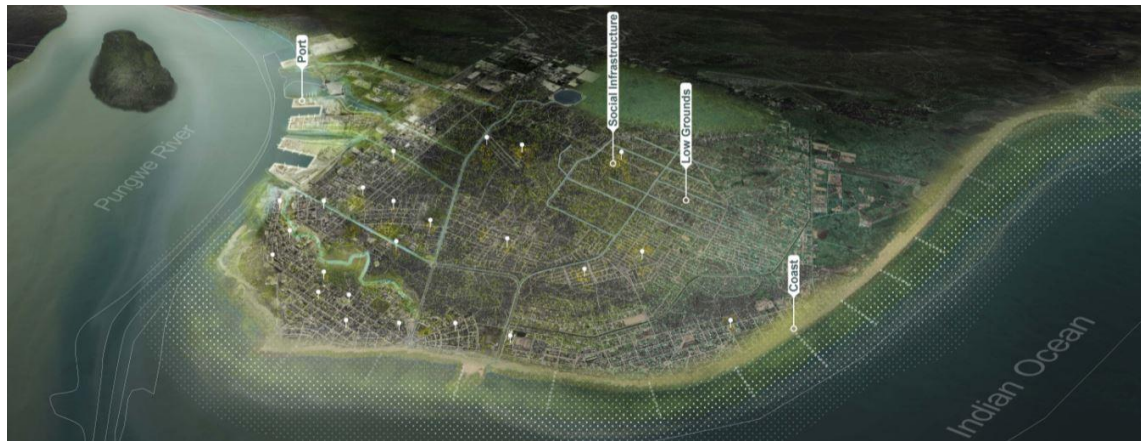


Figure 5: Representation of the Beira city with its main elements: the port, the coast, the social infrastructures. Source: <https://storymaps.arcgis.com/stories/2112d5d782004c9ea79069c2de881748>

## 1.2 Climate extremes, how are they monitored?

This study consists of an investigation of future temperature and precipitation extremes over the area of Beira, Mozambique, through the analysis of data derived from state-of-art General Circulation Models (see Chapter 2).

First of all, what is meant by an ‘extreme’?

Building on the definition given in the last IPCC report, an *extreme weather event* is “an event that is rare at a particular place and time of year” and an *extreme climate event* is “a pattern of extreme weather that persists for some time, such as a season” (IPCC, 2021).

The concept of ‘extreme’ in climatology is not straightforward. The complex nexus of dynamic and thermodynamic processes that happen in the atmosphere as well as the hydrosphere or the terrestrial environment, results in highly variable conditions including temperature and precipitation, which can be defined as ‘extreme’. Extreme events can extend over different spatial and temporal scales, including, for instance, the passage of a tornado for a few minutes or a drought condition in a region that lasts for decades (IPCC, 2012). Moreover, the extremity of an event depends on the geographical context. For instance, the occurrence in Northern Europe of one month of daily temperatures that



normally occur in Beira would be considered as a heat wave. In this thesis, the focus is given on climate extremes rather than weather extremes, although the concepts are interconnected. Sometimes the term ‘extreme’ includes also the outcomes that physical phenomena have on human society or the natural environment. In this case, the definition becomes even more complex, since it is strictly dependent on the stakeholders involved and their critical thresholds (social, ecological or physical). Nonetheless, in this thesis, a climate extreme refers only to the physical dimension; in contrast, the term ‘impact’ is used for the resulting outcomes on society and ecosystems (section 5.5).

A changing climate leads to a variation in the intensity, frequency, duration, timing and geographical extent of climate extremes (IPCC, 2012). Figure 6 shows that the change of the probability distribution of a climate variable (e.g. daily maximum temperature) is linked to the changes in the extremes. In a changing climate, the distribution might shift (change of the mean), widen/narrow (change in variability), change its shape or of all these together. Thus, an increase in the occurrence of warm days (daily maximum temperature above a certain threshold) may result from an increase in the mean daily maximum temperature, a change in the variance or shape of its frequency distribution.

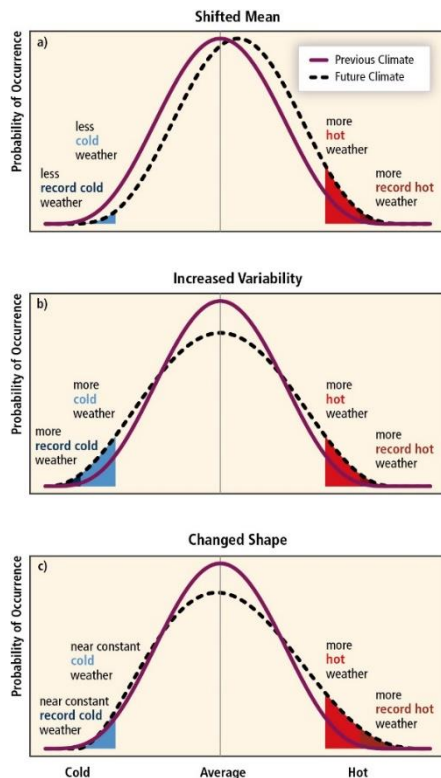
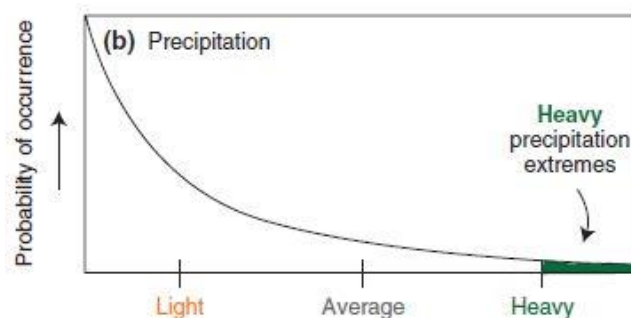


Figure 6: Left: The effect of changes in temperature distribution on extremes. a) effects of a shift of the entire distribution toward a warmer climate; b) effects of an increased temperature variability; c) effects of a variation in the shape of the distribution, i.e. an increased asymmetry toward the hotter part of the distribution. **Source: IPCC, 2012** Right: probability distribution of daily precipitation. The extremes are located at the right-tail of the distribution. **Source: Zhang et al. (2011)**



A relevant question is how regional changes in the extremes can be inferred from the mean global climate changes. This is important because of the implications that global mean temperature targets have on climate extremes<sup>7</sup>. Due to the complex nature of the climate systems, there is not necessarily a linear relation, especially for precipitation, between the global mean climate and the local mean or extreme climate. For instance, regional feedbacks such as soil moisture-temperature feedback<sup>8</sup>, enhances temperature extremes compared to mean changes. Especially in coastal regions like the coastline of Mozambique, regional changes depend on how the global forcings influence the atmospheric patterns (IPCC, 2012). Regional analysis is, therefore, necessary to investigate changes in the extremes.

Moreover, these non-linearities may eventually bring to abrupt changes in the climate systems, leading to variations in the extremes greater than could be expected with gradual warming. If tipping points are crossed, the result could be a high impacts scenario for society.

Among these challenges, how are climate extremes monitored and studied?

A large quantity of the literature on climate extremes is based on the usage of so-known ‘extreme indices’. They began to appear and spread during the 1990s when there was a distinct need for a standardised methodology in the global scientific community to study climate extremes, exchange results and data among different studies and countries (Alexander et al., 2019). Although many different indices have been proposed and used, the most commonly employed are the internationally recognised ETCCDI indices. They were formulated by the Expert Team on Climate Change Detection and Indices (ETCCDI), a group of experts co-sponsored by the World Meteorological Organisation (WMO) Commission for Climatology (CCI), the World Climate Research Programme (WCRP) and the Joint Technical Commission for Oceanography and Marine Meteorology (JCOMM). A set of 27 core indices that measures the frequency, intensity, and duration of temperature and precipitation extremes at the *annual timescale* employing *daily climate data*<sup>9</sup>. They can be sub-divided into three subgroups. The first

---

<sup>7</sup> For instance, the Paris Agreement, whose target is to keep the mean global temperature anomaly compared to pre-industrial era “well below 2°C”

<sup>8</sup> increasing temperatures result in a higher atmospheric moisture demand, which can induce soil drying and further enhance the temperature increase, in a positive feedback mechanism

<sup>9</sup> [http://etccdi.pacificclimate.org/list\\_27\\_indices.shtml](http://etccdi.pacificclimate.org/list_27_indices.shtml)

type of indices describes the maximum or minimum annual temperature or precipitation amount. They have been employed to infer design values for engineering structures (Zhang et al., 2011). The second type measures the number of days in a year in which absolute or relative thresholds are exceeded. Relative thresholds are based on percentiles of the base period climate<sup>10</sup> computed for each calendar day, and for this reason, they are meaningful in every region regardless of the local climate. However, this approach can lead, for instance, to a ‘heat wave’ in the middle of the winter and to a ‘wet day’ in the middle of the dry season. Therefore, the choice of the index can vary depending on the application: for impact studies, absolute thresholds are preferred, while for climate change studies percentile-based thresholds are favoured. The third type of indices measures the annual maximum duration of periods of wetness, dryness, heat or cold. All the indices describe ‘moderate climate extremes’ i.e. events occurring one or a few times in a year. Therefore, they do not characterize rare events located at the very end of the tail of the distributions (with high return periods), which are instead studied with the Extreme Value Theory (ETV)<sup>11</sup>.

The full set of 27 core indices is listed in Zhang et al. (2011). In the following pages, a subset of these is computed and analysed. Moreover, some more indices have been defined to deepen the characterization of climate extremes over the area of Beira. The rationale of using those indices, their formulation, and their meaning is going to be detailed in the correspondent section of the methodology (3.1).

The next chapter (Ch. 2) describes the climate data and models employed. Chapter 3 details the methodology for investigating future climate change extremes in the area of interest. Chapter 4 is devoted to the results obtained, while chapters 5 and 6 are dedicated to the discussion of the results and conclusions, respectively.

---

<sup>10</sup> e.g. 95<sup>th</sup> percentile of 1961-1990 daily precipitation time series

<sup>11</sup> A statistical methodology to model the probability of the least probable events (Abarbanel et al., 1992)

## 2. DATA AND MODELS

### 2.1 Climate Models

The fulfilment of the purpose of this work, described above, is implemented through the manipulation and statistical analysis of climate data. Particularly, the Climate Extremes Indices (ETCCDI) are computed starting from daily data, namely maximum and minimum temperature and precipitation. These were retrieved as the outputs of climate models, numerical representations of the climate system that allow the understanding of how the climate may change in the future. General Circulation Models (GCMs), and more, in particular, the Earth System Models (ESMs), are the most complex class of climate models simulating the physics, chemistry and biology of the atmosphere, land and oceans in great detail all around the globe. For this reason, they require supercomputers to generate their outputs. GCMs describe the climate using a three-dimensional grid on the globe, each model being characterized by a certain horizontal, vertical resolution and grid type. Differential equations (converted in computer codes), representing physical processes of the climate system, are solved giving as output the climate variables characterizing each box at each time step. Regional Climate Models (RCMs) are built from the GCMs by employing downscaling techniques to solve the climate system to higher spatial resolution ( $\sim 10 - 50km$ ) compared to GCM ( $\sim 100 - 1000km$ ). They are important for impact analyses at the regional scale, providing projections with greater detail and a more accurate representation of localised extreme events<sup>12</sup>. Although this study is concerned with analysing future climate projections at a local scale (the area surrounding Beira) and therefore regional models would be more suitable, it was decided to use state-of-the-art global models instead of more aged regional models.

---

<sup>12</sup> <https://cordex.org/about/what-is-regional-downscaling/>

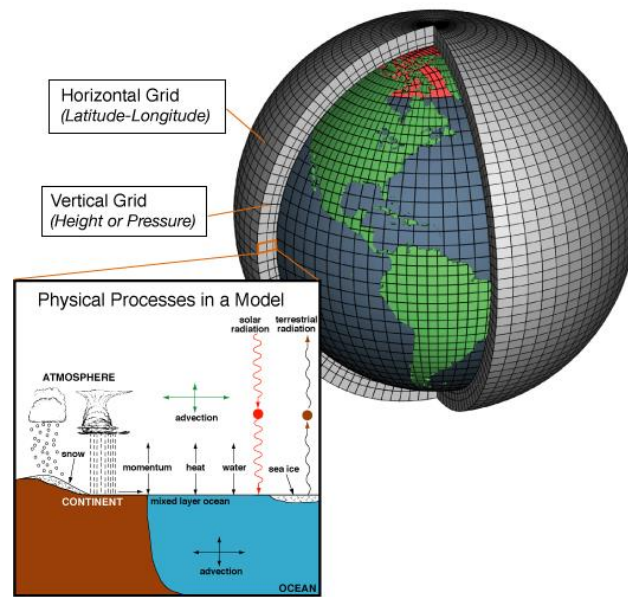


Figure 7: A representation of a General Circulation Model. The Earth is subdivided into boxes that are connected through fluxes of mass and energy. In each box, numerical equations representing physical and chemical processes are solved.<sup>13</sup>

The Working Group on Coupled Modelling (WGCM) of the World Climate Research Programme (WCRP) started the Coupled Model Intercomparison Project (CMIP) in 1955<sup>14</sup>. Its objective is to set up a collaborative framework in which scientists can share and compare their models, that guarantees high quality gridded data across the globe in a standardized format. A multi-model context is crucial to international climate change assessments (Li et al., 2021). This coordinated effort, in which multiple climate models have been run for a common set of experiments (common experiment protocols, forcings and outputs), allows performing Multi-Model Ensembles (MMEs) analyses. MMEs are a set of simulations derived from structurally different models. They allow to assess the structural uncertainty of the models (i.e. the uncertainty introduced by choices in the model design), essential to quantify the full uncertainty in climate change projections (Hawkins, 2011). Moreover, it has been demonstrated that MMEs increase the reliability and consistency of the model projections (Tebaldi, Knutti, 2007).

<sup>13</sup> [http://celebrating200years.noaa.gov/breakthroughs/climate\\_model/welcome.html](http://celebrating200years.noaa.gov/breakthroughs/climate_model/welcome.html)

<sup>14</sup> <https://www.wcrp-climate.org/wgcm-cmip>

**CMIP6** is the 6<sup>th</sup> phase of the Coupled Model Intercomparison Project. Its data coming from state-of-art global climate models underpin the Intergovernmental Panel on Climate Change 6th Assessment Report, the most authoritative report on the state of global climate change. CMIP6 consists of around 100 models run produced by 49 different modelling groups<sup>15</sup>. It includes both historical and future simulations (like the other CMIP phases). Historical runs span the period between 1850 and 2014, in other words from when the instrumental measurements of climate variables exist until the near-present. They are forced by externally imposed forcing based on observations, such as the atmospheric composition of GHGs caused by human activities. They serve to assess models performance (comparing their output with the observations), to perform attribution studies (unfold the causes of climate change), and to track changes over the different generations of models belonging to CMIPs (Eyring et al., 2016).

Future simulations span the period between 2015 and 2100 (2300 for some extended simulations). They are based on future scenarios relevant to societal concerns about climate change mitigation, adaptation and impacts, described in detail in O'Neill et al. (2016). The Shared Socio-economic Pathways (SSPs) are five alternative narratives describing the evolution of society throughout the 21<sup>st</sup> century. They take into account elements such as future population, urbanization, GDP and the type of policies implemented. Based on them, emissions and land-use scenarios are generated with an Integrated Assessment Modelling<sup>16</sup> (IAMs) approach. Thereby, each SSP can result in different radiative forcing outcomes by the end of the century. For instance, mitigation policies applied to each one of the SSPs could produce a forcing pathway that stabilized at 4.5Wm<sup>2</sup>, as visible in Figure 8. The latter figure shows the full collection of SSPs and forcing outcomes as a matrix of possible integrated scenarios. Scenarios in the context of the CMIP6 are referred to as *SSPx-y*, where x is the SSP code and y is the forcing outcome by the end of the century.

---

<sup>15</sup> <https://www.carbonbrief.org/>

<sup>16</sup> IAMs are models that uses different kind of input data – e.g. physical, economic and social – to produce information useful for decision-making.

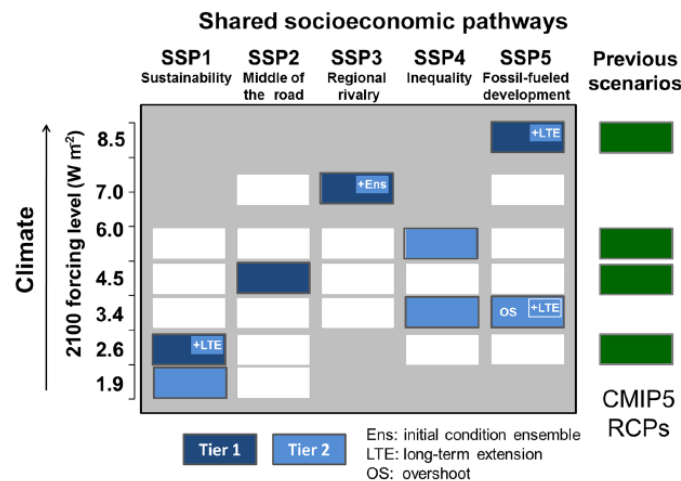


Figure 8: Scenarios matrix for CMIP6 simulations. Each cell is a combination of SSP and climate outcome based on a forcing outcome that IAM demonstrated to be feasible. Green cells represent the corresponding CMIP5 RCPs of each row, the socio-economic scenarios for the older generation of models. Dark blue cells indicate scenarios that will serve as the basis for climate model projections, which have the priority to be run by the modelling groups.  
Source: O'Neill et al., 2016

Graphs in Figure 9 represent the evolution of the CO<sub>2</sub> emissions, concentrations, anthropogenic radiative forcing and global mean temperature corresponding to different SSPx-y.

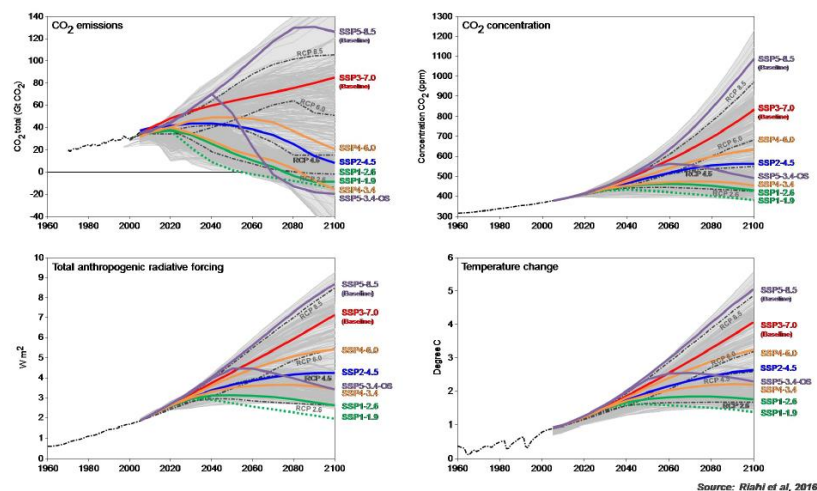


Figure 9: Evolution of the CO<sub>2</sub> emissions, concentrations, anthropogenic radiative forcing and global mean temperature for the scenarios defined in the context of the CMIP6. Grey areas represent scenario variability.  
Source: Riahi et al., 2016

For climate change studies, it is increasingly common to present future projections based on global average temperature change that predict (i.e. global warming levels, **GWLs**) instead of indicating a future epoch or scenario. In Chapter 5, the results will be compared

with the present literature, and therefore the GWLs are going to be employed to describe future projections.

CMIP6 simulations are the main source of data used in this study. For future projections, two scenarios were selected, respectively **SSP1-2.6** and **SSP5-8.5**. SSP1-2.6 updates the RCP2.6 pathway from CMIP5 and represent a scenario of sustainable-oriented growth (*“Taking the green road”*). It represents the best-case scenario producing mean global warming by the end of the century below 2°C compared to the pre-industrial era, and so is suitable to support policy goals. SSP5-8.5 on the contrary is the worst-case scenario (producing mean global warming of 4-5°C by the end of the century compared to the pre-industrial era), updating the RCP8.5 pathway from CMIP5. It represents a scenario with unconstrained economic growth and fossil-fuel use (*“Taking the highway”*) (Li et al., 2021). They are the low and high end of the range of future pathways, and therefore they were chosen to summarise the full range of possibilities regarding climate extremes on Beira.

In addition to data derived from climate model simulations, data based on climate observations were also used in this work. The **ERA5** reanalysis dataset, the latest generation of ECMWF reanalyses of the global climate, is the source of observation data for this study. ERA5 provides hourly estimates of a large number of climate variables covering the Earth on a 30km grid and resolves the atmosphere using 137 levels and covering the period between 1979 and 2020. By using advanced modelling and data assimilation systems, model data are combined with observations into a consistent dataset (Hersbach, 2018). Reanalysis data are employed in this thesis in different contexts as described in sections 2.3.2, 3.2, 3.4.

## 2.2 Climate data

As previously stated, data for future projections were retrieved from an ensemble of climate models part of the last phase of the Coupled Model Intercomparison Project



,CMIP6. They were downloaded by the Climate Data Store<sup>17</sup> (CDS) following specific guidelines through the Climate Data Store Application Program Interface. CDS provides a single point of access to a wide range of quality-assured climate datasets via a searchable catalogue<sup>18</sup>. Models used for the analysis were chosen, among the different simulations of CMIP6, depending on the availability on the portal. Particularly, depending on the availability of daily data of maximum and minimum temperature and precipitation for both the historical and the future projection run.

As a result, among the models which are part of the CMIP6, an ensemble of **18** simulations made by models were selected based on the SSP5-8.5 and **12** based on the SSP1-2.6. Description of climate variables is provided in Table 1. Moreover, the complete set of models which are part of the ensembles is listed in Table 2, together with their horizontal resolution and the institution that built up the model. Reanalysis climate data were equally downloaded from CDS<sup>19</sup>, having an hourly temporal resolution and  $0.25^\circ \times 0.25^\circ$  lon-lat spatial resolution

*Table 1: Description of daily variables used in this study, output of the ensemble of simulations*

<b>Variable</b>	<b>Unit</b>	<b>Definition</b>	<b>Abbreviation</b>
Daily maximum near-surface air temperature	°C	Daily maximum temperature of air at 2m above the surface of land, sea or inland waters.	<i>T<sub>x</sub></i>
Daily minimum near-surface air temperature	°C	Daily minimum temperature of air at 2m above the surface of land, sea or inland waters.	<i>T<sub>n</sub></i>
Precipitation	<i>mm</i>	The sum of liquid and frozen water, comprising rain and snow, that falls to the Earth's surface. It is the sum of large-scale precipitation and convective precipitation. This parameter does not include fog, dew or the precipitation that evaporates in the atmosphere before it lands at the surface of the Earth. This variable represents amount of water per unit area and time.	<i>pr</i>

<sup>17</sup> <https://cds.climate.copernicus.eu>

<sup>18</sup> <https://climate.copernicus.eu/climate-data-store>

<sup>19</sup> <https://cds.climate.copernicus.eu/cdsapp#!/dataset/reanalysis-era5-single-levels?tab=overview>

Table 2: Information about the CMIP6 models used in this study

<b>Model</b>	<b>Modelling centre</b>	<b>Scenario</b>	<b>Resolution (lon × lat)</b>
ACCESS-CM2	CSIRO-ARCCSS (Australia)	SSP1-2.6 SSP5-8.5	1.875° × 1.25°
CMCC-ESM2	Centro Euro-Mediterraneo per I Cambiamenti Climatici (Italy)	SSP1-2.6 SSP5-8.5	1.25° × 0.94°
CNRM-CM6-1-HR	CNRM-CERFACS (France)	SSP5-8.5	0.5° × 0.5°
CNRM-CM6-1	CNRM-CERFACS (France)	SSP1-2.6 SSP5-8.5	1.4° × 1.4°
CNRM-ESM2-1	CNRM-CERFACS (France)	SSP1-2.6 SSP5-8.5	1.4° × 1.4°
CanESM5	Canadian Centre for Climate Modelling and Analysis (Canada)	SSP5-8.5	2.8° × 2.8°
EC-Earth3-CC	EC-Earth-Consortium (Europe)	SSP5-8.5	0.7° × 0.7°
EC-Earth3-Veg-LR	EC-Earth-Consortium (Europe)	SSP5-8.5	1.125° × 1.125°
GFDL-ESM4	Geophysical Fluid Dynamics Laboratory (USA)	SSP1-2.6 SSP5-8.5	1.25° × 1°
INM-CM4-8	Institute of Numerical Mathematics (Russia)	SSP1-2.6 SSP5-8.5	2° × 1.5°
INM-CM5-0	Institute of Numerical Mathematics (Russia)	SSP1-2.6 SSP5-8.5	2° × 1.5°
KACE-1-0-G	National Institute of Meteorological Sciences (South Korea)	SSP5-8.5	1.875° × 1.25°
MIROC-ES2L	MIROC (Japan)	SSP1-2.6 SSP5-8.5	2.8° × 2.8°
MIROC6	MIROC (Japan)	SSP1-2.6 SSP5-8.5	1.4° × 1.4°
MPI-ESM1-2-LR	Max Planck Institute for Meteorology (Germany)	SSP1-2.6 SSP5-8.5	1.875° × 1.865°
MRI-ESM2-0	Meteorological Research Institute (Japan)	SSP1-2.6 SSP5-8.5	1.125° × 1.121°
NESM3	Nanjing University of Information Science and Technology (China)	SSP5-8.5	1.875° × 1.865°
NorESM2-MM	Norwegian Climate Centre (Norway)	SSP1-2.6 SSP5-8.5	0.25° × 0.94°

## 2.3 Pre-processing

### 2.3.1 Cut and Remap original data

Raw data were processed to compute the extreme climate indices. For doing that, CDO – Climate Data Operators – has been used. It is a collection of command-line Operators developed by the Max Planck Institute for Meteorology to manipulate climate data<sup>20</sup>.

First, historical runs for each model and variable (with period 1850-2014) were cut to daily datasets with period 1961-2014 and time-merged with the corresponding projections (2015-2100) to have the full-time interval (1961-2100). Secondly, for each dataset, only one grid cell has been selected with the *nearest neighbor (NN)* approach on Beira coordinates  $34.85^{\circ}N$  -  $19.83^{\circ}E$ . This choice was made since working with data deriving from a single grid cell allows to avoid having time series resulting from a spatial average that would risk “dampening” the signal coming from a change in the extremes. The final product is a set of time series of daily maximum and minimum temperature and precipitation for each model and both socio-economic scenarios.

### 2.3.2 Bias Correction

Climate models are affected by systematic errors that are essentially due to the simplification with which they inevitably represent the real-world climate. Indeed, since the climate is an extremely complex system, it remains fundamentally impossible to describe all its processes. Therefore, in a climate model, several approximations are present, in particular linked to the parameterizations of sub-grid processes (IPCC, 2015). For this reason, statistics of temperature and precipitation projections derived from climate models in a certain period do not usually fit those of observations in the same period. Bias correction methods try to improve the fitting of climate model simulations to observations in a control period and to enhance the reliability of future projections

---

<sup>20</sup> <https://code.mpimet.mpg.de/projects/cdo/>

(Enrique Soriano, 2019). Therefore, before proceeding in the calculation of indices, temperature and precipitation daily time series have been corrected by using a simple bias correction method. The ERA5 reanalysis dataset is used as the source of observation data for the bias correction. Reanalyses datasets are often used for model evaluation due to their gridded outputs, directly comparable with model simulations (Sillmann et al., 2013). Moreover, they are the only source for publicly available information about temperature and precipitation extremes in the area of interest. However, this approach also has some limitations, especially concerning precipitations. Indeed, precipitation data derived from reanalysis are less constrained to real observations and more to the reanalysis model (Kistler et al., 2001), and therefore are affected by biases and less reliable than temperature data (Zhang et al., 2011). Nevertheless, in the context of bias correction, these errors are often argued to be acceptable since they are much smaller than biases present in the models (Glencker et al., 2008). The bias correction method employed is very simple. The purpose is to align the means of the raw temperature and precipitation datasets and the observation dataset in the period in which reanalysis data are available. The original time series is “scaled” to the observational time series (as visible in Figure 10, bottom). This is done by removing from each time step the mean of the entire dataset and adding the mean of the reanalysis dataset for daily maximum and minimum temperatures. Instead, for precipitation, this would not be possible since it would lead to days of negative rainfall. Hence, the mean of the reanalysis data is multiplied while the mean of the simulated dataset is divided to each time step. This simple manipulation of raw time series allows to preserve the variability of the models’ output and so is the climatic signals connected with climate extremes that are of interest for this study. The following formulas are applied to the original datasets.

$$\triangleright T_{BC}(i) = T_{raw}(i) - \bar{T}_{raw} + \bar{T}_{obs} \quad (1)$$

$$\triangleright pr_{BC}(i) = \frac{pr_{raw}(i)}{\bar{pr}_{raw}} * \bar{pr}_{obs} \quad (2)$$

Where  $\bar{T}_{raw}$  and  $\bar{pr}_{raw}$  represents the averages of the raw datasets in 1979-2020 while  $\bar{T}_{obs}$  and  $\bar{pr}_{obs}$  represents the averages of the reanalysis dataset in the same period.  $T_{raw}(i)$  and  $pr_{raw}(i)$  are the original data for each time step  $i$ , while  $T_{BC}(i)$  and  $pr_{BC}(i)$  are the data at the same time step  $i$  after the bias correction.

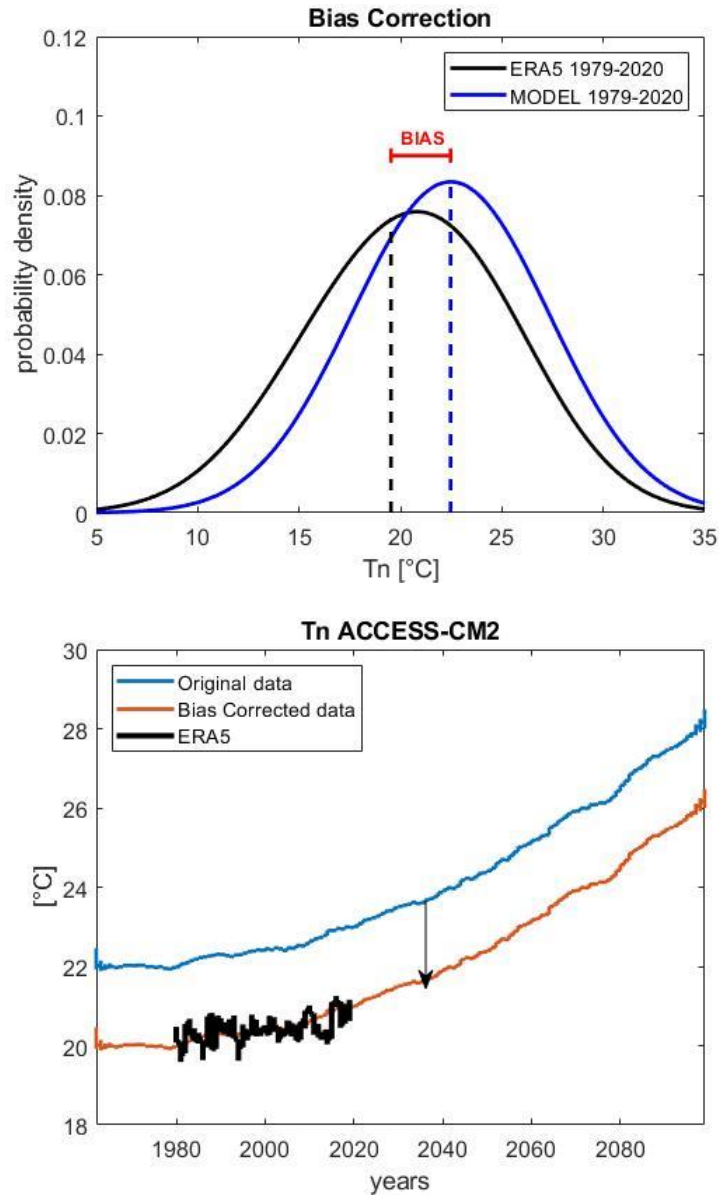


Figure 10: Representation of the bias correction applied to daily minimum temperature simulated by ACCESS-CM2. Up: PDFs of the observed and simulated Tn in the reanalysis period. The bias is the difference between the means. Bottom: The simulated time series is scaled readjusting the mean to the observed one. A 10-years moving average is applied to the time series to smooth them.

The subsequent analyses, which are going to be described in detail in the next chapters, have been performed using codes developed from scratch in Matlab® and R programming languages.

### 3.METHODOLOGY

The methodology developed in this work aims at investigating future scenarios regarding extreme climate in areas around the city of Beira.

Figure 11 is a diagram showing the main steps of the methodology. To begin, Climate Extremes Indices were selected and defined. Indices were then calculated. Before analysing what models say about the future, their performance to predict reality was assessed. For doing that, the time series of annual indices were compared to the time series of indices computed through observational data. Afterwards, future projections of indices were taken into consideration. To assess the temporal change of the indices, different analyses were conducted.

The core analysis is the assessment and computation of trends in the time series of indices (i.e. Trend Analysis). Complementary to that, a temporal comparison of probability density functions and mean absolute anomalies was performed to have a better insight into the way the indices are projected to change. The latter temporal comparisons were made on three sub-periods of the main study period (1961-2100): the baseline period (1981-2010), the near future (2026-2055) and the far future (2071-2100).

In addition, the correlation between the indices and the extreme events that had dramatic consequences for the city of Beira was investigated. To this end, the cross-correlation between the indices was first explored using the rank correlation coefficient by Spearman. Finally, a procedure was developed to correlate the indices and the “critical events” over Beira and to assess whether they are going to increase or decrease in the future.

Each of these steps is going to be described in detail in this chapter.

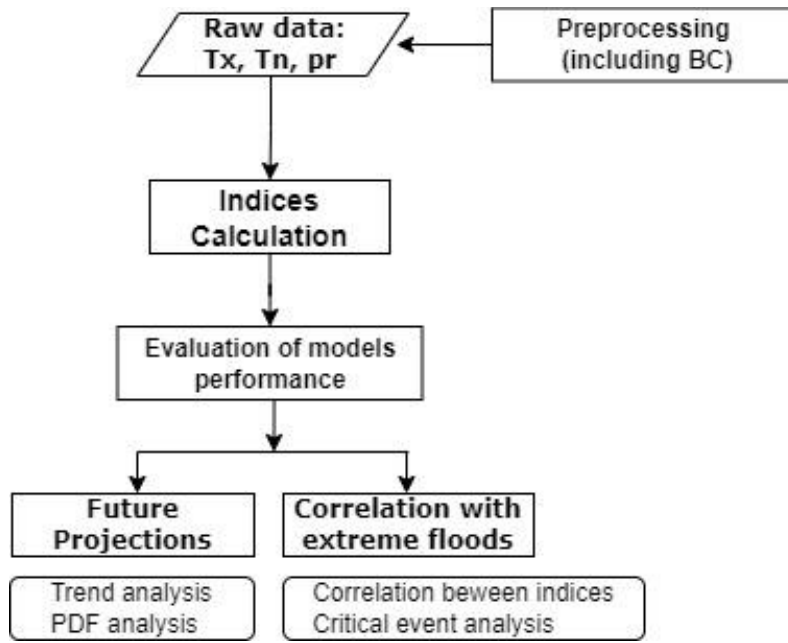


Figure 11: Diagram showing the methodology of the work. All the steps are performed using raw data derived from the two different socioeconomic scenarios (SSP1-2.6, SSP5-8.5).

### 3.1 Indices Definition and Calculation

Among the 27 ETCCDI conventionally used to assess climate moderate extremes, 16 were selected since they were considered as more relevant for the analysis and the study area. Of these, half describe extreme temperature events and the other half describe extreme rainfall events.

In addition, four more indices have been analysed, whose ID names are ETR, nR95p, inR95p, and cwd95. ETR has been defined following Frinch et al. (2002) while the others have been directly suggested here as complementary information to get a more complete framework about the precipitation extremes over Beira. Overall, **20 indices** are computed from daily temperature and precipitation data using Climate Data Operator line commands<sup>21</sup>.

<sup>21</sup> [https://gitlab.dkrz.de/k204210/cdo\\_cei](https://gitlab.dkrz.de/k204210/cdo_cei)

The following Table 3 displays the selected indices and their definitions. *T<sub>x</sub>* stands for daily maximum temperature, *T<sub>n</sub>* stands for daily minimum temperature and *pr* stands for daily precipitation. For the calculation of the percentile-based indices, a bootstrapping procedure is employed within the base period (on which percentiles are computed), in order to avoid artificial discontinuities are reported in Zhang et al. (2005).

Table 3: Extreme Climate Indices used in this study. Percentiles are computed over the base period 1981-2010.  
\* Non-ETCCDI

ID	Indicator Name	Definition	Unit
<b>TX<sub>x</sub></b>	Maximum annual temperature	Annual maximum value of daily maximum temperature	°C
<b>TN<sub>n</sub></b>	Minimum annual temperature	Annual minimum value of daily minimum temperature	°C
<b>DTR</b>	Daily temperature range	Annual mean difference between <i>T<sub>x</sub></i> and <i>T<sub>n</sub></i> .	°C
<b>ETR*</b>	Extreme temperature range	Difference between <i>TX<sub>x</sub></i> and <i>TN<sub>n</sub></i>	°C
<b>Tn10p</b>	Warm nights	Percentage of days when <i>T<sub>n</sub></i> < 10 <sup>th</sup> percentile	%
<b>Tx10p</b>	Cold days	Percentage of days when <i>T<sub>x</sub></i> < 10 <sup>th</sup> percentile	%
<b>Tn90p</b>	Warm nights	Percentage of days when <i>T<sub>n</sub></i> > 90 <sup>th</sup> percentile	%
<b>Tx90p</b>	Warm days	Percentage of days when <i>T<sub>x</sub></i> > 90 <sup>th</sup> percentile	%
<b>wsdi</b>	Warm spell duration index	annual count of days with at least 6 consecutive days when <i>TX</i> > 90 <sup>th</sup> percentile	days
<b>sdii</b>	Simple daily precipitation index	Annual total precipitation divided by the number of wet days ( <i>pr</i> > 1mm)	mm
<b>Rx1day</b>	Max 1-day precipitation	Annual maximum 1-day precipitation	mm
<b>Rx5day</b>	Max 5-day precipitation	Annual maximum 5-day precipitation	mm



<b>PRCPTOT</b>	<i>Annual total precipitation</i>	<i>annual total precipitation in wet days (<math>pr &gt; 1</math> mm)</i>	mm
<b>R95p</b>	<i>Very wet days</i>	<i>Total precipitation when <math>pr &gt; 95</math>th percentile</i>	mm
<b>cdd</b>	<i>Consecutive dry days</i>	<i>Annual maximum number of consecutive days with <math>pr &lt; 1</math> mm</i>	days
<b>cwd</b>	<i>Consecutive wet days</i>	<i>Annual maximum number of consecutive days with <math>pr &gt; 1</math> mm</i>	days
<b>R20</b>	<i>number of heavy precipitation days</i>	<i>annual count of days when <math>pr &gt; 20</math> mm</i>	days
<b>nR95p*</b>	<i>Number of very wet days</i>	<i>Annual count of days in which <math>pr &gt; 95</math>th percentile</i>	days
<b>inR95p*</b>	<i>Number of independent extreme precipitation events</i>	<i>Annual count of very wet days (<math>pr &gt; 95</math>th percentile) divided by at least 7 dry days (<math>pr &lt; 1</math> mm)</i>	events
<b>Cwd95*</b>	<i>Consecutive very wet days</i>	<i>Annual maximum number of consecutive days with <math>pr &gt; 95</math>th percentile</i>	days

***TXx*** and ***TNn*** are direct indicators of the intensity of warmest and coldest annual temperatures. They are intuitive absolute measures of how hot or cold a year has been.

***DTR*** is a measure of the average thermal excursion between day and night. Analysing its changes is interesting to understand how the temperature regime changes.

***ETR*** is a measure of the width of temperature distribution across the year. It is computed as the annual difference between ***TXx*** and ***TNn***. If the yearly minimum temperature increases faster than the yearly maximum, the temperature distribution becomes narrower (and vice versa). Therefore, an increase in this index might indicate that temperature variations become more extreme.

***Tx10p***, ***Tn10p***, ***Tn90p***, and ***Tx90p*** are measures of the annual frequency of extreme temperature events, in terms of exceedance (or not-exceedance) of percentile thresholds. They allow stating if the “extreme event” defined as belonging to the first and last portion (10%) of the temperature distribution, is going to happen more or less often in the future.

Therefore, they are useful to understand if the definition of “extreme event”, as defined in a reference period, is appropriate also for the future.

***wsdi*** is an index concerning heat waves. According to its definition, a heatwave is a period of at least six consecutive days in which temperature is above the 90<sup>th</sup> percentile. The indicator counts the number of days characterized by a heatwave in one year. Heatwaves are important temperature extreme events that need to be assessed due to the serious implications on human health (McGregor et al., 2015).

***sdi*** is a very simple and intuitive measure of average precipitation intensity. It measures how much it rains when it rains.

***Rx1day*** and ***Rx5day*** are measures of the short-term extreme precipitation intensity. They are flood indicators and because of that, they are essential for the present analysis.

***PRCPTOT*** is the measure of the total annual rainfall amount and it is connected to water availability. As a matter of fact, the region of Beira is characterized by a large amount of fallen precipitation compared to the more internal part of Mozambique. It is of interest to understand how the annual rainfall pattern is projected to change.

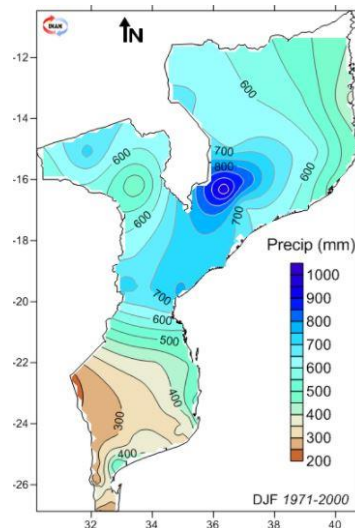


Figure 12: Rainfall amount over Mozambique in December, January and February, during the rainy season. The area of the city of Beira presents relatively high values of precipitation with respect to other parts of the country.  
Source: INAM, Instituto Nacional de Meteorologia ([www.inam.gov.mz](http://www.inam.gov.mz))

***R95p*** is a measure of the cumulative intensity of the extreme precipitation events, that are of particular interest for the present study. It is correlated with both the number and the intensity of extreme events.

***cdd*** is a duration index connected to meteorological droughts. An increase would mean a dryer climate, with potentially important consequences on natural and social systems due to reduced water availability.

***cwd*** is a duration index connected to high flood risk. An increase in this index would mean higher chances of flooding. Hence, it is important for this study.

***R20*** is a measure of the frequency of heavy precipitation days in a year, where a “heavy precipitation day” is defined as a day with precipitation greater than 20mm. Thus, it is related to flood frequency and flood risk. Nonetheless, considering the climate features of Mozambique<sup>22</sup>, the threshold of 20mm used to define a precipitation extreme is only representative of the wet season and not of the dry season (Tinley, K.L., 1982). In other words, future projections of *R20* successfully allow analysing how the frequency of the rainiest days in the year is going to change but do not give any information about the dry season.

For this reason, ***nR95p*** is defined. For this index, the “very wet day” is a day in which the 95<sup>th</sup> percentile is overcome (in the same way as for *R95p*). Given that the percentile is a threshold that varies depending on the day of the year, also changes in the rainfall regime of the dry season may be detected. Indeed, an “extreme precipitation event” defined in this way might be a day in which the fallen precipitation is low in absolute values, but high if compared to the usual precipitation that falls on that particular day of the year.

The ***inR95p*** index aims at describing the frequency of meteorologically independent extreme events. It is the annual count of the number of very wet days (above 95th percentile) that are separated between each other by at least 7 consecutive dry days (with  $pr < 1\text{mm}$ ). For the determination of the 7-day threshold, the IETD (Inter-Event Time Definition) approach was used. The IETD is the minimum dry period between two independent events. If the time between two wet days is greater than the IETD, they are

---

<sup>22</sup> <https://www.inam.gov.mz/>

considered separated events. One traditional determination method for IETD is the “average annual number of events analyses” (Joo et al. 2014). This consists of determining IETD as the point where increasing IETD does not change the annual number of rainfall events significantly. The following Figure 13 shows the variation of the number of independent extreme events as the IETD value changes. Applying a conservative approach, the value of IETD= 7 days has been chosen to separate independent extreme events.

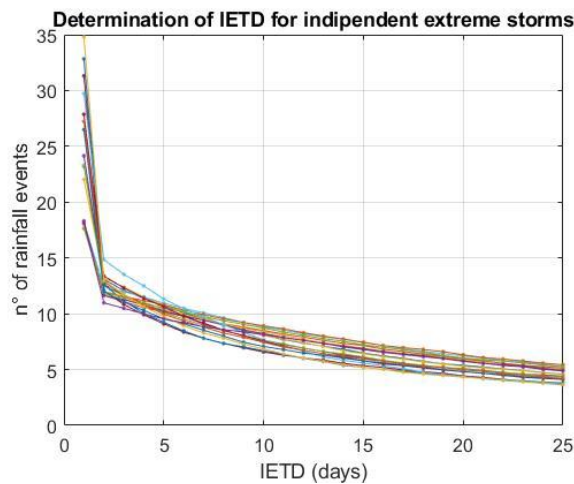


Figure 13: determination of IETD for defining independent extreme storms in the inR95p index. Different lines represent the different models. Changing the IETD value results in changing the number of detected annual independent extreme events in the rainfall time series. IETD =7 was chosen because the number of events does not change “significantly” after that.

**cwd95** is the measure of the annual maximum duration of consecutive wet days above the 95<sup>th</sup> percentile. Consequently, it is an indication of the length of precipitation extremes that is noticeably an important factor concerning the risk of flooding.

The last three indices (not part of the core ETCCDI list) are very much connected, and therefore it might be interesting to see if there is some pattern emerging by looking at them together.

### 3.2 Ability of models to simulate temperature and precipitation extremes

The evaluation of climate models through the comparison of their outputs with observations is a prerequisite for applying them confidentially (Flato et. al, 2013). Therefore, before going further into the analysis of projected indices, the performance of the models in simulating temperature and precipitation extremes needs to be evaluated. This is done by comparing the simulated indices to the indices produced starting from daily data provided by the reanalysis data (ERA5) as it is frequently done in literature, for instance in Li et al. (2021), Sillmann et. al. (2013), Gleckler et al. (2008).

The quantitative assessment of the performances of the models was accomplished by computing a **Performance Index**. It is defined as the relative error (i.e. bias) between the mean, along the period 1979-2014, of an index simulated by the models and the mean of the same index calculated from ERA5 data. The period of 35 years was chosen since it is the intersection of the reanalysis period (1979-2020) and the historical run period (1961-2014). The bias is normalized, in a way to make values between the indices comparable to each other. Formula 3 represents the Performance Index calculation for a generic index “*Ind*”. The subscript “*m*” stands for the model to which the Performance Index is referred.

$$PI_{Ind,m} = \frac{\overline{Ind_m - Ind_{era5}}}{\overline{Ind_{era5}}} \quad (3)$$

This procedure roughly follows Sillmann et al. (2013) that had analysed the performance of CMIP5 models in simulating ETCCDI indices through the Root Mean Square Error (RMSE) computed on spatial patterns. However, contrarily to their study in which the whole globe is considered, here only one-grid cell is taken. Hence, the measure of performance is different.

The results are collected in the following Figure 14, a Portrait Diagram (Gleckler et. al, 2008), to have a compact graphical overview of the performance of the models. Each column contains one of the 18 models, while each row is one of the 20 indices. The analysis was performed before and after Bias Correction (Figure 14) to assess the efficiency of the bias removal. A white box indicates a very low bias between models and ERA5. A blue box indicates that the model tends to underestimate the value of the index, while the value tends to be overestimated in a red box.

Moreover, the statistical significance of the agreement between the simulations of the models and the observations is tested with the Two-sample Kolmogorov-Smirnov test (Smirnov, N.V., 1939). The statistical test compares the cumulative distributions of the time series and accepts or rejects the Null Hypothesis of the same distribution underlying the data.

The results are yet shown in Figure 14, by indicating a black dot on the boxes for which the Null Hypothesis is not rejected, i.e. the model and the reanalysis distributions are not significantly different, and therefore there is good agreement between predictions and observations.

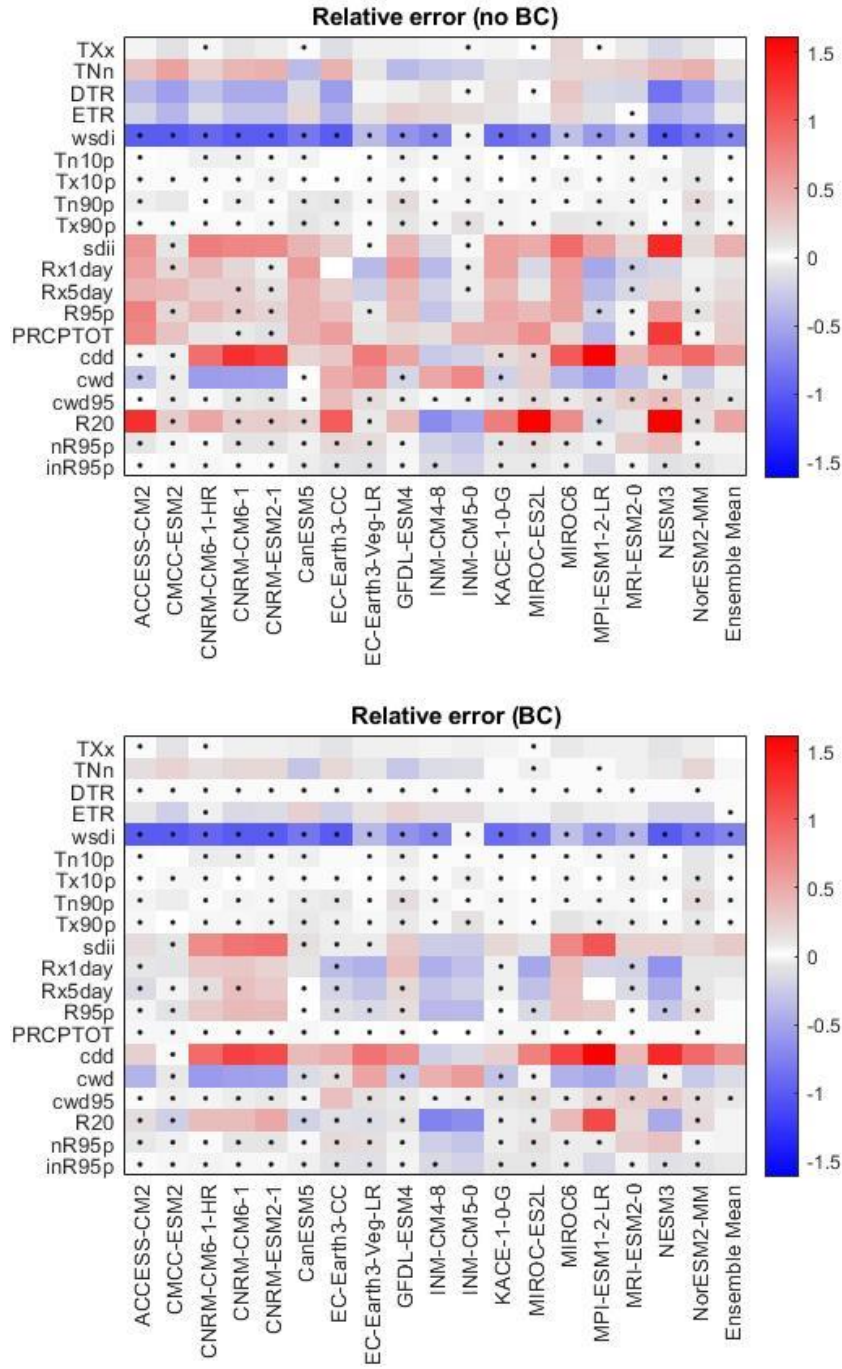


Figure 14: Portrait Diagrams displaying the Performance Index (normalized bias between models' projections and reanalysis over the period 1979-2014) with a blue-red color scale. In this way, the performance of models is evaluated. The black dots indicate where the null hypothesis of the Kolmogorov-Smirnov test of the same underlying cumulative distribution is not rejected. Up: Indices computed starting from data not-bias corrected. Bottom: Indices computed starting from bias-corrected data

The overall **Model Performance** is obtained by averaging the *Performance Index* over the indices (over each column of the Portrait Diagram). This quantity is contained in Table 4 in which is applied the same colour scale as in Figure 14.

Table 4: Model Performance Index before bias correction (left) and after bias correction (right).

Model	Model Performance (no BC)	Model	Model Performance (BC)
ACCESS-CM2	0.152	ACCESS-CM2	-0.034
CMCC-ESM2	0.006	CMCC-ESM2	-0.068
CNRM-CM6-1-HR	0.076	CNRM-CM6-1-HR	0.065
CNRM-CM6-1	0.056	CNRM-CM6-1	0.109
CNRM-ESM2-1	0.037	CNRM-ESM2-1	0.110
CanESM5	0.093	CanESM5	-0.009
EC-Earth3-CC	0.107	EC-Earth3-CC	-0.033
EC-Earth3-Veg-LR	0.047	EC-Earth3-Veg-LR	0.021
GFDL-ESM4	0.107	GFDL-ESM4	0.053
INM-CM4-8	-0.117	INM-CM4-8	-0.142
INM-CM5-0	-0.002	INM-CM5-0	-0.079
KACE-1-0-G	0.117	KACE-1-0-G	-0.025
MIROC-ES2L	0.151	MIROC-ES2L	-0.025
MIROC6	0.234	MIROC6	0.146
MPI-ESM1-2-LR	0.010	MPI-ESM1-2-LR	0.147
MRI-ESM2-0	0.013	MRI-ESM2-0	0.030
NESM3	0.292	NESM3	-0.038
NorESM2-MM	0.005	NorESM2-MM	0.044
Ensemble Mean	0.077	Ensemble Mean	0.015

The **Index Agreement** is obtained by averaging the Performance Index over the models (over each row of the Portrait Diagram). This quantity is contained in Table 5 in which is applied the same colour scale as in the above Figure 14.



Table 5: Index Agreement before bias correction (left) and after bias correction (right).

Model	Index Agreement (no BC)	Model	Index Agreement (BC)
TXx	-0.009	TXx	0.014
TNn	0.127	TNn	0.038
DTR	-0.224	DTR	0.002
ETR	-0.072	ETR	0.003
wsgi	-0.737	wsgi	-0.737
Tn10p	-0.006	Tn10p	-0.006
Tx10p	0.005	Tx10p	0.005
Tn90p	0.050	Tn90p	0.050
Tx90p	0.037	Tx90p	0.037
sdii	0.448	sdii	0.286
Rx1day	0.105	Rx1day	-0.072
Rx5day	0.162	Rx5day	-0.028
R95p	0.242	R95p	0.036
PRCPTOT	0.273	PRCPTOT	0.012
cdd	0.589	cdd	0.666
cwd	-0.062	cwd	-0.137
cwd95	0.090	cwd95	0.090
R20	0.529	R20	0.052
nR95p	0.050	nR95p	0.051
inR95p	-0.059	inR95p	-0.059

Overall, the models compare well with the ERA5 reanalysis. However, there are some differences, particularly regarding WSDI, which is heavily underestimated by all the models. By looking at the single simulated and observed time series in Figure 15, one very large value is recorded in the year 1993 that is not reproduced by the models. This outlier is probably the main source of the large bias between the means of the time series. On the contrary, CDD and SDII tend to be overestimated by the majority of the models, as clearly visible in the time series in Figure 15 - bottom.

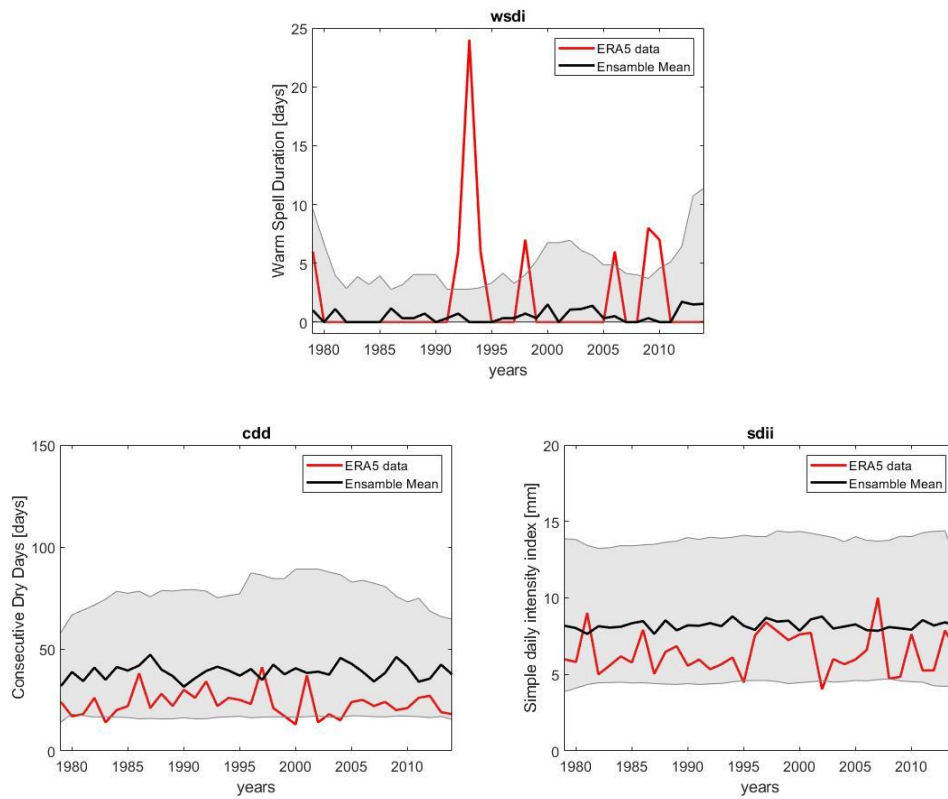


Figure 15: Comparison between ERA5 and models time series after the Bias Correction. The thick black line represents the Ensemble Mean, while the shading is the area between the 5th and 95th percentile.

In general, by looking at the portrait diagrams in Figure 14 and Table 5, it is possible to say that annual values of precipitation extremes tend to be overestimated by the models. This divergence is in part corrected by the bias correction. This procedure does not have a uniform effect on the agreement between models and observations. The *Index Agreement* shows well this behaviour. For many indices, the *Index Agreement* remains constant after the BC while for others it increases or decreases. This depends on how the indices are defined. For instance, the temperature indices based on percentile threshold exceedances remain the same, since the bias correction changes both the value of the data and the value of the thresholds so that the number of exceedances remains unchanged. However, by comparing the two portrait diagrams, it can be said that bias correction brings the relative errors towards more “faded” colours and more statistically significant agreements. Indeed, the number of black dots increase, 186 before bias correction and 225 after. The Model Performance of 11 models out of 18 increases after the Bias

Correction and in particular the Ensemble Mean, which is the most statistically robust reference for future predictions (Flato et al, 2013), outperforms most models and has its bias decreased after BC procedure.

The validation of climate performances of the models in simulating indices of precipitation and temperature extremes over Beira gives confidence to future predictions.

### 3.3 Future Projections

The analysis of projected future tendencies of climate extremes is the core part of the present work. For this investigation, three 30-year periods are used as a reference for the baseline period (1981–2010), the near future (2026–2055), the far future (2071–2100). Different analyses have been conducted to determine the projected changes of the indices. Firstly, the climate change signal was highlighted as the *difference between the mean* over future periods and the mean over the reference period. This provides an overview of the sign and the magnitude of change that we are going to expect in climate extremes over Beira (Sillman et al., 2013). Secondly, the *presence and the magnitude of trends* in the extreme indices time series are assessed. This is widely documented as the statistically most robust way to detect the rate of change of climate indices (Zhang et al., 2011). Lastly, *probability density functions* are computed and their evolution in time is studied. The trend analysis and the analysis are described in detail in this section. The results are going to be displayed in the following Chapter 4.

### 3.3.1 Trend Analysis

The traditional approach of time series analysis assumes time-series data to be generated by a process composed of a deterministic part and a stochastic part. The time-evolution of the deterministic component can be described by a mathematical equation that while the stochastic is unpredictable and makes the climate variables as ‘random variables’. The deterministic part of climatic a time series can be, broadly speaking, separated into the Trend and the Periodical (or Seasonal) components. The Periodical component is any regular oscillation around the trend of data values. In climate science, it can be attributed to any physical process for instance seasonality or long-term climatic oscillations such as El Niño-Southern Oscillation. The Trend component is the long-term pattern or tendency of the data. The presence or not of this component in the data determines if the time series is stationary (no trend) or non-stationary (trend presence) (Dagum, E. B. 2001).

Trend analysis is a central process in assessing the state of the climate and provides an overall estimate of the variations in the climate variables (Mahmood, R., Jia, S., 2017). Regression Analysis is the main statistical approach to estimate the trend component. In particular, OLS (ordinary least square) is the best-known estimation method and its fields of application are very diverse, including climatology (Tank et al., 2003). An important assumption underlying this linear regression model is that the data under study are attributable to a normal distribution. An initial sample analysis of the time series of indices of temperature and precipitation extremes highlighted their non-conformity to the normal distribution. Hence, different techniques have been used for the trend analysis in this study. The Slope Estimator by Sen (Sen, 1968) was used to provide the estimate of the trend, while the Mann-Kendall test (Mann 1945; Kendall, 1948), was applied to the time series to evaluate the significance of the trend at the 5% level ( $p=0.05$ ). An insight of the two statistical techniques is clearly explained in Wang, X.L., Swail, V.R. (2001) and Pohlert, T. (2020).

The Sen Slope Estimator is a non-parametric estimation method, i.e. it does not make specific assumptions about the distribution of the data under consideration. Moreover, it

is a “robust” estimator, i.e. is less sensitive to the presence of outliers. The slope of the line is given by the median of the slopes that can be calculated for each pair of points in the data set.

A set of linear slopes is calculated as follow:

$$s_k = \frac{X_j - X_i}{t_j - t_i} \quad \text{for } 1 \leq i < j \leq n \quad (4)$$

Where:  $s$  is the slope,  $X$  denotes the variable,  $n$  is the number of data, and  $i, j$  are indices.

The slope is then calculated as the median from all slopes:

$$b = \text{median}(s_k) \quad (5)$$

The intercepts are computed for each time step  $t$  as:

$$a_t = X_t - b * t \quad (6)$$

On the other hand, the Mann-Kendall test is a nonparametric test for randomness against trend. As for the Sen Estimator, the use of the Mann-Kendall test is well documented in climate extreme analysis (for instance Dagum, et al., 2001; Zhang et al., 2011; Russo et al., 2011). The null hypothesis,  $H_0$ , is that the data are Independent and Identically Distributed (IID). The alternative hypothesis,  $H_A$ , is that the data follow a monotonic trend. The test statistics  $S$  is defined as:

$$S = \sum_{k=1}^{n-1} \sum_{j=k+1}^n \text{sgn}(X_j - X_k) \quad (7)$$

where

$$\text{sgn}(x) = \begin{cases} 1 & \text{if } x > 0 \\ 0 & \text{if } x = 0 \\ -1 & \text{if } x < 0 \end{cases} \quad (8)$$

The variance of  $S$  is given by:

$$V_s = n(n-1)(2n+5)/18 \quad (9)$$

The significance of the trend is assessed using a  $Z$  value defined as:

$$Z = \begin{cases} \frac{S-1}{\sqrt{V_s}} & \text{if } S > 0 \\ 0 & \text{if } S = 0 \\ \frac{S+1}{\sqrt{V_s}} & \text{if } S < 0 \end{cases} \quad (10)$$

This value is compared with  $Z_{\frac{\alpha}{2}} \mid F_n \left( Z_{\frac{\alpha}{2}} \right) = \frac{\alpha}{2}$  (11)

$F_n$  being the standard cumulative Distribution and  $\alpha$  being the significance level for the test. **H0 is accepted if  $|Z| \leq Z_{\frac{\alpha}{2}}$**

The  $(1-\alpha)$  confidence interval of estimator  $b$  is  $(X_{M_1}, X_{M_2+1})$ , with:

$$n^* = Z_{\frac{\alpha}{2}} V_s \quad ; \quad M_1 = \frac{n - n^*}{2} \quad ; \quad M_2 = \frac{n + n^*}{2} \quad (12)$$

To sum up, the Trend Analysis gives as output the magnitude and the significance of a trend in each of the time series. Therefore, the analysis is repeated for each index, for each model (including the Ensemble Mean time series), and both the future socio-economic scenarios.

### 3.3.2 Probability Density Functions

Empirical Probability Density Functions (PDF) have been computed as further analysis to deepen the knowledge about future temporal changes of indices.

The comparison of empirical density functions over time has been widely used in literature as a way to analyse changes in climate variables (Fallmann et al.,2017; Xu et al.,2015; Ongoma et al.,2018). In this work, PDFs are produced by binning annual values of the indices for the 30 years sub-periods: base period (1981-2010), near future (2026-2055), far future (2071-2100). In this case, data from all the models are used without distinction. Hence, the number of data points used to compute each PDF is equal to the number of models multiplied by the number of years in a sub-period:  $18 \cdot 30 = 540$  for

SSP5-8.5 and  $12 \cdot 30 = 360$  for SSP1-2.6. This is the same procedure as the one performed by Russo et al. (2011).

For each index, the probability distributions relative to different periods are tested to be significantly different between each other with the two-tailed Kolmogorov-Smirnov test (Smirnov, N.V., 1939) with the null hypothesis that the cumulative distribution functions computed for two periods are identical.

Subsequently, statistics of the distributions i.e. Median, standard deviation and 95<sup>th</sup> percentile, are computed to assess their changes in time. It should be remarked that these statistics are computed over data coming from different models. Hence, for instance, an increase of the standard deviation in the far future compared to the reference period indicates a greater disagreement between models and not a greater climate variability in physical terms.

The empirical distribution functions are estimated employing the Kernel Density Estimation (Rosenblatt, M., 1956). It is a nonparametric technique for the estimation of the empirical probability density function. Unlike a histogram, which is the traditional empirical PDF representation, it produces a smooth PDF based on individual locations of all sample data. Therefore, it allows for better visual comparisons of distributions over time and does not suffer from the subjectivity of the binning procedure, which strips data of their position by replacing them with an interval (Węglarczyk, S. 2018). The drawback is that the smoothing may hide some features of the distribution, for instance, high peaks or bi-modality.

Kernel estimate  $\hat{f}(x)$  assigns each  $i$ -th sample data point  $x_i$  a function  $K(x_i, t)$  called a kernel function:

$$\hat{f}(x_i) = \frac{1}{nh} \sum_{i=1}^n K\left(\frac{x - x_i}{h}\right) \quad (13)$$

where parameter  $h$ , called smoothing parameter, governs the amount of smoothing applied to the sample. A compromise between over-smoothing (too high  $h$  value) and under-smoothing (too low  $h$  value) is needed (Węglarczyk, S. 2018). The  $h$  parameter is

empirically determined for each index, by comparing the resulting PDFs with the corresponding histograms (Figure 16).

As a result, the kernel transforms the point location of  $x_i$  into an interval centered in  $x_i$ . Many types of kernel functions exist. Here, the *Gaussian kernel function* is employed, that produces the smoothest estimate:

$$K(t) = \frac{1}{\sqrt{2\pi}} e^{-\frac{t^2}{2}} \quad (14)$$

To sum up, PDFs are produced for each index and each of the three sub-periods. The distributions relative to the future periods are tested to be significantly different from the one of the base period and relevant statistics are computed.

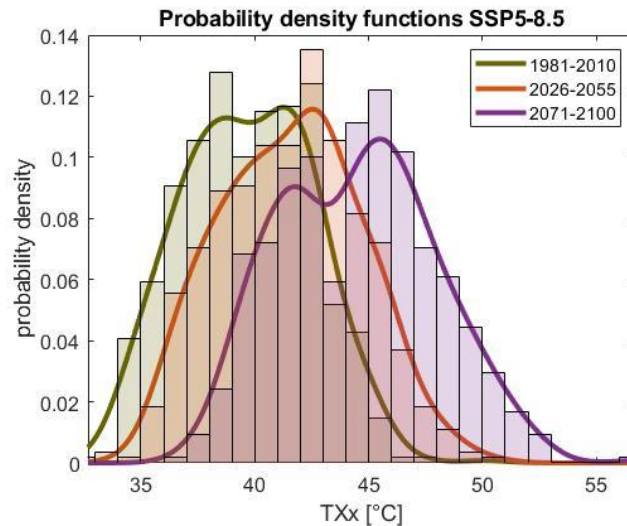


Figure 16: PDFs of the maximum annual temperature ( $TXx$ ) computed by binning values from all the models over the 30-years subperiods, through the Kernel Density Estimator. Histograms are plotted for comparison. The curve allows a better view of the distributions and their evolution over time, but it "abates" some probability peaks.



### 3.4 Correlation between extreme indices and critical events in Beira

The whole province of Sofala in Mozambique, and especially the city of Beira, have experienced numerous disasters in the past, which are linked to extreme precipitation and tropical cyclones, including the cyclone Idai in March 2019, which is the actual trigger for this thesis project. One fundamental question this work aims to answer is the following: is there any connection between the climate extreme indices and these kinds of disasters? If so, how can it be useful in predicting how climate change will affect their frequency?

As just recalled, the present analysis is based on climate extremes that describe “moderate” extreme events with return periods of generally less than one year, and therefore are not directly representative of events with very high return periods that have dramatic impacts on the study area. Therefore, an additional investigation was performed to evaluate if the ETCCDI can provide information about the destructive events that upset the province of Sofala and Beira. In such a manner, through the analysis of standard internationally recognised indices relatively simple to compute, it would be possible to infer on more complex-to-handle weather features such as extreme rainfalls caused by tropical cyclones, that from now on will be simply called “*critical events*”. This term is not meant to indicate a single abrupt physical phenomenon, but also the combination of several phenomena of the same or different nature, connected or consecutive, which result in putting the city of Beira under serious stress in terms of large-scale destruction and loss of human life.

Subsequently, once the correlation pattern is found, a final investigation aims at determining if climate models, through the indices projections, provide a signal of change for future critical frequency of events.

How to put in relation gridded annual indices and this kind of events?

In the analyses described so far, only one grid cell was considered for the computation of the indices. Namely, from each gridded dataset the closest cell to the coordinates of the

city of Beira was extracted. However, the spatial scale of one single grid cell cannot fully represent the *critical events* (Konrad et al., 2002). To obtain reliable results, a larger area is therefore used for this analysis: a  $3^\circ \times 3^\circ$  lon-lat, from  $33^\circ$  to  $36^\circ$  in longitude and from  $-18^\circ$  to  $-21^\circ$  in latitude. Such indices are computed for each model grid cell and following spatially averaged. The resulting time series are more suitable to represent large-scale extreme events.

Figure 17 exhibits an overview of the analysis that is going to be described in this section. Further details are reported in the corresponding results section (4.2).

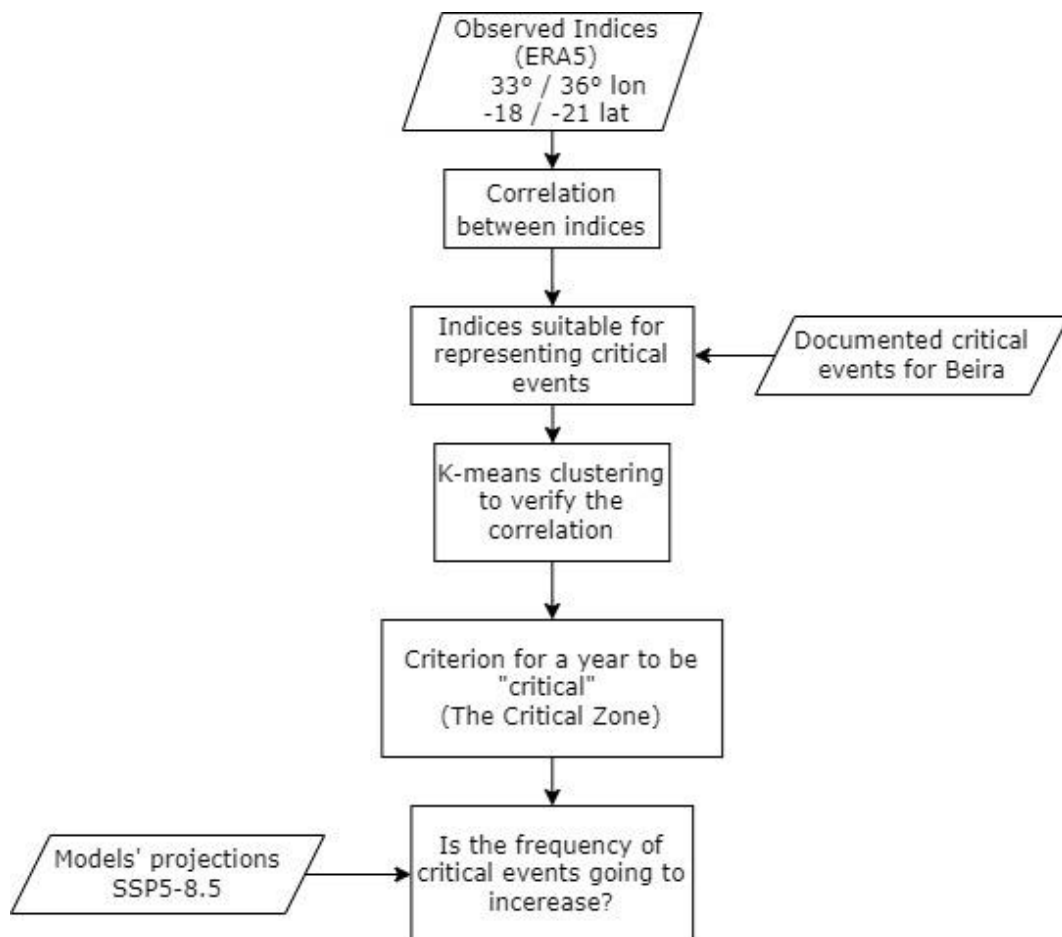


Figure 17: Flow diagram showing the steps of the approach applied in order to infer about critical destructive precipitation events by the analysis of moderate climate extremes indices.

Firstly, the correlation between the indices themselves is analysed. In this way, relationships between the indices are explored and more knowledge is acquired for their use in subsequent analyses. A similar approach as in Seo et al. (2019) is followed, computing the rank correlation coefficient by Spearman (Spearman, C., 1904). The aforementioned statistical measure was chosen since its use is often reported in climate extreme studies (Zhang et al., 2019), and more specifically because of the non-linear relationships between the indices (Pesce et al., 2020) as opposed to the correlation coefficient by Pearson, more suitable for detecting linear relationships.

Secondly, after the most disruptive events for the city of Beira have been identified, visually inspecting the time series of observed indices results in a subset of the indices that are best suited to correlate with the *critical events*. This is done by evaluating the index values in the years in which the critical events occurred: is the index recoding a relatively high value in these years?

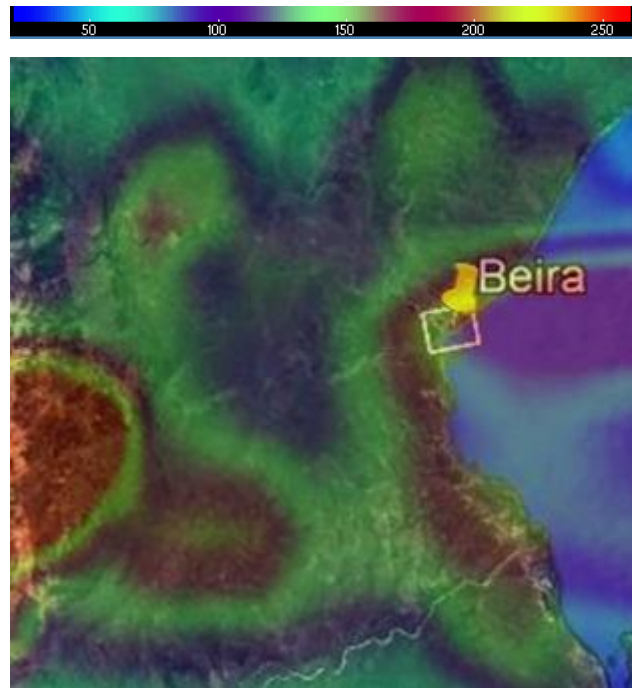


Figure 18: Representation of the values of Rx1day computed starting from reanalysis data, for the year 2019 over the area of interest. This image demonstrates that the index of extreme rainfall contains information about the criticality of that year for Beira, given the high values reported (reddish areas). From this point, an empirical approach described in this paragraph was developed to construct a criterion whereby, starting from indices values, one year is defined as “critical” for Beira.

Thirdly, the correlation between the subset of indices and the *critical events* is assessed through the K-mean clustering algorithm (MacQueen, J., 1967). The algorithm partitions data into  $k$  mutually exclusive clusters based on their attributes. It is an iterative procedure that aims at minimizing the sum of the distances between the centroid and all the points of the cluster. Indeed, ***critical years*** (i.e. years in which one or more *critical events* occurred) can be identified as a part of a cluster of points in the  $n$ -dimensional space where  $n$  is the number of the selected indices. In other words, by putting together all the information coming from the selected indices, the critical years stand out from the rest. As a result, the indices were found to capture the criticality that a year had for Beira. Thereafter, a criterion has been defined for a year to be defined as *critical*. To do that, the ***Critical Zone*** is defined.

An  $n$ -dimensional point, representing one year characterized by  $n$ -index values  $(x_1, x_2 \dots x_n)$ , belongs to the *Critical Zone* if  $x_i \geq c_i \ \forall \ i = 1 \dots n$ , with  $c$  being the vector containing properly defined thresholds.

Thresholds are defined for each index from the values of the critical years. In this way, a criterion is established to determine whether a year characterised by any value of the indices is critical or not for the city of Beira and its surroundings.

Finally, once the correlation between the observed indices and documented critical events is established, it is time to make future considerations. Through model projections of indices values, the frequency of critical events is studied to see how it will change over the century.

## 4.RESULTS

### 4.1 Future Projections

This section presents the results regarding future changes in the indices of climate extremes over Beira. A complete report of future projections of indices is reported in Appendix B. For ease of reading, this section aims at showing only the most relevant results. The indices have been grouped into four categories regarding their interpretation: intensity of extreme temperatures, frequency of extreme temperatures, the intensity of extreme precipitation, and frequency of extreme precipitation. The grouping is only indicative and is a way to provide the results more clearly. The **Mean Trend (MT)**, i.e. trend computed over the multi-model ensemble mean, is the main reference for providing results. Therefore, it will be referred to as simply “trend”. However, in order not to neglect the information deriving by individual models, the percentage of models that detect a significant trend is also indicated. Moreover, as a measure of the spread of the magnitude of the detected trends by different models, the **Trend Variability** is computed, i.e. the standard deviation of the slopes of the models ( $b_i$ ) expressed as a percentage of the *Mean Trend (MT)* (Russo and Sterl, 2011):

$$\text{➤ } \sigma_n = \sigma(b_i) / MT ; \quad (15)$$

A low  $\sigma_n$  indicates a little dispersion around the Mean Trend (i.e. good agreement in the MT value), while high values of  $\sigma_n$  indicates disagreement in the magnitude of the trend across the models. Therefore, it can be interpreted as a measure of the reliability of the *Mean Trend*.

Complementary to the analysis along the entire study period (1961-2100), sub-periods of 30-years have been analysed and compared to each other: the base period (1981-2010), the near future (2026-2055), and the far future (2071-2100). Over these temporal windows, mean absolute differences are computed and represented as box plots showing the models spread, and Probability Density Functions are compared to each other as described in section 3.3.2.

### 4.1.1 Intensity of Extreme Temperatures

The projections regarding temperature extremes are unequivocally consistent with a warming tendency. All the models agree on future warmer extreme temperatures. This is visible in Figure 19, which shows the mean absolute anomalies of temperature intensity indices for both scenarios and future periods. The box plots illustrate the inter-model spread: the middle line represents the multi-model median and the box boundaries represent the upper and lower quartiles.

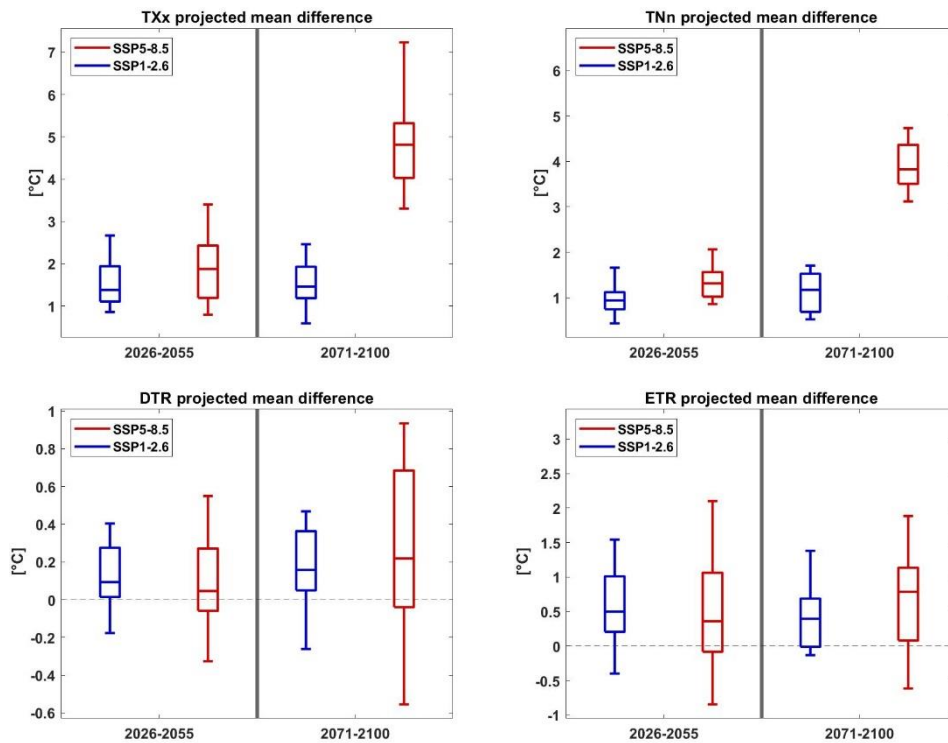


Figure 19: Box plots representing the intermodal variability of the mean absolute anomalies in the near future (2026-2055) and far future (2071-2100) of Temperature Intensity indices compared to the baseline period (1981-2010), for both scenarios.

All the models agree on a significant positive trend for the maximum and minimum annual temperatures (**TXx** and **TNn**) in both scenarios. Regarding SSP5-8.5, **TXx** presents a trend of  $0.48^{\circ}\text{C}/\text{decade}$  while **TNn** is increasing to the lesser extent of  $0.41^{\circ}\text{C}/\text{decade}$ . The same pattern but more attenuated is conserved for SSP1-2.6:  $0.18^{\circ}\text{C}/\text{decade}$  for **TXx** and  $0.16^{\circ}\text{C}/\text{decade}$  for **TNn**. As visible in the following Figure 20 as well as in the above boxplots, by the end of the 21st century, the lower emission scenario predicts a stabilization of the temperature values, while in the higher emission scenario staggering

values are reached. The standard deviation of the trend  $\sigma_n$  is very low for these indices, meaning that there is very good agreement between the models and therefore the results are very much reliable.

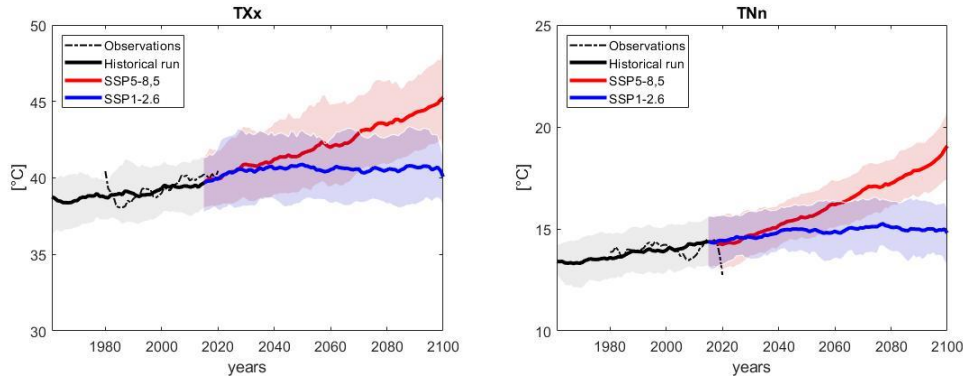


Figure 20: Temporal evolution of maximum of daily maximum temperature (TXx) and minimum of daily minimum temperature (TNn). A moving average of 10 years is applied to the Ensemble Means (thick lines). The shadings represent the areas between the 75<sup>th</sup> and 25<sup>th</sup> percentiles. The black line represents the historical period simulation, the dashed line represents the observed values of the indices, and the red and blue lines are the future scenarios.

By looking at the probability distributions (Figure 21), the change that the maximum and minimum annual temperatures will undergo is evident. The displacement of the mean of the distribution is consistent with the increase of global mean temperature under global warming (around 5°C by the end of the century compared to the baseline period according to SSP5-8.5). In the far future under SSP5-8.5, a bi-modal distribution indicates that the predictions made by the models split into two groups, in which temperature peaks reach different intensities.

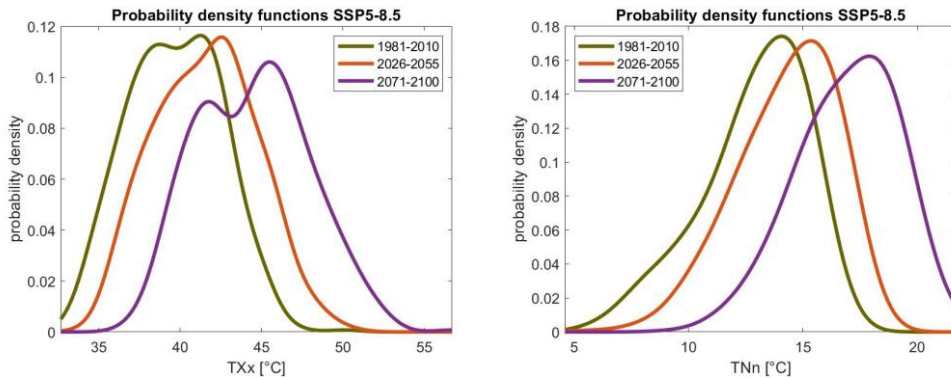


Figure 21: Temporal evolution over the three sub-periods of probability density functions of TXx (left) and TNn (right) in the scenario SSP5-8.

**DTR** shows a positive trend of  $0.02^{\circ}\text{C/decade}$  for SSP5-8.5 and  $0.01^{\circ}\text{C/decade}$  for SSP1-2.6. More than 2/3 of the models detect a significant trend, but the model spread ( $\sigma_n$ ) is very large (in the order of 200%) indicating low agreement around the precise magnitude of the *mean trend*. Overall, the emerging signal indicates that the day-to-night temperature difference is going to increase but at a relatively slow rate. Indeed, less than  $0.3^{\circ}\text{C}$  increase over one century in the average daily thermal excursion does not represent a dramatic change.

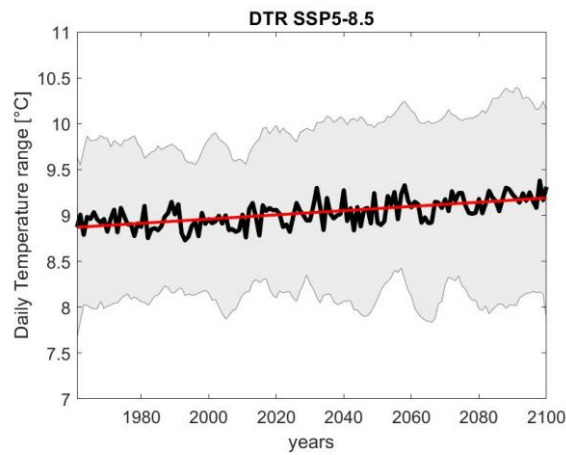


Figure 22: Trend detected for the Daily Temperature Range over the scenario SSP5-8.5. Thick line is the Ensemble mean. The shading represents the area between the 95<sup>th</sup> and 5<sup>th</sup> percentile

The extreme temperature range **ETR** shows a slow positive rate of change and high uncertainty as well. In both scenarios, a positive trend emerges, but only in the higher emission scenario this is statistically significant and its value is  $0.07^{\circ}\text{C/decade}$ . Only half of the models agree on the statistical significance of a trend and the trend spread is even in this case very high (159%). The slightly positive signal is consistent with the difference in the trend magnitude between *TXx* and *TNn* being *ETR* the annual difference between these indices. Table 6 summarises the results of the trend analysis described so far.



Index	unit	Scenario	Mean Trend [unit/year]	% of significant trends	$\sigma_n$ [%]	Slope Range [unit/year]	
TXx	°C	SSP5-8.5	0.048	100.0	26.632	0.030	0.076
		SSP1-2.6	0.018	100.0	37.483	0.008	0.030
Tn <sub>n</sub>	°C	SSP5-8.5	0.041	100.0	19.398	0.031	0.066
		SSP1-2.6	0.016	100.0	25.166	0.010	0.022
DTR	°C	SSP5-8.5	0.002	77.8	211.437	-0.008	0.010
		SSP1-2.6	0.001	75.0	225.920	-0.004	0.007
ETR	°C	SSP5-8.5	0.007	50.0	159.213	-0.009	0.035
		SSP1-2.6	0.001	75.0	225.920	-0.004	0.007

Table 6: Sum up of Trend Analysis results for Temperature Intensity indices. Yellow coloured cells in the Mean Trend column indicate a statistically significant trend.

#### 4.1.2 Frequency of Temperature Extremes

Percentile-based temperature indices - Tn10p, Tx10p, Tn90p, Tx90p – are the ones that present the strongest positive signal with the lowest uncertainty. All the models agree on a significant positive change. The following Figure 23 provides an overview of the average variations that these indices, as well as the heatwave index – wsd<sub>i</sub> – will undergo in the near and far future.

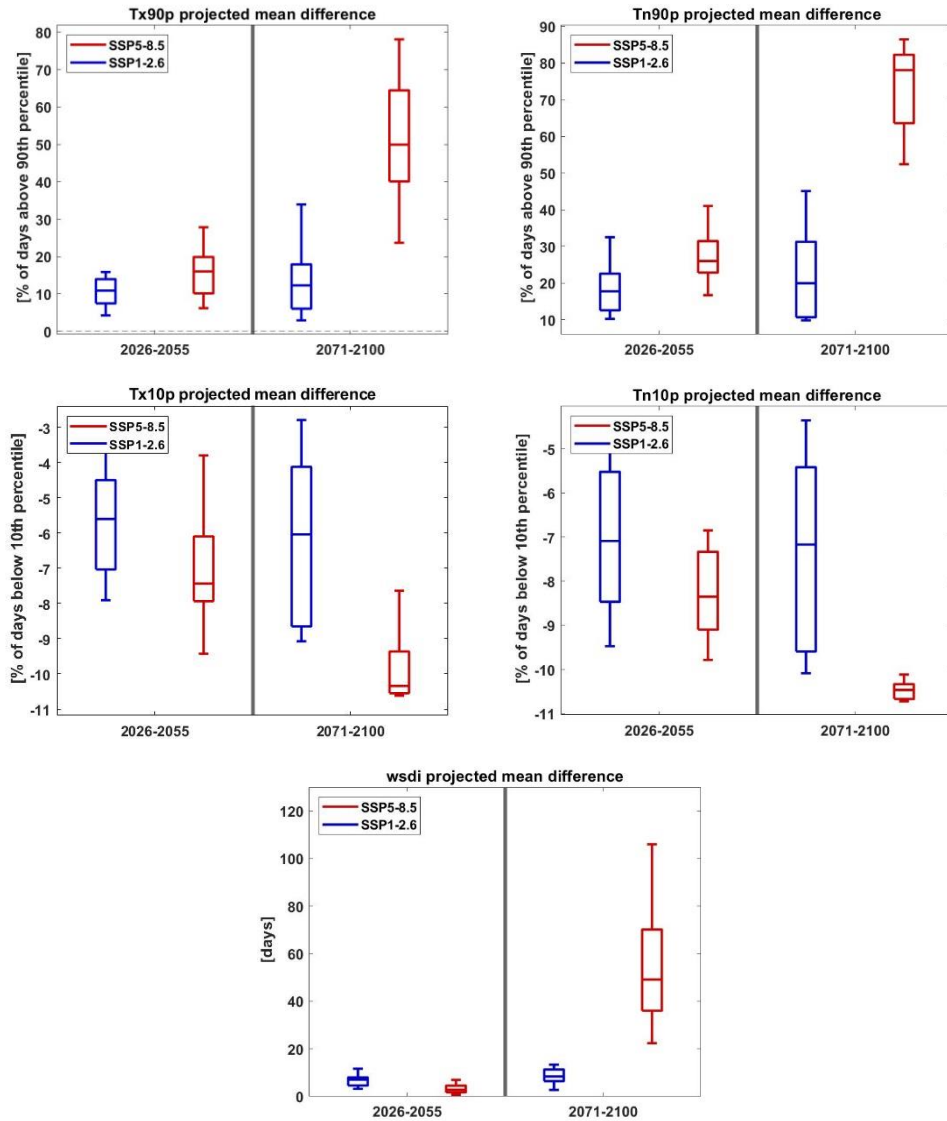


Figure 23: Box plots representing the intermodal variability of the mean absolute anomalies in the near future (2026-2055) and far future (2071-2100) of Temperature frequency indices compared to the baseline period (1981-2010), for both scenarios.

Warm days (Tx90p) and warm nights (Tn90p) are bound to increase. The trend for **Tn90p** is 7.29%/decade in SSP5-8.5 and 2.55%/decade in SSP1-2.6. This is approximately an increase of 26 and 9 warm nights per decade respectively, with  $\sigma_n$  values of 16.5% and 47%. **Tx90p** presents a positive trend of 4.89%/decade in SSP5-8.5 and 1.47%/decade in SSP1-2.6. This is approximately an increase of 18 and 5 warm days per decade

respectively, with  $\sigma_n$  equal to 33% and 57% (very good agreement between models). In conclusion, results indicate that warm nights are increasing faster than warm days.

Figure 24 illustrates the difference between the two future scenarios. Over the SSP1-2.6, the warm nights and cold nights occurrences tend to stabilise after mid-century. On the contrary, over the SSP5-8., they keep increasing until they reach the point where almost all the days in a year the thresholds are overcome. Therefore, the temperature regime is projected to change so that what was defined in the reference period as a heat extreme will become the norm. This is a symptom of a radical shift in the temperature distribution and indicates that the definition of temperature extremes will not be the same in the future. Indeed, by looking at the  $Tn90$  graph, is visible that the median by the end of the century approaches 100%. A fixed threshold being exceeded as a normal occurrence leads to the saturation of the probability increase and may result in an underestimation of the trend.

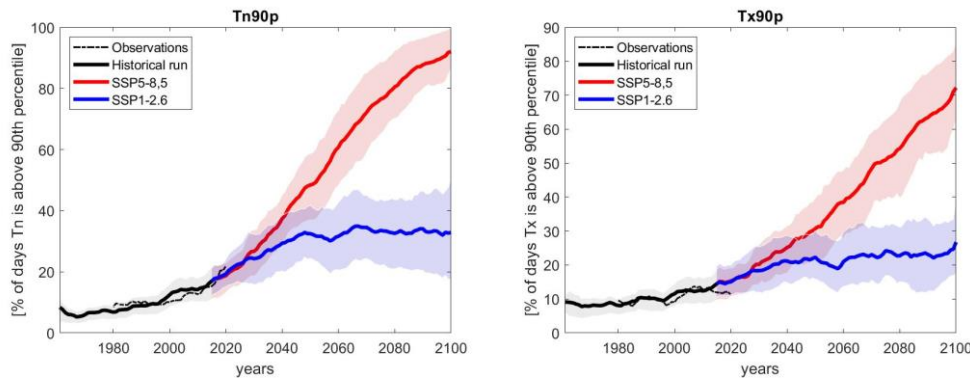


Figure 24: Temporal evolution of warm nights ( $Tn90p$ ) and warm days ( $Tx90p$ ). A moving average of 10 years is applied to the Ensemble Means (thick lines). The shadings represent the areas between the 75<sup>th</sup> and 25<sup>th</sup> percentiles. The black line represents the historical period simulation, the dashed line represents the observed values of the indices, and the red and blue lines are the future scenarios.

Figure 25 further shows the radical change that the distributions of frequency of warm days and night would undergo under the two scenarios. The baseline period distribution is also compared to the ERA5 distribution. The difference between the scenarios is once again very evident by looking at the far-future distribution, which under SSP1-2.6 remains similar to the near-future distribution while under SSP5-8.5 completely diverges.

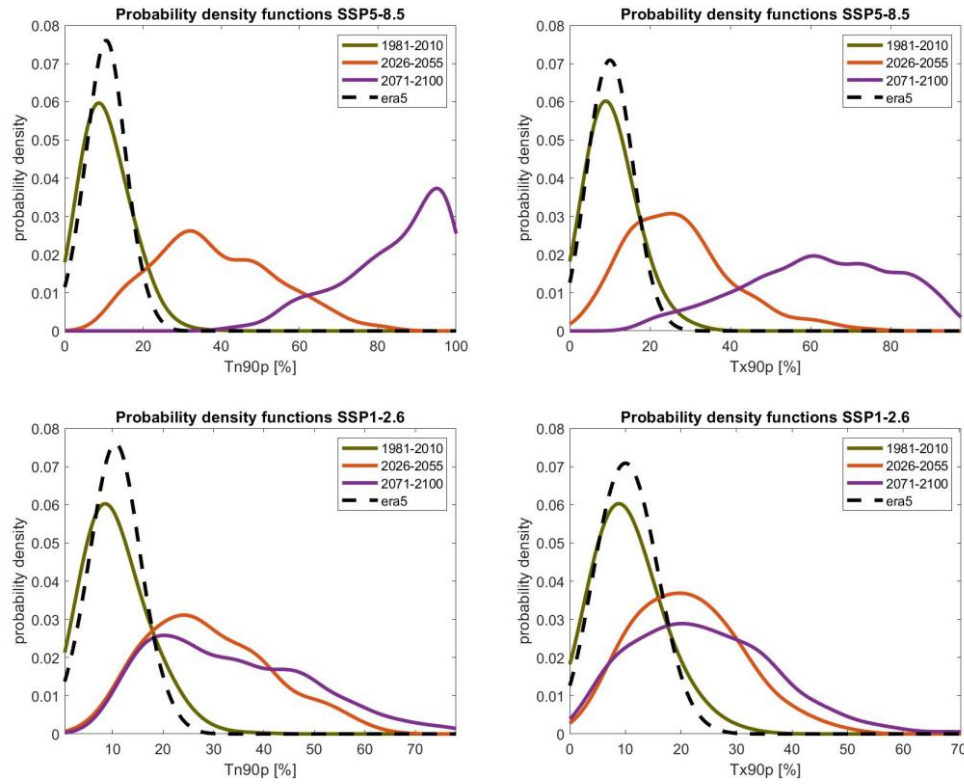


Figure 25: PDFs temporal evolution and comparison with ERA5, regarding  $Tn90p$  and  $Tx90p$  under SSP5-8.5 (up) and SSP1-2.6 (bottom).

On the other hand, as can be expected, cold days ( $Tx10p$ ) and cold nights ( $Tn10p$ ) are bound to decrease. The *trend* recorded for  $Tn10p$  amounts to  $-1,27\%$  per decade in the higher radiative forcing scenario and  $0.97\%/decade$  in the lower higher radiative forcing scenario. This is approximately a reduction of 4.5 and 3.5 cold nights per decade respectively, with  $\sigma_n$  equal to 6.9% and 17% (very good model agreement). The *trend* detected for  $Tx10p$  is  $-1.12\%/decade$  under SSP5-8.5 and  $0.74\%/decade$  under SSP1-2.6. This is approximately a reduction of 4 and 3 cold days per decade respectively, with  $\sigma_n$  values of 7% and 17% (very good model agreement). Therefore, cold nights are projected to decrease faster than cold days.

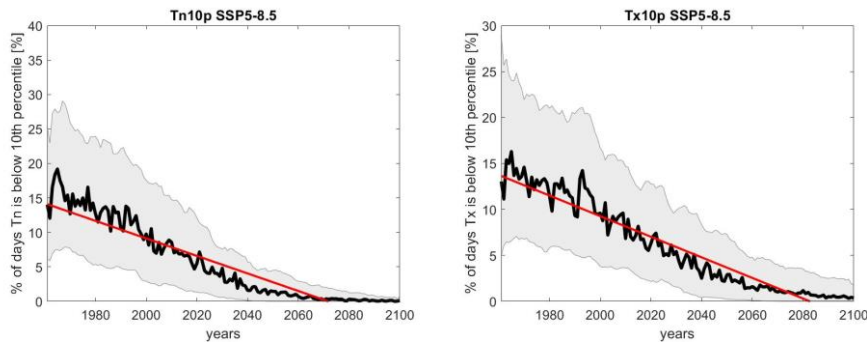


Figure 26: Temporal evolution of Tn10p and Tx10p with relative negative trends. The thick line is the ensemble mean while shading represents the area between the 5<sup>th</sup> and 95<sup>th</sup> percentile.

The above Figure 26 shows the temporal evolution of the two indices under SSP5-8.5. The Ensemble Mean converges to the 0-value because following the half of the century none of the days in one year are projected to have a minimum or maximum temperature below the 10<sup>th</sup> percentile. Once more, the definition of cold extreme (10<sup>th</sup> percentile) made on the baseline period (1981-2010) is not suitable for the future because of the change in the temperature regime. As a consequence, the computed trend is lower than it would be with a more “updated” extreme definition. In Figure 27, trends are computed over the three sub-periods (baseline, near future, far future) to visualize how they change because of the obsolete definition of the extreme. The trend computed over the baseline period is not affected by it and is therefore reported in the Table 7 below.

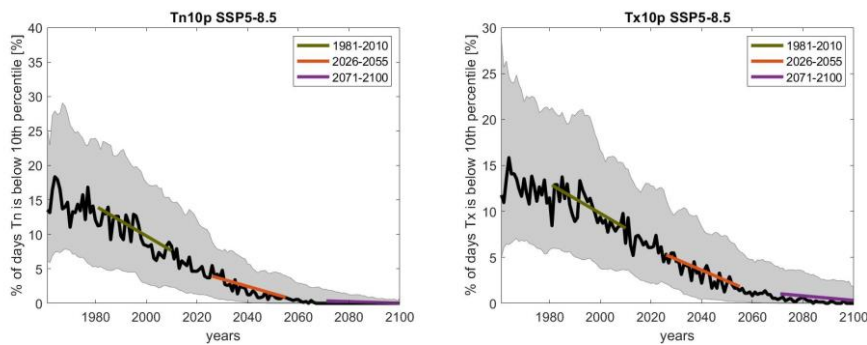


Figure 27: Trend computed over sub-periods for Tn10p and Tx10p. Is evident the effect of trend "flattening" as a result of the obsolete threshold definition

Index & Scenario	Trend over the baseline period [% of days/decade]
Tn10p SSP5-8.5	-2.16
Tn10p SSP1-2.6	-1.78
Tx10p SSP5-8.5	-1.61
Tx10p SSP1-2.6	-1.15

Table 7: Trend values for Tn10p and Tx10p under SSP5-8.5 and SSP1-2.6 considering only the baseline period, not affected by the "flattening effect"

The Warm Spell Duration Index, **wsgi**, is also projected to increase in both scenarios although in different ways. In the low emission scenario, the positive trend value is  $0.88 \text{ days/decade}$  with a good agreement between models ( $\sigma_n = 24\%$ ). In the high emission scenario, the trend value is  $2.74 \text{ days/decade}$  with higher disagreement between the models ( $\sigma_n = 98\%$ ). However, as clearly visible in Figure 28 below, after mid-century in the high-emission scenario index values rise monotonically year after year reaching very high values by the end of the century. This behaviour was also evident by looking at the boxplots anomalies (Figure 23).

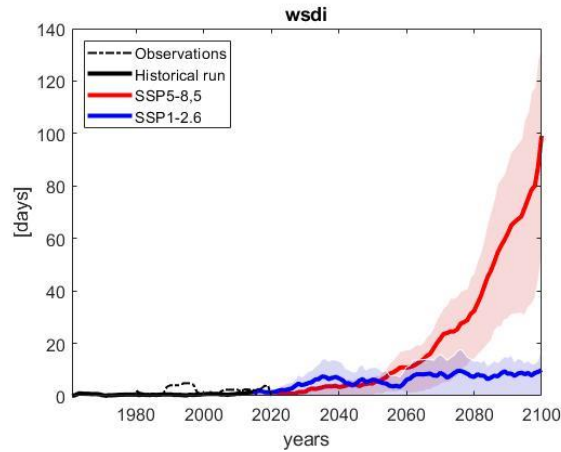


Figure 28: Temporal evolution of warm spell duration index (wsgi) under the two future scenarios. A moving average of 10 years is applied to the Ensemble Means (thick lines). The shadings represent the areas between the 75<sup>th</sup> and 25<sup>th</sup> percentiles. The black line represents the historical period simulation, the dashed line represents the observed values of the indices, and the red and blue lines are the future scenarios.

Therefore, it is of interest to estimate the trend only in the last portion of the time series, where the models project this steep increase. The *trend* value in the far future (2071-2100) is  $26 \text{ days/decade}$ , which is surprisingly high. After the mid-century according to the worst-case scenario, every year on average an increase of 2.6 days of heat waves is projected. These very high values can be explained by remembering the definition that has been given to the ‘heat wave’: at least 6 days consecutive days with a maximum daily temperature greater than 90<sup>th</sup> percentile (computed on 1981-2010). The projected shift in

the temperature regime results, as for the other temperature frequency indices, in what is termed extreme in the base period being the norm in the future in this scenario. In particular, by the last quarter of the century, the ‘extreme event’ will occur so commonly as to make almost one-third of the year to be classified as ‘heatwave period’.

The following Table 29 summarises the results of the trend analysis for indices of frequency of extreme temperature.

Index	unit	Scenario	Mean Trend [unit/year]	% of significant trends	$\sigma_n$ [%]	Slope Range [unit/year]	
wsdi	days	SSP5-8.5	0.274	100.0	98.646	0.000	1.176
		SSP1-2.6	0.088	91.7	24.425	0.000	0.075
Tn10p	% of days	SSP5-8.5	-0.127	100.0	6.969	-0.117	-0.081
		SSP1-2.6	-0.097	100.0	17.000	-0.111	-0.063
Tx10p	% of days	SSP5-8.5	-0.112	100.0	9.346	-0.112	-0.076
		SSP1-2.6	-0.074	100.0	32.841	-0.106	-0.033
Tn90p	% of days	SSP5-8.5	0.729	100.0	15.569	0.493	0.860
		SSP1-2.6	0.266	100.0	47.561	0.134	0.494
Tx90p	% of days	SSP5-8.5	0.489	100.0	33.119	0.201	0.768
		SSP1-2.6	0.147	91.7	57.432	0.031	0.314

Table 8: Sum up of Trend Analysis results for Temperature frequency indices. Yellow coloured cells in the Mean Trend column indicate a statistically significant trend.

### 4.1.3 Intensity of Precipitation Extremes

Indices of precipitation extremes do not show such a clear direction of change. Indices of precipitation intensity show the weakest change over time and low agreement between the predictions made by the models.

This is visible in the projected absolute differences in the following Figure 30. Here, the high variability between model predictions is demonstrated by the fact that box plots cross the zero-line, meaning that many models project an opposite sign of change. However, by looking at the median of the models (the thick middle line in the boxplot), especially for SSP5-8.5, an increasing signal emerges for the indices concerning short-term extreme

precipitation (Rx1day, Rx5day, sdii) and a decreasing signal emerges for the indices concerning cumulative annual precipitation sum (PRCPTOT, R95p). More details are provided through the trend and the probability density functions analysis.

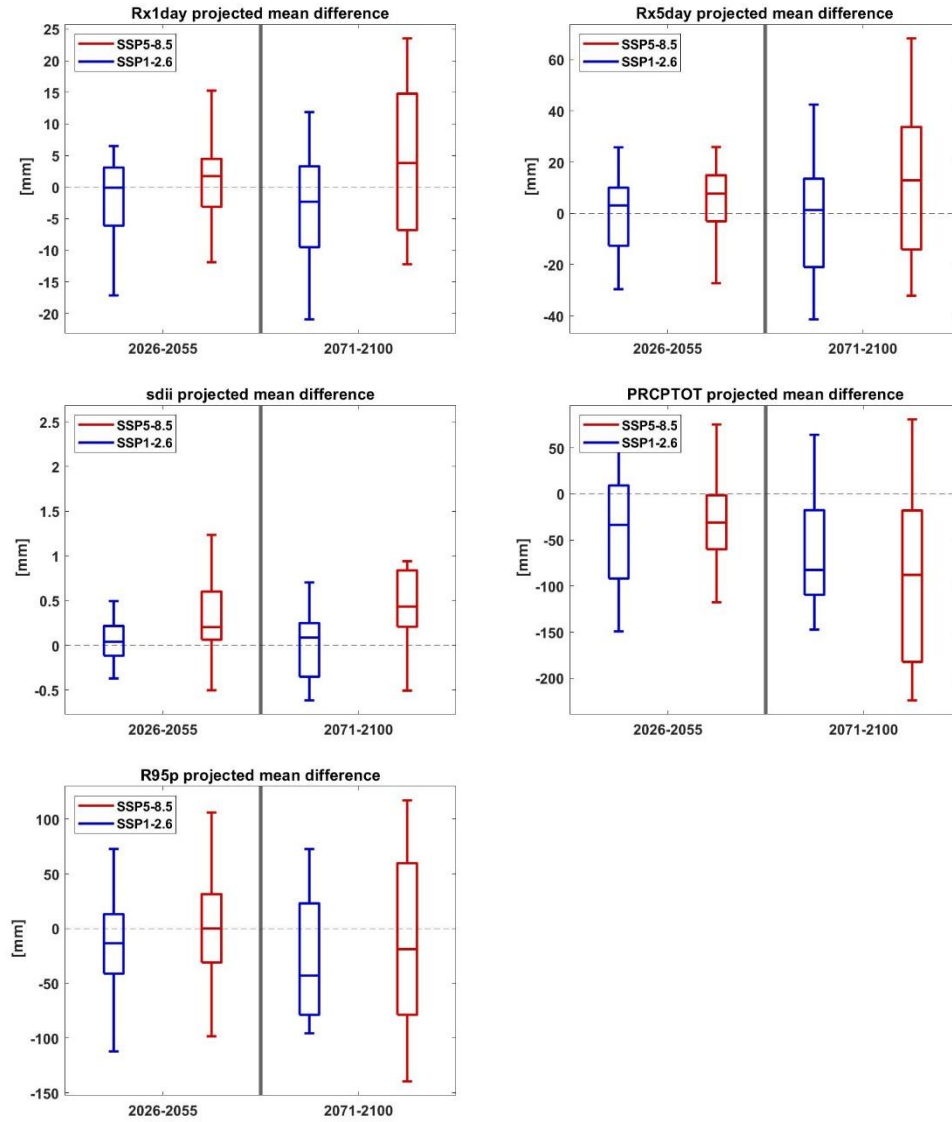


Figure 29: Box plots representing the intermodal variability of the mean absolute anomalies in the near future (2026-2055) and far future (2071-2100) of Precipitation intensity indices compared to the baseline period (1981-2010), for both scenarios.

**Rx1day** and **Rx5day** show positive trends under the SSP5-8.5 scenario respectively of  $0.49\text{mm/decade}$  and  $1.13\text{mm/decade}$  with the trend variability of 142% and 156%. Only



one-third of models detect a significant trend in this scenario for these indices. Besides, under the SSP1-2.6, no significant *trend* is detected. Probability distributions over the three sub-periods are not significantly different from each other in either scenario. However, the increase in the 95<sup>th</sup> percentile under SSP5-8.5 is remarkable. It increases by *17mm* for Rx1day and *54mm* for Rx5day over 2071-2100 compared to 1981-2010. The most extreme rainy events are projected to intensify more than the moderate extreme events.

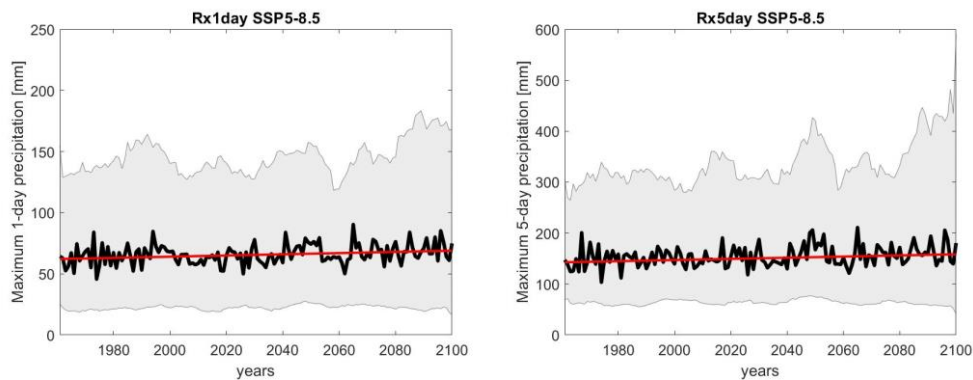


Figure 30: Positive trends detected for Rx1day and Rx5day under SSP5-8.5

For the Simple Daily Intensity Index (*sdi*) a positive *trend* of *0.06mm/decade* is recorded under SSP5-8.5. Fifty percent of the models agree on a significant trend and the trend variability is high, 104%. Concerning the PDFs, a significant change compared to the baseline period is recorded only in the far future, with a slight increase of the median (from 7.7 to 8.2 mm) in standard deviation (from 2.8 to 3.5 mm) and the 95<sup>th</sup> percentile (from 13.8 to 15.8 mm). The slight shift is visible in Figure 32 together with the distribution of observed data. The difference between the projected index and the observation is larger than the evolution of the projected indices over time. This gives less confidence in the interpretation of future changes. Under SSP1-2.6 instead, no significant trend is present.

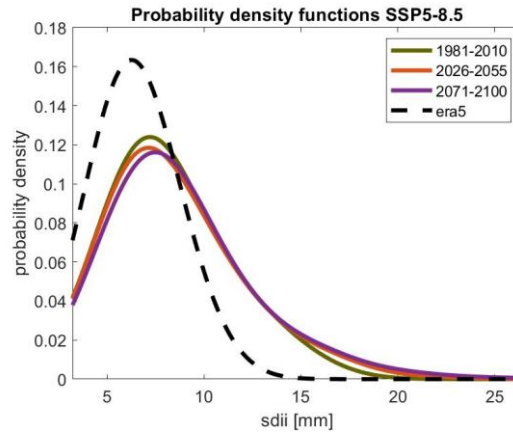


Figure 31: PDFs evolution under SSP5-8.5 and the observed PDF in the baseline period (dashed line)

A decreasing tendency is to be expected for the total annual precipitation **PRCPTOT**. The *trend* is equal to  $-8.16\text{mm/decade}$  under SSP5-8.5 and  $-5.09\text{mm/decade}$  under SSP1-2.6 with *trend variability* of 122% and 161%. The PDFs show a significant decrease in the median from 929 mm (1981-2010) to 827 mm under SSP5-8.5 and 841mm under SSP1-2.6 (2071-2100).

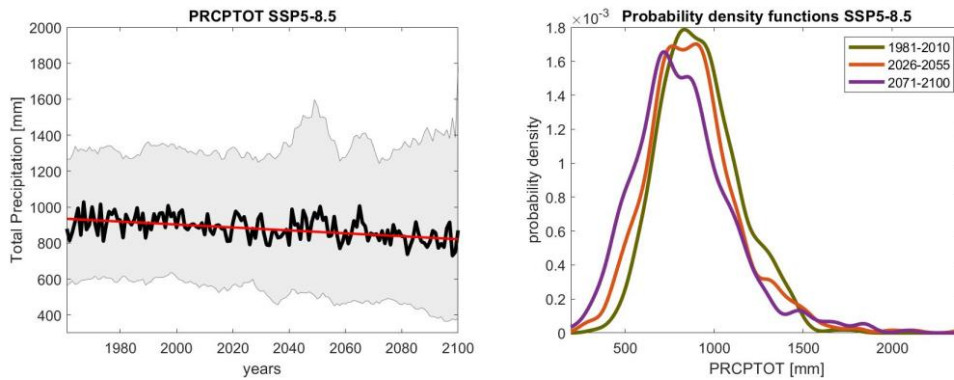


Figure 32: Trend (left) and PDF (right) evolution of PRCPTOT under SSP5-8.5.

The very wet days, **R95p**, show a decreasing *trend* only for SSP1-2.6, equal to  $-1.52\text{mm/decade}$ , while no significant trend is detected under SSP5-8.5. This is unusual since normally the higher radiative forcing scenario is the one with a more robust trend. Nonetheless, this “role-reversal” is due to the very high disagreement between the models, as visible in the absolute anomaly in the above Figure 30 (boxplots). Therefore,

the predictions concerning R95p turned out to be unreliable due to very high inter-model variability.

Table 9 summarises the results of the trend analysis for indices of intensity of extreme precipitation.











Index	unit	Scenario	Mean Trend [unit/year]	% of significant trends	σn [%]	Slope Range [unit/year]	
sdii	mm	SSP5-8.5	0.006	 50.0	104.236	-0.004	0.024
		SSP1-2.6	0.001	 16.7	445.257	-0.008	0.010
Rx1day	mm	SSP5-8.5	0.049	 33.3	142.867	-0.082	0.196
		SSP1-2.6	-0.030	 8.3	164.693	-0.111	0.034
Rx5day	mm	SSP5-8.5	0.113	 38.9	156.017	-0.300	0.333
		SSP1-2.6	0.004	 25.0	4464.567	-0.296	0.185
R95p	mm	SSP5-8.5	0.001	 27.8	118799.580	-1.538	1.488
		SSP1-2.6	-0.152	 25.0	456.966	-1.121	0.954
PRCPTOT	mm	SSP5-8.5	-0.816	 55.6	122.850	-2.172	1.398
		SSP1-2.6	-0.509	 58.3	161.195	-1.503	0.663

Table 9: Sum up of Trend Analysis results for Precipitation intensity indices. Blue colored cells in the Mean Trend column indicate a statistically significant trend.

#### 4.1.4 Frequency of Precipitation Extremes

The analysis of the frequency of precipitation extremes led interesting patterns of change to emerge. From the following Figure 34 may be noticed that the models agree more on the sign of change compared to the precipitation intensity indices.

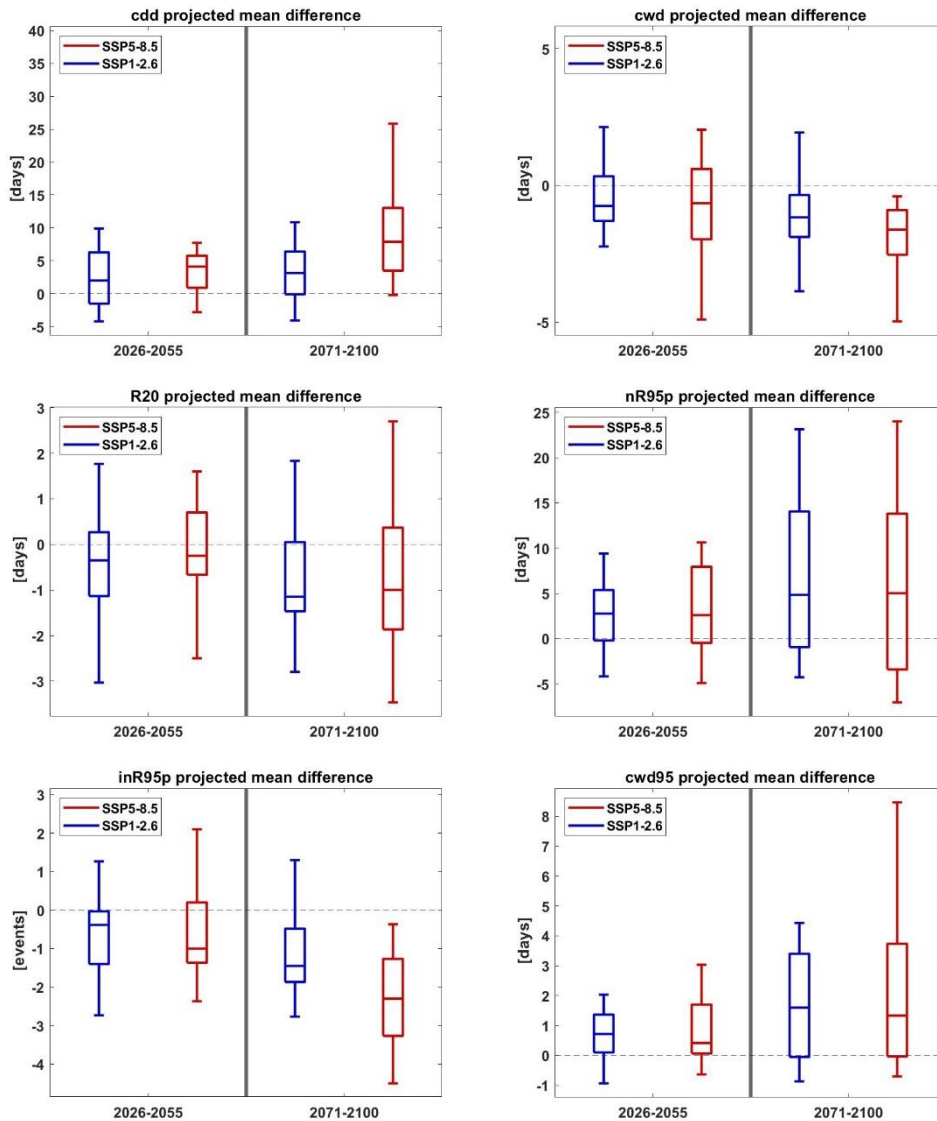


Figure 33: Box plots representing the intermodal variability of the mean absolute anomalies in the near future (2026-2055) and far future (2071-2100) of Precipitation frequency indices compared to the baseline period (1981-2010), for both scenarios.

Consecutive Dry Days (*cdd*) are projected to increase over Beira in both scenarios. A positive trend is detected, consisting of *1.15 days/decade* (78% of models report a significant trend,  $\sigma_n = 78\%$ ) under SSP5-8.5 and *0.62 days/decade* (33% of models report a significant trend,  $\sigma_n = 79.5\%$ ) under SSP1-2.6. The PDF analysis results in a consistent upward shift of the median, the standard deviation, and the upper tail of the distribution, which is statistically significant only in SSP5-8.5 (Figure 35).

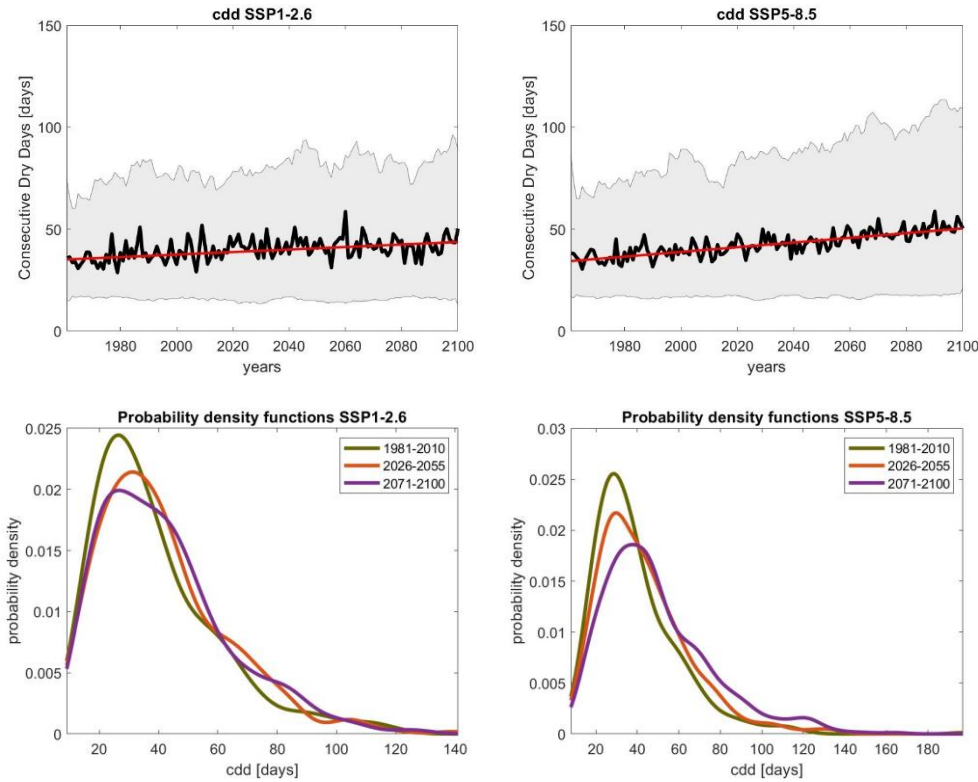


Figure 34: Consecutive dry days. Up: time series and trends for both scenarios. Shading indicates the area between the 95<sup>th</sup> and 5<sup>th</sup> percentile. Bottom: evolution of the pdf over the three reference periods under the two scenarios.

Consecutive Wet Days (*cwd*) report a trend of *-0.12 days/decade* (27% of models detect a significant trend,  $\sigma_n = 174\%$ ) under SSP5-8.5, while under SSP1-2.6 no significant trend is detected (*none of the models detects a significant trend*). Therefore, the decreasing signal about this index is very fragile. A decreasing of the median and the 95<sup>th</sup> percentile of the PDF is recorded, but also in this case the magnitude of change is very low.

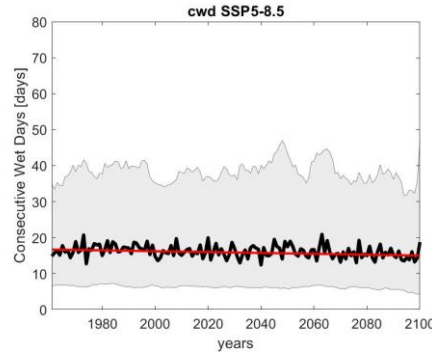


Figure 35: Time series of Consecutive wet days and the detected trend. Shading indicates the area between the 95<sup>th</sup> and 5<sup>th</sup> percentile. Thick line represents the ensemble mean.

The number of Heavy Precipitation days, **R20**, do not show any statistically significant change in both scenarios.

On the contrary, the number of very wet days, **nR95p**, show an evident increasing trend with a very similar magnitude for both scenarios: *0.68days/decade (83% of models report a significant trend,  $\sigma_n = 150\%$ )* under SSP5-8.5 and *0.67 days/decade (67% of models report a significant trend,  $\sigma_n = 120\%$ )* under SSP1-2.6. Figure 36 below shows the trend and the PDF evolution under SSP5-8.5. The increased probability of the right tail of the distribution is evident, the 95<sup>th</sup> percentile increases from 34 days in the base period to 54 days in the far-future.

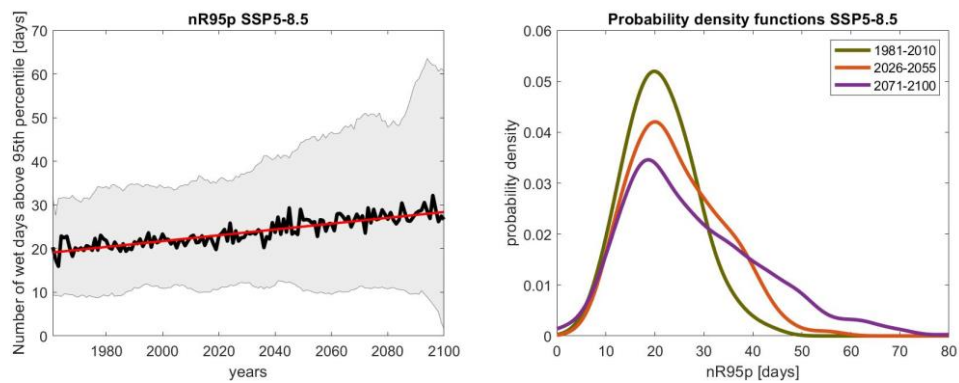


Figure 36: nR95p time series and trend under SSP5-8.5. Shading indicates the area between the 95<sup>th</sup> and 5<sup>th</sup> percentile (left). Thick line represents the ensemble mean. Evolution of the PDFs over the three reference periods under SSP5-8.5.

The number of independent extreme precipitation events, *inR95p*, show a negative trend of  $-0.21$  events/decade SSP5-8.5 (94% of models report a significant trend,  $\sigma_n = 106\%$ ) and  $-0.13$  independent events/decade under SSP1-2.6 (92% of models report a significant trend,  $\sigma_n = 117\%$ ). Therefore, the analysis reveals a decreasing frequency of independent extreme events for both scenarios.

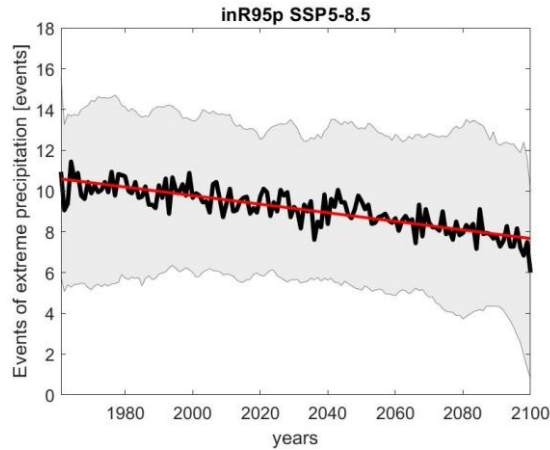


Figure 37: *inR95p* time series and trend under SSP5-8.5. Shading indicates the area between the 95th and 5th percentile (left). The thick line represents the ensemble mean.

Finally, the maximum number of consecutive extreme precipitation events, *cwd95*, is simulated to increase for both scenarios:  $0.21$  events/decade SSP5-8.5 (78% of models report a significant trend,  $\sigma_n = 111\%$ ) and  $0.16$  independent events/decade under SSP1-2.6 (98% of models report a significant trend,  $\sigma_n = 117\%$ ). The major change regarding the evolution of the PDFs is the increase of the 95<sup>th</sup> percentile: from 7 days to 11 days under SSP1-2.6 and 15 days under SSP5-8.5.

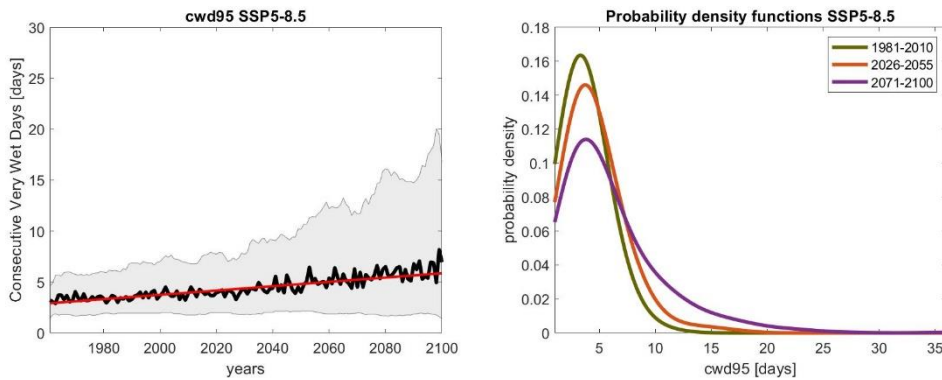


Figure 38: *cwd95* time series and trend under SSP5-8.5. Shading indicates the area between the 95th and 5th percentile (left). Evolution of the PDFs over the three reference periods under SSP5-8.5.

Table 10 summarises the results of the trend analysis for indices of frequency of extreme precipitation.

Index	unit	Scenario	Mean Trend [unit/year]	% of significant trends	$\sigma_n$ [%]	Slope Range [unit/year]	
cdd	days	SSP5-8.5	0.115	77.8	77.916	0.000	0.347
		SSP1-2.6	0.062	33.3	79.560	0.000	0.157
cwd	days	SSP5-8.5	-0.012	27.8	174.325	-0.042	0.045
		SSP1-2.6	-0.006	0.0	159.048	-0.027	0.010
cwd95	days	SSP5-8.5	0.021	77.8	111.558	0.000	0.066
		SSP1-2.6	0.016	75.0	98.637	0.000	0.040
R20	days	SSP5-8.5	-0.003	38.9	477.353	-0.031	0.036
		SSP1-2.6	-0.004	41.7	340.518	-0.026	0.022
nR95p	days	SSP5-8.5	0.067	83.3	149.778	-0.080	0.234
		SSP1-2.6	0.068	66.7	120.143	-0.062	0.227
inR95p	events	SSP5-8.5	-0.021	94.4	106.585	-0.045	0.039
		SSP1-2.6	-0.013	91.7	117.352	-0.031	0.016

Table 10: Sum up of Trend Analysis results for Precipitation frequency indices. Blue coloured cells in the Mean Trend column indicate a statistically significant trend.

#### 4.1.5 Summary

The analysis of the indices has revealed a picture of future climate extremes in the area of the Beira city according to two future scenarios. Figure 39 summarises the projected changes by the end of the century on Beira, compared to the base period. The boxplots, showing the inter-model variability, are drawn on the standardised anomalies of the indices *i.e. the absolute anomaly divided by the standard deviation in the baseline period*. Indeed, from Figure 39 the different impacts that the two scenarios have on the extremes may be captured. As far as temperature extremes are concerned, SSP5-8.5 leads to warmer extreme conditions than SSP1-2.6. In particular, the standardised anomaly of wsd<sub>i</sub> “blasts” by the end of the century, to the point of having a different scale of values from the other indices, and therefore having to be represented in a different graph. For precipitation extremes, the high emissions scenario leads to a general emergence of a signal of change by the end of the century, despite greater model variability than SSP1-2.6.



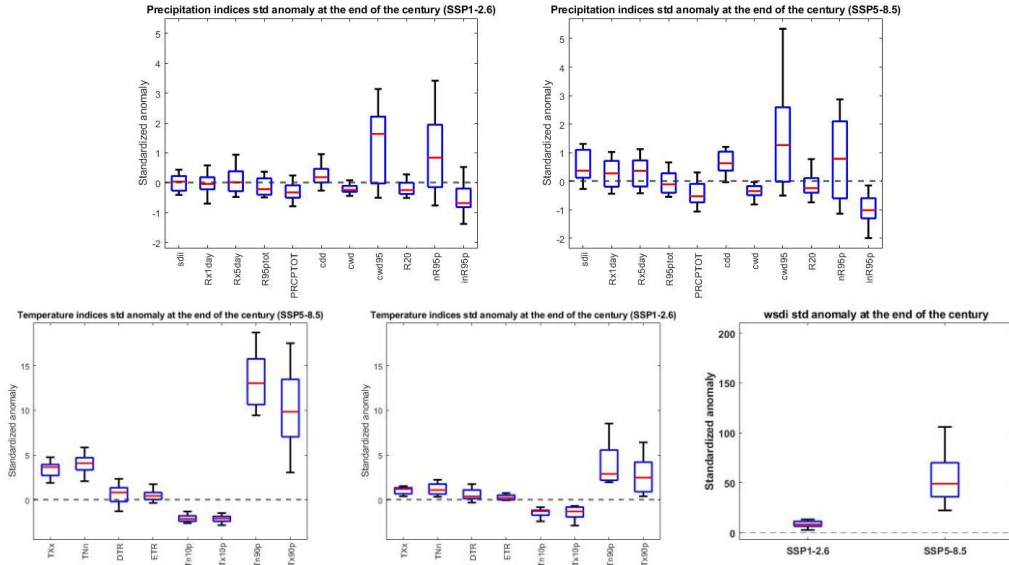


Figure 39: Box plots of the 20 indices showing the standardised anomaly at the end of the century 2071-2100, compared to the baseline period 1981-2010. wsdI is represented in a different box because its values are out of scale compared to the others, due to the very large increasing at the end of the century, as described in 4.1.1

## 4.2 Correlation between extreme indices and critical events in Beira

This section presents the relationship between the indices of extremes and the destructive events that upset Beira. The aim is to suggest an empirical methodology to use the indices of extremes as an indicator of critical destructive events with high impact for the city of Beira. More in particular, a combination of the indices is used to highlight a space of phases that defines one year as "critical", i.e. one year in which one or more destructive events occurred.

### 4.2.1 Indices cross-correlation

As described in the methodology, the first step was to describe the correlation between the indices themselves through the correlation coefficient by Sparkman. Figure 40 shows the correlation tables in which correlation values are replaced with a colour scale. The first table displays the cross-correlation of indices computed starting from observations (ERA5), while the second table (below) displays the cross-correlation of indices computed starting from model simulations. Here, the “mean correlation” is displayed, meaning that each value within a cell is the average over the eighteen correlation values from the models. The almost perfect equivalence of the two tables confirms the reliability of models in simulating the indices.

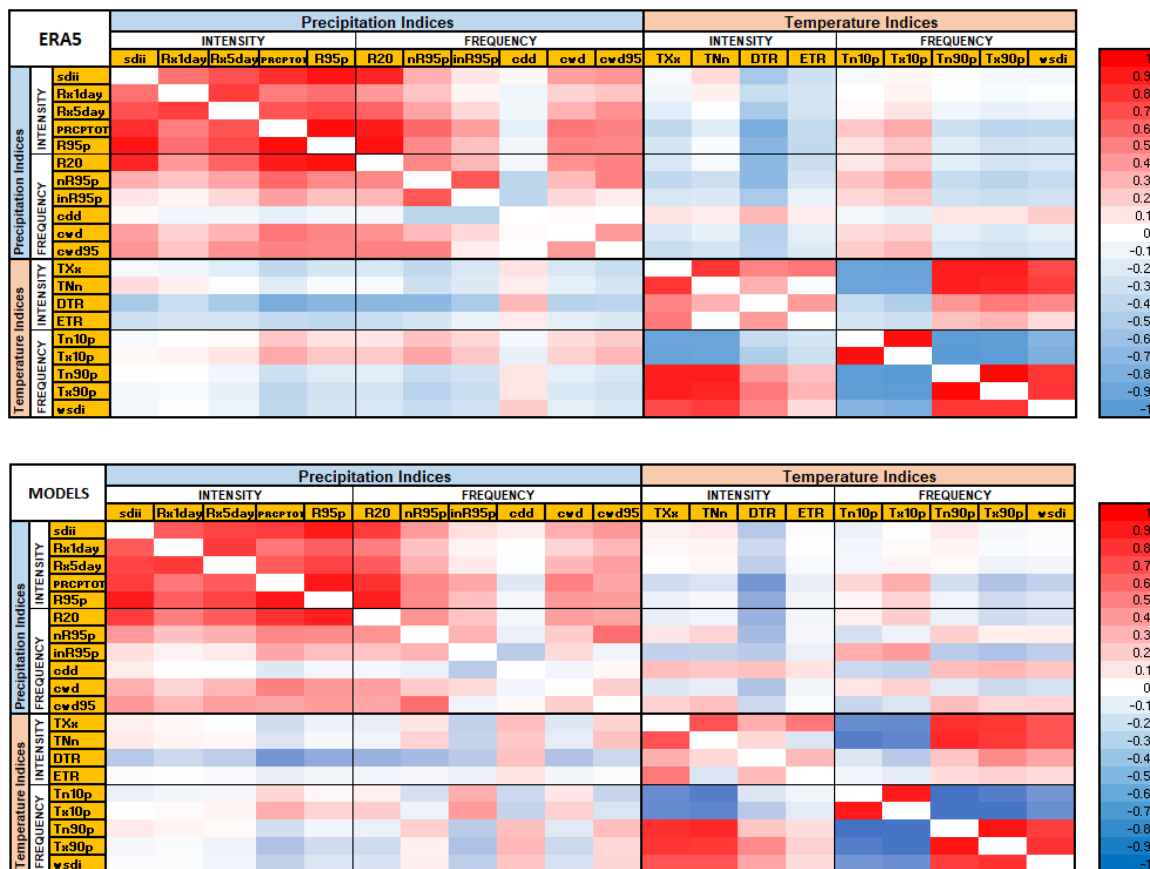


Figure 40: Correlation Tables. The colours scales with values of the non-dimensional Spearman's correlation coefficient (that varies between -1 and 1). Above, the correlation table of observed indices (ERA5). Below, the correlation table of simulated indices (mean value over the 18 models' correlations).

Several interesting pieces of information emerge from the preliminary correlation analysis.

Firstly, there is a strong correlation between the indices concerning the intensity of precipitation (upper left quadrant). On the contrary, low correlation values are recorded between the frequency precipitation indices. Moreover, by looking at the correlation between intensity and frequency precipitation indices, the situation appears to be “faded”. Only the Number of Heavy precipitation days (R20), show a high correlation in particular with the intensity index (sdii), the total precipitation (PRCTOT), and the total precipitation above 95<sup>th</sup> percentile (R95p).

A strong correlation is also recorded between temperature frequency indices (lower right quadrant) and between temperature frequency indices and temperature intensity indices. This means that, for instance, a high value of annual maximum (TXx) or minimum (TNn) temperature corresponds on average a high duration value of heat waves (wsdi). This is not surprising, but not obvious either.

The correlation between precipitation and temperature indices is very low, as expected. The negative correlation between Daily Temperature Range (DTR) and almost all the precipitation indices is remarkable. In particular, a very low correlation is computed between the above-mentioned index and the total annual precipitation (PRCTOT). One explanation of this result might be related to the fact that on average the daily temperature range is smaller on rainy days. If the sky is cloudy, the daily maximum temperature is reduced, and the minimum temperature may be increased due to less heat being lost to the upper atmosphere and retained near the ground.

#### 4.2.2 Identification of critical destructive events

The second step is to identify which are the destructive events that occurred in Beira, to evaluate if the indices are able to reproduce their criticality. The EM-DAT disaster database<sup>23</sup> provides information about the past disasters that happened in Mozambique and the province of Sofala. Moreover, the humanitarian information service provided by the United Nations Office for the Coordination of Humanitarian Affairs (OCHA) provides a record of the ongoing and past disasters around the globe, including floods that happened in Mozambique<sup>24</sup>. The main source of information regarding the tropical cyclones that affected the area of interest was the Direction of Météo-France in La Réunion<sup>25</sup>, which has been designated as the Regional Specialized Meteorological Centre (RSMC) for Tropical Cyclones in the South-West Indian Ocean by the World Meteorological Organization (WMO) in 1993 (Draxler et al., 1993). Further knowledge was acquired from the Australian Severe Weather website<sup>26</sup>, and from FAO documentation (Adriana Herrera et al., 2010). Table 11 reports the main destructive events connected to extreme precipitation that happened in the province in Sofala from 1985 onwards (because of information availability). These events caused thousands of fatalities and billions of dollars of damages. A more detailed insight on this topic is reported in Appendix A.

---

<sup>23</sup> <https://www.emdat.be>

<sup>24</sup> <https://reliefweb.int/disasters>

<sup>25</sup> <http://www.meteofrance.re/cyclone/>

<sup>26</sup> <http://www.extremestorms.com.au/>

<b>Critical Events that affected the city of Beira</b>				
Year	Months	Event	People affected	People killed
1997	January to February	Riverine floods and Tropical Storm Lisette	400.000	87
2000	January to March	Floods and Tropical Cyclone Eline-Leon	>2.000.000	800
2001	January to April	Riverine floods	500.000	115
2007	January to February	Floods and Tropical Cyclone Favio	400.000	150
2019	March	Tropical Cyclone Idai	>2.000.000	>1300

*Table 11: Description of the most critical events for the city of Beira. Data about people affected and killed are estimations. Source: <https://www.emdat.be>*

A Tropical Cyclone, like in the case of Idai, combines extreme winds, extreme rainfall and can trigger storm surges. However, it should be specified that these events are rarely the result of a single “climatic hazard”, but they are the consequence of compound events affecting the area over a relatively short period. For instance, a severe rainy season characterised by torrential rain followed by a tropical cyclone, or multiple storms in sequence. In addition, is essential to bear in mind that disasters are not only the result of a natural hazard but of the complex interrelation between the severity of one event, the vulnerability, and the exposure to that event. However, in these analyses the focus is only on the physical dimension of the event, leaving aside the social and economic dimensions.

### 4.2.3 Indices and Critical events

At this point, the time series of the observed indices (ERA5) were visually inspected to answer the following question: is there a signal emerging from the time series of the indices in correspondence with the years in Table 11? Figure 41 shows the indices that were selected since they present relatively high values in correspondence to 1997, 2000, 2001, 2007 and 2019. Hence, a correlation is potentially present.

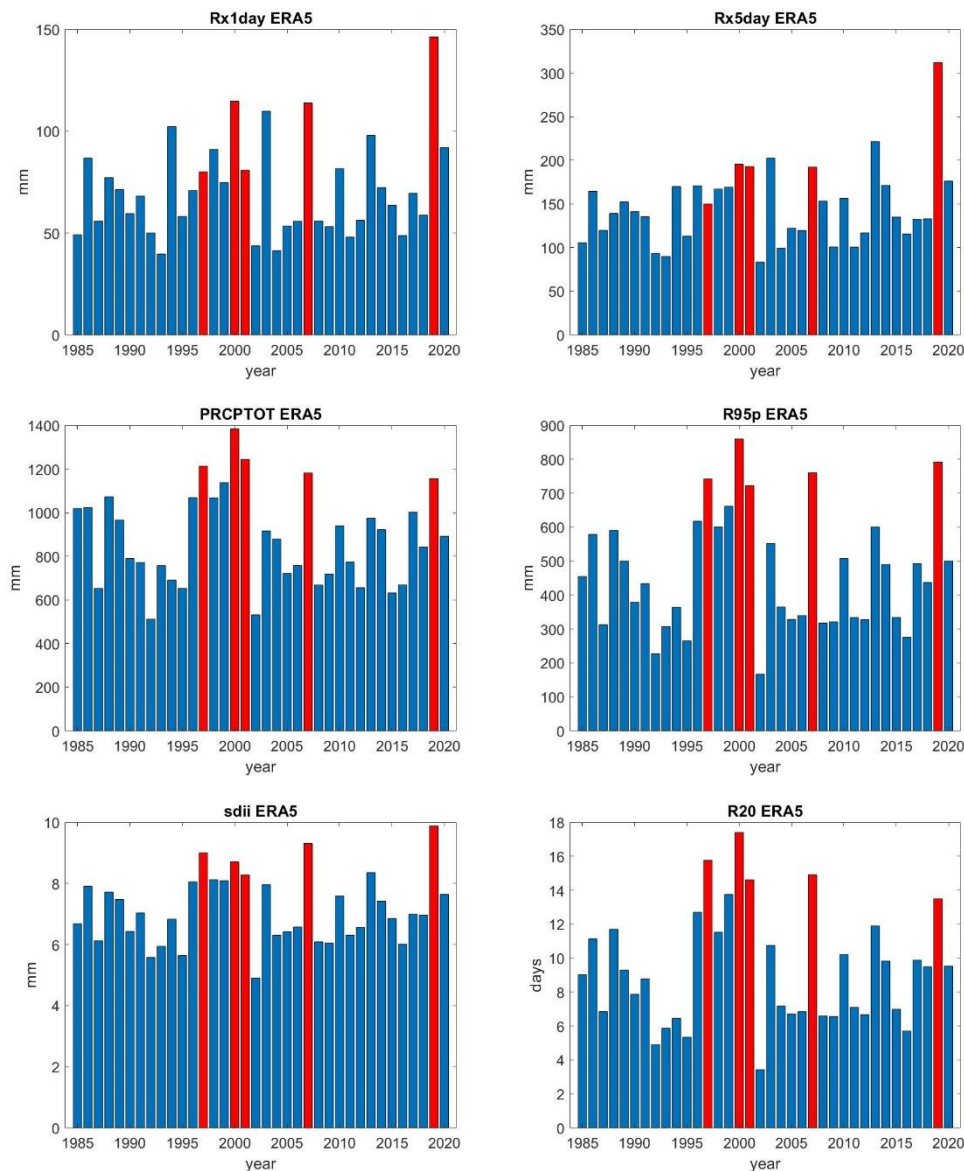


Figure 41: Bar diagram for the time series of selected indices. Red bars are located in correspondence to the years 1997, 2000, 2001, 2007 and 2019, where relatively high values are recorded

The indices for which high values are present in correspondence to the critical years are the ones that most intuitively are connected with the extreme rainfall. However, the indices taken individually do not manage to distinguish unambiguously the three critical years from the others. Nevertheless, criticality is successfully isolated by taking into account the years in which more than one index has relatively high values. In other words, the years in which Beira suffered from extreme critical events can be identified by considering the information from *all* the indices in Figure 42. Here, the K-means clustering algorithm (MacQueen, J., 1967) has been applied to verify whether the three-dimensional scatter plot generated by the indices successfully manages to isolate the critical years (Figure 42). Running the algorithm with a predefined number of  $k = 5$  clusters results in the critical years to be part of a single group. This demonstrates that some of the indices of moderate extremes if combined can reveal the years in which Beira and the province of Sofala experienced one or more destructive critical events. In other words, the observed precipitation indices reveal the signal that critical events have had on precipitation and are therefore possible to infer about these events from the analysis of the indices.

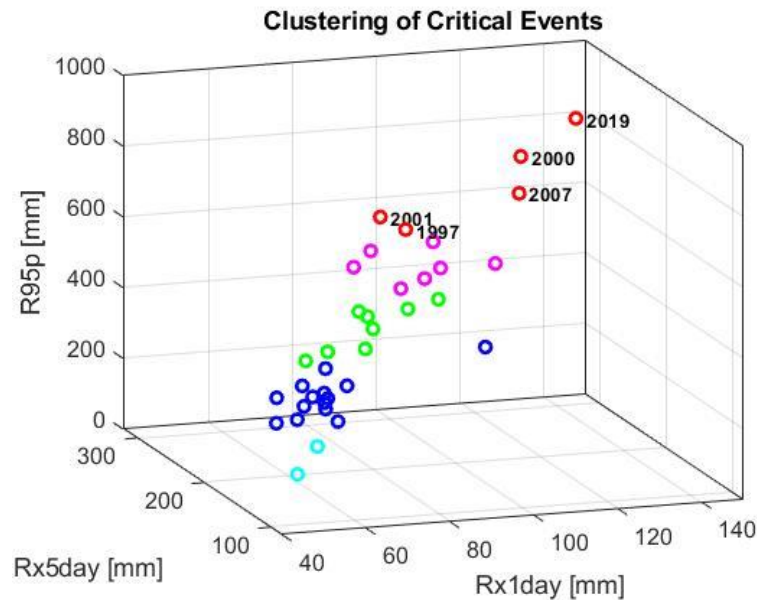


Figure 42: Three-dimensional scatter plot of the indices chosen to correlate with the critical events. K-means clustering is used to divide the 30 years into 5 clusters. In red is the critical cluster, grouping the critical years for the city of Beira.

At this point, it is necessary to identify what defines a year as belonging to the “red” group. In this respect, the “*Critical Zone*” is defined as *the 6-dimensional open sub-space* so that appropriate index values are *simultaneously* exceeded. These thresholds have been established, with a certain degree of subjectivity, taking into account the values of the indices in the critical years, i.e. rounding down the minimum value of the five *critical years*. Table 12 contains the threshold values and Figure 43 displays them on the indices time series.

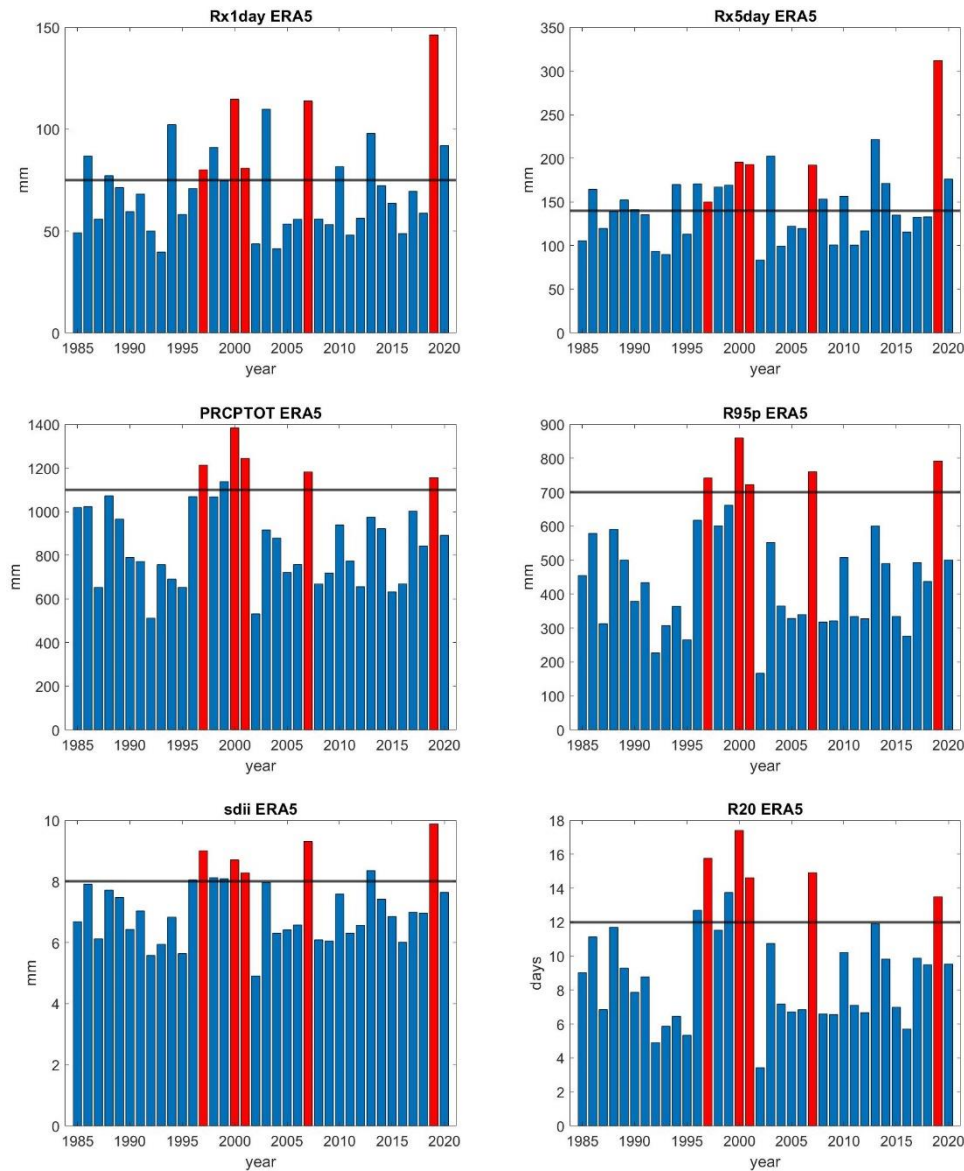


Figure 43: Timeseries of observed indices and relative thresholds used to define the  $n$ -dimensional Critical Zone



<i>Index values that if simultaneously exceeded define a critical event</i>					
Rx1day	Rx5day	sdii	R95p	PRCPTOT	R20
75 mm	140 mm	8 mm	700 mm	1100 mm	12 days

Table 12: Threshold values for each index. They are used to define a year as critical

In addition, Figure 44 shows the representation of the *Critical zone* in 3D (for obvious reasons a 6D representation would not be possible). In conclusion, one point falling into the *Critical zone* is defined to represent a year in which Beira and the province of Sofala experienced one or more destructive critical events.

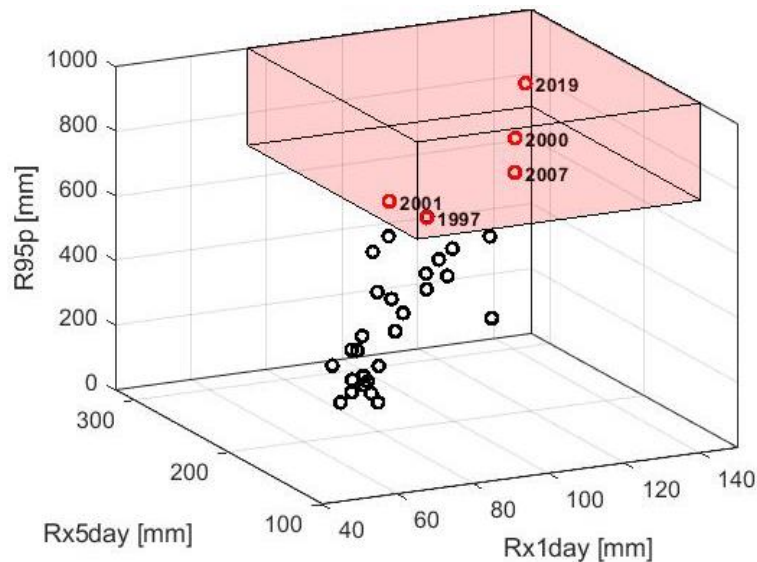


Figure 44: The concept of Critical Zone. Three-dimensional representation of the Critical Zone (red parallelepiped) within the 3D scatterplot of Rx1-Rx5-R95p.

To summarize, a correlation between the values of a subset of extreme precipitation indices and the most dramatic events that upset Beira in the past was established. In doing that, a criterion has been set, according to which a year is defined to be or not to be “critical”.

#### 4.2.4 Future projections of critical events

In the last place, it is interesting to assess what the models project about the future of *critical events*. Namely, is the frequency of these kinds of disasters going to increase or decrease according to model projections under the high radiative forcing scenario (SSP5-8.5)?

For each model, the frequency of projected *critical events* is computed as the count of years falling within the *Critical Zone* in the past (1981-2020), the mid-term (2021-2060), and the far future (2061-2100). Afterwards, the mean of the model results is computed, reported in Table 13. The three graphs in Figure 45 show this analysis in 2D for Rx1day, Rx5day, and R95p for the sake of understanding.

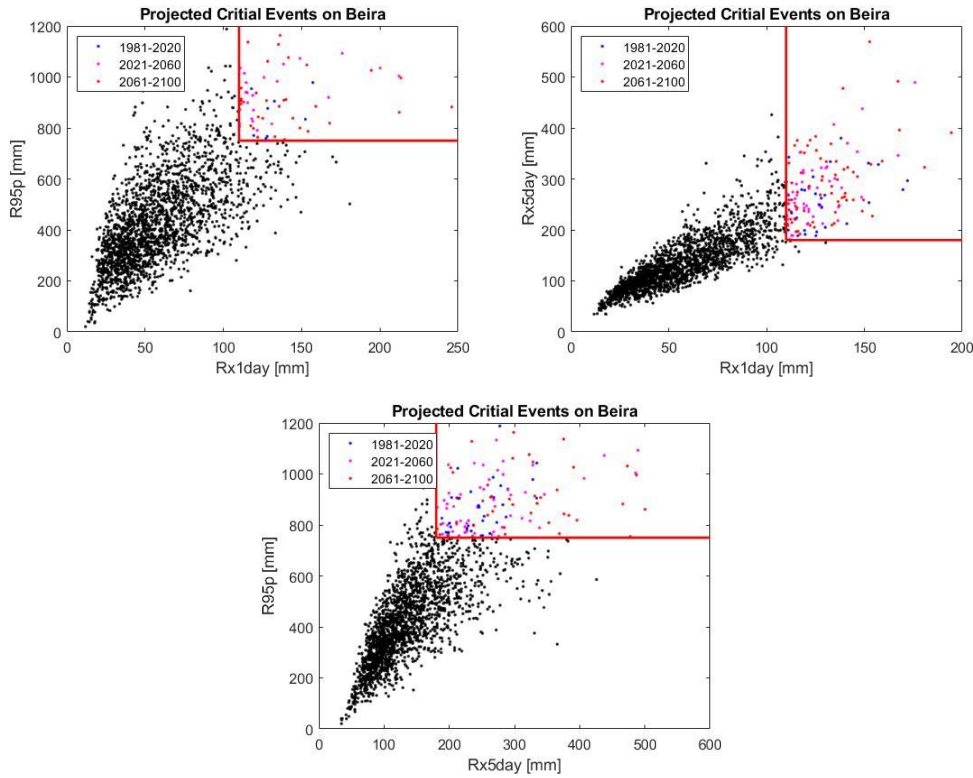


Figure 45: Representation of the position of simulated years in 2D. Red lines are the boundaries of the Critical Zone.

	<b>Past (81-20)</b>	<b>Mid-term (21-61)</b>	<b>Long-term (61-100)</b>
Mean n. of simulated critical events	1.94	3.11	2.17

Table 13: Count of years falling in the Critical Zone on the three sub-periods averaged over the models.

By looking at Table 13, a sign of an increase in the frequency of these events emerges clearly in the medium term with an increase in the order of 60%, while the increase seems to attenuate in the long term (around 10% increase compared to the past).

To have a measure of the uncertainty of these measures, a bootstrap resampling procedure is applied. Half of the models are randomly selected iteratively ( $n^\circ$  iterations = 100) and the previous computation is repeated each time. In this way, the standard deviation of the different realizations for the three results is computed, as reported in Table 14.

	<b>Past (81-20)</b>	<b>Mid-term (21-61)</b>	<b>Long-term (61-100)</b>
Mean (bootstrapping)	1.87	3.07	2.10
Standard deviation (bootstrapping)	0.56	0.82	0.63

Table 14: Mean and standard deviation of the sampling distribution resulted from the bootstrapping procedure. Data are resampled using 9 out of 18 models 100 times, and the results about the frequency of critical events are each time recorded.

As visible in Table 14, the magnitude of the uncertainty does not allow making predictions confidentially, since the sample distributions of the results over the three periods overlap each other. In other words, the increase in the frequency of projected critical years is not statistically significant, especially concerning the long-term projections. To be noted is that the mean number of the simulated past critical events (1.94) is lower than the critical events that happened, suggesting that the models tend to underestimate the magnitude of extreme precipitation.

For this reason, the analysis was repeated by taking a smaller subset of indices ( $n=3$ ), namely Rx1day, Rx5day and R95p. They were chosen among the others since they do not show a high correlation between each other (*correlatio coefficient*  $\rho_s < 0.7$ ),

meaning that they reveal independent information. The clustering algorithm (K-means), applied with a predefined number of  $k=5$  clusters, resulted in the ‘critical cluster’ to be composed by the *years 2000, 2007 and 2019* that were without any doubt the most stressful for Beira because of the intense tropical cyclones that devastated the area (Appendix A). Table 15 reports the thresholds used to define the *Critical Zone*, which this time is a 3-dimensional parallelepiped subspace (as in the above Figure 44).

<b><i>Index values that if simultaneously exceeded define a critical event</i></b>		
Rx1day	R95p	Rx5day
110 mm	750 mm	180 mm

Table 15: Threshold values for the subset of three indices used to define a year as critical.

Results are given in the Tables below. Table 16 reports the mean number of simulated critical events over the three periods. Table 17 reports the results of the bootstrapping procedure to assess the uncertainty of results.

	<b>Past (81-20)</b>	<b>Mid-term (21-61)</b>	<b>Long-term (61-100)</b>
Mean n. of simulated critical events	0.5	1.44	2.17

Table 16: Count of years falling in the newly defined Critical Zone on the three sub periods averaged over the models.

	<b>Past (81-20)</b>	<b>Mid-term (21-61)</b>	<b>Long-term (61-100)</b>
Mean (bootstrapping)	0.49	1.42	2.15
Standard deviation (bootstrapping)	0.01	0.12	0.09

Table 17: Mean and standard deviation of the sampling distribution resulted from the bootstrapping procedure. Data are resampled using 9 out of 18 models for 100 times.

Given that 2000, 2007 and 2019 were the most critical for Beira compared to 1997 and 2001, it was to be expected that the mean number of projected future critical events would be lower than in the previous analysis.

All in all, predictions about future critical events made using only these three indices results in their sharper and gradual increase over time. Moreover, the standard deviations of the sampling distributions are very low and therefore the results are to be said to be statistically significant.

## 5. DISCUSSION

The study conducted so far has led to an insight into the extreme temperature and precipitation conditions projected along the 21st century in the area of the city of Beira. This section aims at summarising and interpreting the results into a coherent picture, by focusing also on their impacts on socio-economic and natural systems (section 5.5). Given the complex interrelationship between climate change and the different scales on which it acts, it is interesting to put in relation the findings of this study at the local scale (area of Beira) with global and regional (South Eastern Africa region – SAEF) observations and projections. The aim is to confirm whether the results of this work are in line with findings at larger scales and to put them into a broader context with the support of relevant literature. In particular, the main reference for discussion are the recently published IPCC assessment reports, AR6 working groups I, II (IPCC, 2021), and the more outdated SREX report (IPCC, 2012).

### 5.1 Extreme Temperatures

The future projections over the area of Beira highlight a consistent increase of intensity and frequency of the temperature extremes for both scenarios, with a unanimous consensus among the models. However, while in the best-case scenario (SSP1-2.6) in the long-term (after mid-century) extreme temperatures tend to stabilise, the worst-case scenario predicts that extreme temperatures would continue to rise to very high levels by the end of the century.

Temperature peaks will increase in intensity: by the end of the century (2071-2100) a median increase of the maximum annual temperature (*TXx*) of  $4.8^{\circ}\text{C}$  under SSP5-8.5 and  $1.4^{\circ}\text{C}$  under SSP1-2.6 is predicted compared to the baseline period (1981-2010). Minimum temperatures (*TNn*) will rise accordingly, with a slightly lower extent. Heatwaves' days (*wsdi*) are projected to increase consistently: by the end of the century a median increase of *49 days* under SSP5-8.5 and *9 days* under SSP1-2.6 is predicted.

The increase in the frequency of warm days (*Tx90p*) and nights (*Tn90p*) suggests a future radical change in the temperature regime compared to 1981-2010 according to the worst-case scenario, given that temperature extremes in the base period will be the normality by the end of the century. To explain this, it must be taken into account that the tropical climate of Mozambique implies that the 90<sup>th</sup> percentile and the median daily maximum temperatures are not too far apart. For this reason, a shift of about 4-5°C in the maximum daily temperature distribution (according to the global warming scenario under SSP5-8.5) towards higher temperatures results in a saturation of the probability of occurrence of the 90<sup>th</sup> percentile, since the ‘future mean maximum daily temperature’ has the same value of the past ‘extreme’. The same can be said by looking at the decrease in the frequency of cold days (*Tx10p*) and cold nights (*Tn10p*). Warm nights are projected to increase faster than warm days and, accordingly, cold nights are projected to decrease faster than warm nights (see 4.1.2, 4.1.3).

Studies conducted at the global scale have led to consistent evidence of warming of observed temperature extremes. It has been demonstrated that changes in temperature extremes are driven by human-induced climate change (IPCC, 2012; IPCC, 2014). Extreme temperatures warming robustly scales with global warming. However, local and regional feedbacks strongly influence extreme temperatures (e.g. soil moisture-evapotranspiration-temperature feedback), as well as external forcings (land use/cover changes and aerosol concentrations), so that changes in extreme temperatures are often greater than those in average temperatures (Seneviratne et al, 2021). At the regional scale, not many studies have been conducted on the observed changes in South-Eastern Africa –SEAF– due to a lack of data, however among the existing studies an increase in the intensity and frequency of hot extremes is detected (Seneviratne et al, 2021).

Regarding future projections, at the global scale models predict substantial warming in temperature extremes by the end of the 21st century. There will be more frequent hot extremes and fewer cold extremes in a warmer climate and is very likely heatwaves will occur with a higher frequency and longer duration, especially considering global warming scenarios above 2°C (IPCC, 2012). In ESAF, projections are in line with the results of this study. For instance, Li et al. (2021) describe at the 4°C warming level a median

increase of almost 5°C in annual TXx and TNn compared to pre-industrial levels, which agrees with the results over Beira, described in section 4.1.1.

## 5.2 Heavy Precipitation

Projections about heavy precipitations over Beira contain a large degree of uncertainty. The latter is somewhat reduced by considering the highest emissions scenario (SSP5-8.5) in the distant future, where significant and consistent changes emerge. In this case, the intensity of precipitation extremes is set to increase. Heavy precipitation events become heavier (***Rx1day***, ***Rx5day***). The change is non-linear: the rarest and most extreme events (that occur in average 1 time over 20 years) are projected to intensify more. As regards the frequency of precipitation extremes, the future context for the city of Beira according to the SSP5-8.5 scenario is to be predicted as follows. The *number of heavy precipitation days* (***R20***, *pr* greater than 20mm) will not change significantly. Nonetheless, the *number of wet days* (***nR95p***, *pr* greater than 95<sup>th</sup> percentile) is projected to increase. This means that consistent rainy days are going to increase in the dry season, since the threshold of 20mm is representative only of the wet season, whereas the percentiles are thresholds that depend on the day of the year, thus including also the dry season. Independent extreme meteorological events (***inR95p***) are projected to be less frequent but to last significantly longer (***cwd95***).

At the global scale, there is consistent evidence of an increase in heavy precipitation events over land, although there are wide seasonal and regional variations (IPCC,2012; IPCC,2014). In general, warming increases the atmospheric vapour holding capacity following the Clausius-Clapeyron relationship (~7% increase/°C). Consequently, the hydrological cycle tends to intensify, leading to more extreme rainfall. The increase of ***Rx1day*** over the last decades of the 20th century is estimated to be consistent with C-C concerning global mean temperature rise (Fischer et al., 2016). However, extreme precipitation is very much connected with the large-scale modes of variability such as El Niño-Southern Oscillation, whose warming-induced changes are complex and uncertain.



Moreover, precipitation extremes are also affected by local forcings including changes in aerosols, land cover change and urbanization (Seneviratne et al, 2021). This makes changes in extreme precipitation heterogeneous and complex to model, which explains the large uncertainty in model projections.

CIMP6 models indicate on the ESAF region a future increase of intensity and frequency of heavy precipitation extremes. Li et al., (2021) show at the 4°C warming level a median increase of more than 15% in the 50-year Rx1day and Rx5day events compared to the 1°C warming, that is a similar increase to the one found in this study for the area of Beira (4.1.3, increase on the 95<sup>th</sup> percentile of the probability distribution).

## 5.3 Droughts

Droughts refer to periods with below-average moisture conditions and limitations in water availability (Wilhite and Pulwarty, 2017).

Future projections indicate increasing dry conditions over Beira. Meteorological droughts (lack of precipitation) are expected to increase for both future scenarios. Indeed, the total annual precipitation (*PRCPTOT*) is projected to decrease by around 10% under SSP5-8.5 and 7% under SSP1-2.6 by the end of the century compared to the baseline period. Consistently, the number of consecutive dry days (*cdd*) is projected to increase (4.1.4).

Atmospheric dynamics is the dominant factor in precipitation deficiency, with mechanisms taking place on different spatial and temporal scales (e.g. blocking patterns); droughts are therefore phenomena strictly region-dependent (Seneviratne et al, 2021).

Studies conducted at the global and regional scale confirm the projected increase of meteorological droughts in the area of Beira. A strong increase in *cdd* is indeed projected for 4°C of global warming over most of the African continent (Sillmann et al., 2013). In the ESAF, there is evidence of a change in meteorological droughts already at the 1.5°C warming level (Xu et al., 2019).

## 5.4 Extreme weather events

Within sections 3.4 and 4.2, an empirical approach was developed to relate selected annual indices of moderate precipitation extremes to the extreme weather events that led to severe damage in the city of Beira. In particular, the focus was on the heavy rainfall associated with tropical cyclones that had caused extensive floods in the city.

After determining a criterion that, starting from the values of the reanalysis-derived indices, makes it possible to infer about this type of events, future assumptions were made using indices computed under the SSP5-8.5 scenario. A signal of future increases in the frequency of extreme weather events emerged from the analysis (see 4.2.2).

In the 11<sup>th</sup> chapter of AR6 (Seneviratne et al, 2021) the challenges of the quantification of climate change effects on extreme storms are remarked. This is in part because they are rare, local, and influenced by stochastic variability. Models do not manage to accurately represent the small-scale physical processes that drive changes in the extreme storms, and therefore future projections are challenging. Identifying past trends of Tropical Cyclones metrics is a challenge because of the heterogeneous instrumental data that collect the long-term records. Using only the most recent homogenized data (acquired by satellites) it has been observed a global tendency towards an increase of intensity of tropical cyclones (Knutson et al. 2020). In addition, the widening of the Hadley cell has likely caused the poleward shift of cyclones tracks (Sharmila and Walsh, 2018) which poses an increased threat on Beira. Moreover, there is evidence of the increased TC intensification rates (Kishtawal et al. 2012). In the ocean that bathes the city of Beira, South-West Indian Ocean, an increase of the most intense cyclones (category 3-5) has been observed in recent decades (Fitchett, 2018). Specifically, it has been observed a more frequent landfall of tropical cyclones over central to northern Mozambique (Malherbe et al., 2013).

Future projections for this basin, and in other basins worldwide, agree on a general reduction in the total number of tropical cyclones, but in the increase in the proportion of most powerful and dangerous tropical cyclones (category 4-5). These studies show that heavy rainfall associated with TCs is likely to increase with warming at a greater rate than the C-C scaling (Malherbe et al., 2013; Knutson et al., 2020). These findings are

consistent with the projected increase in the number of critical precipitation events over the area of Beira.

## 5.5 Impacts

Studying and monitoring the extreme climate events described in the previous paragraphs is crucial, since the impacts they have on human conditions and assets, on ecosystems and the natural physical environment. Predicting the impacts of this kind of events is a complex task since involves elements from different fields of knowledge, entailing earth, social and economic sciences. The concept of risk associated with the extreme climate is the result of the interconnection between the entity of the hazardous physical event and the exposure and vulnerability of people, infrastructures, environmental services, etc. Moreover, impacts related to different extreme climatic events are often interconnected, which adds another degree of complexity.

Detailed impact analysis for the area of Beira goes beyond the scope of the present work. This section merely outlines the potential increased risk that the area may experience as a result of the projected changes in climate extremes of temperature and precipitation.

The latest IPCC report, details the past and future impacts of climate change worldwide. Chapter 9 (Trisos et al., 2022) focuses on vulnerabilities and adaptation options for Africa. The following Figure 46 shows the increased risk due to climate change for three selected key risks in Africa. Below, the impacts of precipitation and temperature extremes changes are identified by the sectors they affect, focusing on the case of Beira.

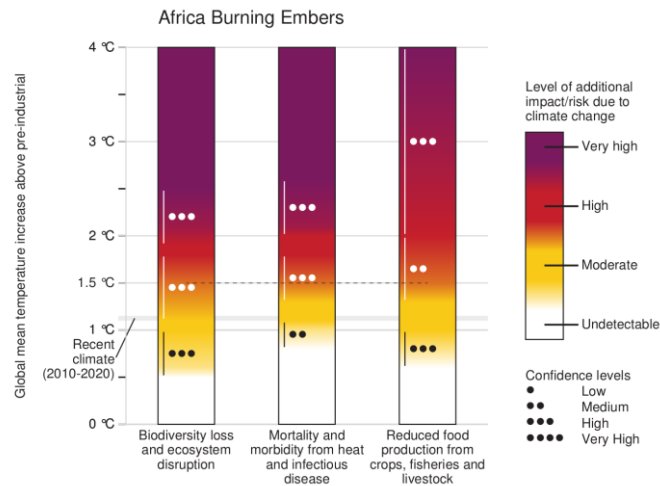


Figure 46: Burning embers showing the increased risk due to climate change for selected key risks in Africa. The projected increase is assessed for global warming increasing above pre-industrial levels (1850–1900). At the actual level of global warming (about 1.1°C), all three risks are already classified to moderate risk (IPCC, 2022).

### 5.5.1 Ecosystems

High-temperature extremes, droughts and floods substantially affect ecosystems and ecosystems services. In Africa, communities are particularly dependent on regulating and provisioning ecosystem services (Scholes et al., 2018) such as water quality regulation, coastal protection, crop and livestock productivity, and wild-harvestable food. Extreme climate might severely test the resilience of ecosystems and therefore their services. Dry and hot conditions promote the generation and spread of wildfires, which, although part of the functioning of ecosystems, are going to increase (Jones, et al., 2020). If tipping points are crossed, systems may undergo abrupt changes. For instance, forests may shift from being net carbon sinks to net carbon sources (Hubau,et al. 2020). In South-East Africa, the risk of abrupt disruption of biodiversity largely increases above 2°C. More specifically, models project that at coral reefs of the region are going to be destroyed by bleaching by more than 90% (Hoegh-Guldberg et al., 2018).

Mangrove ecosystems are very important as carbon sequesters and shoreline protection in Mozambique. These are compromised by extreme events. For instance, mangrove cover in Mozambique was reduced by 48% after Cyclone Eline in 2000 (Macamo et al., 2016).

A key sector for Mozambique that is very vulnerable to extreme climatic events is Nature-based tourism (Da Silva, Jose Juliao, 2019). Increased heat stress for tourists and employees, reduced animal mobility, disrupted tourism activities and infrastructures due to extreme weather conditions are among the impacts that threaten this important business.

### 5.5.2 Water scarcity and food security

Water and food availability are strictly connected. Both are largely impacted by climate extremes.

Even though the area of Beira is not characterized by a high vulnerability to water scarcity<sup>27</sup> (Pörtner et al., 2022, figure 7S.6), prolonged droughts might exacerbate water management challenges for municipal and agricultural use. Precipitation deficits might have dramatic consequences also on rain-fed agricultural production. The long droughts that struck Mozambique between 1981 and 1984 have affected more than four million people and killed about one hundred thousand<sup>28</sup>. Besides, heatwaves negatively affect crop yields and livestock productivity (Lobell et al. 2011). Water deficit in rivers or lakes and high temperatures heavily affect the fishery sector as well, which is particularly important for Beira and in general for Mozambique, a country with vast seacoasts whose inhabitants largely depend on small-scale fishing for a living (Bilika et al., 2019). At the 4°C global warming level, models project that the Maximum Catch Potential (MCP, a

---

<sup>27</sup> In the area of Beira a large amount of precipitation falls annually compared to other parts of the country. Moreover, the presence of Pungue and Buzi rivers assure large amount of water.

<sup>28</sup> <https://www.emdat.be>

matrix used for fish biomass abundance) along African coasts would decrease by 12-69% (Golden et al., 2016).

Moreover, floods and severe tropical storms may impact the food supply chains (roads, infrastructures...), driving rising food insecurity. Between 2015 and 2019, an estimated 62 million people in eastern Africa needed humanitarian assistance due to climate-related food emergencies (Gebremeskel et al., 2019).

A 2018 World Bank analysis stated that experiencing a cyclone, flood or drought leads to a reduction of as much as 25-30 percent in per capita food consumption and about 0.4 fewer meals per person per day (Baez et al., 2018).

### 5.5.3 Human Health

Climate extremes, such as heatwaves, droughts and floods influence human health and well-being.

Extreme heat and heat stress might be fatal and are associated with increased hospitalisation. Elevated night-time temperatures, as projected for Beira, does not allow human body relief from heat stress. Even if the proximity of the sea mitigates the effect of urban heat islands, the elevated humidity combined with heatwaves might induce great heat stress. The most vulnerable are young children and the elderly.

Infectious diseases in developing countries like Mozambique have often followed floods. In Beira, in the weeks after Cyclone Idai, a cholera epidemic added to the disaster (Macamo, et al., 2021). Floods might also cause a displacement of malaria epidemic regions by changing the breeding sites for vector mosquitoes. Droughts might affect mosquito-borne diseases as well and they are also linked with meningitis (Molesworth et al., 2003). Indirect health impacts related to extreme events are mental health impacts related to traumatic experiences of loss, disruption and displacement, often under-examined (Neria et al., 2008).

#### 5.5.4 Human settlements and infrastructures

Human settlements concentrate elements of exposure. The coastal city of Beira is especially at risk because of the projected increase in the intensity of extreme coastal storms and heavy precipitation events, and because of the vulnerability of the informal settlements and the inadequate drainage systems. The city is located only a few meters above sea level, and this makes the area much vulnerable to coastal floods. Moreover, in many cases of coastal settlements (including Beira), the ability of natural coastal systems to respond to extreme climate events has been reduced with urbanization, because of the removal of the protection provided by dunes and mangroves ecosystems. Cyclone Idai had a devastating effect on the infrastructure of the city of Beira: approximately 70% of the houses were partially or completely destroyed (Trujillo, M., 2019).

Adaptation actions are required to make the city more resilient to such events, which are bound to increase due to climate change. Many interventions have been designed and are being implemented to enhance the protection of Beira from floods. Grey-green interventions such as the restoration of mangroves ecosystems inside the city (along the Chiveve River) and along the coast, the expansion of sand dunes, breakwaters systems and coastal walls are part of the Beira Recovery and Resilience plan<sup>29</sup> that was developed after the Cyclone Idai disaster.

---

<sup>29</sup> <https://www.slideshare.net/BasAgerbeek/beira-municipal-recovery-and-resilience-plan-volume-1-main-report>

## 6. CONCLUSIONS

In these years, the world is facing a challenge of unprecedented magnitude, in which complex decisions have to be taken to ensure a fair future for the next generations. Sound knowledge of the changes taking place in the climate system is of primary importance to make informed decisions. In particular, the study of climate extremes is relevant because of the large impacts they have on human systems. Beira is one of the cities most threatened by climate change worldwide, highly vulnerable to climatic extremes. This thesis aimed to analyse the changes in temperature and precipitation extremes that are expected in the Beira city area throughout the 21st century. The results provide the latest information on the extreme climate response to two future scenarios (SSP1-2.6 & SSP5-8.5).

Temperature extremes will rise consistently with global warming. In the worst-case scenario (SSP5-8.5), what is considered an 'extreme' today will be the norm by the end of the century. Temperature peaks will increase in intensity and minimum temperatures will rise accordingly, with a slightly smaller extent. The duration and frequency of heatwaves are expected to increase slightly under SSP1-2.6 and consistently under SSP5-8.5. For extreme precipitation, a sign of change emerges only by considering the SSP5-8.5 scenario. The models predict a decrease in total annual rainfall and longer dry spells, indicating increasing risk of droughts. Heavy rainfall is projected to become heavier. An increase in the number of very wet days is expected to happen in the dry season (May-October). In general, extreme precipitation events are going to be less frequent but last longer. The increasing duration of extreme events is the signal that emerges most clearly from data, and that poses a challenge for the drainage system of the city. Certainly, it may be concluded that it would be substantially easier for the community of Beira to adapt to the changing climate extremes if a global socio-economic scenario more similar to SSP1-2.6 than to SSP5-8.5 were to be realised.

A further outcome of this thesis was to develop an empirical approach to relate annual extreme moderate precipitation indices to the disasters caused by the torrential rains that



devastated the city of Beira. This correlation makes it possible to verify that the annual indices manage to capture the criticality of an event of extreme precipitation for the city and to make future assumptions based on model projections under the SSP5-8.5 scenario. The latter reveals that **such events are bound to increase**, although with a certain degree of uncertainty related to some steps of the methodology. Indeed, the limitation of this approach is the subjectivity in the choice of the subset of indices used in the correlation analysis, and criticality thresholds (see paragraph 4.2.1). Future developments of this methodology should include a more objective method for the characterisation of critical events than a set of predefined thresholds, such as the application of machine learning techniques to identify a parametric subspace in the multi-dimensional space of indices. In addition, a dimensionality reduction technique such as PCA (Principal Component Analysis) may be used to determine objectively the optimal combination of indices used as impact predictors.

Several other improvements or developments could be made. For instance, the computation of temperature extremes indices based on percentiles (section 4.1.2) could be repeated using moving reference periods as in Russo et al. (2011), to separate those changes resulting from a shift in PDF from those resulting from an increase in climatic variability. Moreover, the whole study could be repeated employing data from higher resolution regional models (RCMs) that have been proven to simulate better extreme rainfall events compared to their host GCMs thanks to their ability to cope with topography and coastlines. Besides, they are more suitable to simulate tropical cyclones and the associated precipitation (Seneviratne et al, 2021).

In the aftermath of the Cyclone Idai disaster, the municipality of Beira prepared the Beira Recovery and Resilience Plan addressing both immediate recovery needs and longer-term strategies to make Beira a resilient city; a roadmap to ‘Build Beira Back Better (BBBB)’<sup>30</sup>. The plan covers the key areas of infrastructure which proved to be vulnerable during the Idai event, namely the coastal protection, the drainage system, the sewage, the solid waste management, the roads, and the housing.

---

<sup>30</sup> <https://www.slideshare.net/BasAgerbeek/beira-municipal-recovery-and-resilience-plan-volume-1-main-report>

The methodology and the results obtained in this work may provide useful information for updating and calibrating the existing improvement measures or as a basis for designing new adaptation actions. Moreover, it may be trustful support and reference for further investigations on the climate of the area.

## 7. BIBLIOGRAPHY

- Abarbanel, H., Koonin, S., Levine, H., MacDonald, G., Rothaus, O., 1992. Statistics of Extreme Events with Application to Climate. MITRE CORP MCLEAN VA JASON PROGRAM OFFICE.
- Adriana Herrera Garibay, Paul de Wit, Luis Eleazar, Fausto Jordán Bucheli, Simon Norfolk, Raúl Sánchez Mena, Salma A. Shafi, 2010. Land tenure and natural disasters.
- Alexander, L.V., Fowler, H.J., Bador, M., Behrangi, A., Donat, M.G., Dunn, R., Funk, C., Goldie, J., Lewis, E., Rogé, M., Seneviratne, S.I., Venugopal, V., 2019. On the use of indices to study extreme precipitation on sub-daily and daily timescales. *Environ. Res. Lett.* 14, 125008. <https://doi.org/10.1088/1748-9326/ab51b6>
- Baez, J.E., Caruso, G.D., Niu, C., 2018. Extreme Weather and Poverty Risk: Evidence from Multiple Shocks in Mozambique (SSRN Scholarly Paper No. ID 3297323). Social Science Research Network, Rochester, NY.
- Bilika, F., Farooq, H., Alfredo, A. C., Soares, A., & Morgado, F., 2019. Caracterização dos desembarques da pesca na Baía de Pemba: centros de pesca de Pemba e Pemba-Metuge (Norte Moçambique). *Revista Captar: Ciência e Ambiente para Todos* 8(1), 131–143.
- Chemane, D., Motta, H., Achimo, M., 1997. Vulnerability of coastal resources to climate changes in Mozambique: a call for integrated coastal zone management. *Ocean Coast. Manag., Climate Change and Integrated Coastal Management* 37, 63–83. [https://doi.org/10.1016/S0964-5691\(97\)00073-2](https://doi.org/10.1016/S0964-5691(97)00073-2)
- Christie, F., Hanlon, J., 2001. Mozambique & the Great Flood of 2000. Indiana University Press.
- Da Silva, Jose Juliao, 2019. Turismo em Moçambique: Oportunidades, desafios e Riscos AbeÁfrica: Revista da Associação Brasileira de Estudos Africanos.
- Dagum, E. B., 2001. *Analisi delle serie storiche: modellistica, previsione e scomposizione*. Springer Science & Business Media.
- Draxler, R. R., Rolph, G. D., McQueen, J. T., Heffter, J. L., & Stunder, B. J. B., 1993. Capabilities of the NOAA Washington Regional Specialized Meteorological Centre for atmospheric transport model products for environmental emergency response. Presented at the International Workshop on Users' Requirements for the provision of Atmospheric Transport Model Products for Environmental Emergency Response., Canadian Meteorological Service, Canada., Dorval, Quebec.
- Eckstein, D., Künzel, V., & Schäfer, L., 2021. Global climate risk index 2021. Who Suffers Most from Extreme Weather Events, 2000-2019.
- Enrique Soriano, Luis Mediero, Carlos Garijo, 2019. Selection of Bias Correction Methods to Assess the Impact of Climate Change on Flood Frequency Curves. *Water* 11, 2266. <https://doi.org/10.3390/w11112266>
- Eyring, V., Bony, S., Meehl, G.A., Senior, C.A., Stevens, B., Stouffer, R.J., Taylor, K.E., 2016. Overview of the Coupled Model Intercomparison Project Phase 6 (CMIP6) experimental design and organization. *Geosci. Model Dev.* 9, 1937–1958. <https://doi.org/10.5194/gmd-9-1937-2016>
- Fallmann, J., Wagner, S., Emeis, S., 2017. High resolution climate projections to assess the future vulnerability of European urban areas to climatological extreme events. *Theor. Appl. Climatol.* 127, 667–683. <https://doi.org/10.1007/s00704-015-1658-9>
- Fischer, E.M., Knutti, R., 2016. Observed heavy precipitation increase confirms theory and early models. *Nat. Clim. Change* 6, 986–991. <https://doi.org/10.1038/nclimate3110>
- Fitchett, J.M., 2018. Recent emergence of CAT5 tropical cyclones in the South Indian Ocean. *South Afr. J. Sci.* 114. <https://doi.org/10.17159/sajs.2018/4426>
- Flato, G.M., Marotzke, J., Abiodun, B., Braconnot, P., Chou, S.C., Collins, W., Cox, P., Driouech, F., Emori, S., Eyring, V., Forest, C., Gleckler, P.J., Guilyardi, É., Jakob, C., Kattsov, V., Reason, C., Rummukainen, M., 2013. *Evaluation of climate models*. Cambridge University Press. <https://doi.org/10.1017/CBO9781107415324.020>
- Frich, P., 1998. REWARD—A Nordic Collaborative Project. Annex of Meeting of the Joint CCI/CLIVAR Task Group on Climate Indices, Bracknell. Presented at the World Climate Data and Monitoring Programme (1999), Bracknell, UK.

- Frich, P., Alexander, L.V., Della-Marta, P., Gleason, B., Haylock, M., Tank, A.M.G.K., Peterson, T., 2002. Observed coherent changes in climatic extremes during the second half of the twentieth century. *Clim. Res.* 19, 193–212. <https://doi.org/10.3354/cr019193>
- Gebremeskel Haile, G., Tang, Q., Sun, S., Huang, Z., Zhang, X., Liu, X., 2019. Droughts in East Africa: Causes, impacts and resilience. *Earth-Sci. Rev.* 193, 146–161. <https://doi.org/10.1016/j.earscirev.2019.04.015>
- Gleckler, P.J., Taylor, K.E., Doutriaux, C., 2008. Performance metrics for climate models. *J. Geophys. Res. Atmospheres* 113, D06104. <https://doi.org/10.1029/2007JD008972>
- Global increase in major tropical cyclone exceedance probability over the past four decades [WWW Document], n.d. . PNAS. URL <https://www.pnas.org/doi/abs/10.1073/pnas.1920849117> (accessed 3.4.22).
- Golden, C.D., Allison, E.H., Cheung, W.W.L., Dey, M.M., Halpern, B.S., McCauley, D.J., Smith, M., Vaitla, B., Zeller, D., Myers, S.S., 2016. Nutrition: Fall in fish catch threatens human health. *Nature* 534, 317–320. <https://doi.org/10.1038/534317a>
- Gorgulla, C., Boeszoermyeni, A., Wang, Z.-F., Fischer, P.D., Coote, P.W., Padmanabha Das, K.M., Malets, Y.S., Radchenko, D.S., Moroz, Y.S., Scott, D.A., Fackeldey, K., Hoffmann, M., Iavniuk, I., Wagner, G., Arthanari, H., 2020. The projected timing of abrupt ecological disruption from climate change. *GSTDTAP* 580. <https://doi.org/10.1038/s41586-020-2189-9>
- Hawkins, E., Sutton, R., 2011. The potential to narrow uncertainty in projections of regional precipitation change. *Clim. Dyn.* 37, 407–418. <https://doi.org/10.1007/s00382-010-0810-6>
- Hersbach, H., Bell, B., Berrisford, P., Biavati, G., Horányi, A., Muñoz Sabater, J., Nicolas, J., Peubey, C., Radu, R., Rozum, I., Schepers, D., Simmons, A., Soci, C., Dee, D., Thépaut, J.-N., 2018. ERA5 hourly data on single levels from 1979 to present. Copernicus Climate Change Service (C3S) Climate Data Store (CDS) 10.24381/cds.adbb2d47.
- Hoegh-Guldberg, O., Jacob, D., Bindi, M., Brown, S., Camilloni, I., Diedhiou, A., Djalante, R., Ebi, K., Engelbrecht, F., Guiot, J., Hijioka, Y., Mehrotra, S., Payne, A., Seneviratne, S.I., Thomas, A., Warren, R., Zhou, G., Halim, S.A., Achlatis, M., Alexander, L.V., Allen, M., Berry, P., Boyer, C., Byers, E., Brilli, L., Buckeridge, M., Cheung, W., Craig, M., Ellis, N., Evans, J., Fischer, H., Fraedrich, K., Fuss, S., Ganase, A., Gattuso, J.P., Greve, P., Bolaños, T.G., Hanasaki, N., Hasegawa, T., Hayes, K., Hirsch, A., Jones, C., Jung, T., Kanninen, M., Krinner, G., Lawrence, D., Lenton, T., Ley, D., Liverman, D., Mahowald, N., McInnes, K., Meissner, K.J., Millar, R., Mintenbeck, K., Mitchell, D., Mix, A.C., Notz, D., Nurse, L., Okem, A., Olsson, L., Oppenheimer, M., Paz, S., Petersen, J., Petzold, J., Preuschmann, S., Rahman, M.F., Rogelj, J., Scheuffele, H., Schleussner, C.-F., Scott, D., Séférian, R., Sillmann, J., Singh, C., Slade, R., Stephenson, K., Stephenson, T., Sylla, M.B., Tebboth, M., Tschakert, P., Vautard, R., Wartenburger, R., Wehner, M., Weyer, N.M., Whyte, F., Yohe, G., Zhang, X., Zougmore, R.B., 2018. Impacts of 1.5°C Global Warming on Natural and Human Systems.
- Hubau, W., Lewis, S.L., Phillips, O.L., Affum-Baffoe, K., Beeckman, H., Cuní-Sanchez, A., Daniels, A.K., Ewango, C.E.N., Fauset, S., Mukinzi, J.M., Sheil, D., Sonké, B., Sullivan, M.J.P., Sunderland, T.C.H., Taedoumg, H., Thomas, S.C., White, L.J.T., Abernethy, K.A., Adu-Bredu, S., Amani, C.A., Baker, T.R., Banin, L.F., Baya, F., Begne, S.K., Bennett, A.C., Benedet, F., Bitariho, R., Bocko, Y.E., Boeckx, P., Boundja, P., Brien, R.J.W., Brncic, T., Chezeaux, E., Chuyong, G.B., Clark, C.J., Collins, M., Comiskey, J.A., Coomes, D.A., Dargie, G.C., de Haulleville, T., Kamdem, M.N.D., Doucet, J.-L., Esquivel-Muelbert, A., Feldpausch, T.R., Fofanah, A., Foli, E.G., Gilpin, M., Gloor, E., Gonmadje, C., Gourlet-Fleury, S., Hall, J.S., Hamilton, A.C., Harris, D.J., Hart, T.B., Hockemba, M.B.N., Hladik, A., Ifo, S.A., Jeffery, K.J., Jucker, T., Yakusu, E.K., Kearsley, E., Kenfack, D., Koch, A., Leal, M.E., Levesley, A., Lindsell, J.A., Lisingo, J., Lopez-Gonzalez, G., Lovett, J.C., Makana, J.-R., Malhi, Y., Marshall, A.R., Martin, J., Martin, E.H., Mbayu, F.M., Medjibe, V.P., Mihindou, V., Mitchard, E.T.A., Moore, S., Munishi, P.K.T., Bengone, N.N., Ojo, L., Ondo, F.E., Peh, K.S.-H., Pickavance, G.C., Poulsen, A.D., Poulsen, J.R., Qie, L., Reitsma, J., Rovero, F., Swaine, M.D., Talbot, J., Taplin, J., Taylor, D.M., Thomas, D.W., Toirambe, B., Mukendi, J.T., Tuagben, D., Umunay, P.M., van der Heijden, G.M.F., Verbeeck, H., Vleminckx, J., Willcock, S., Wöll, H., Woods, J.T., Zemagho, L., 2020. Asynchronous carbon sink saturation in African and Amazonian tropical forests. *Nature* 579, 80–87. <https://doi.org/10.1038/s41586-020-2035-0>

- IPCC Core Writing Team, R.K. Pachauri and L.A. Meyer, 2014. Climate Change 2014: Synthesis Report. Contribution of Working Groups I, II and III to the Fifth Assessment Report of the Intergovernmental Panel on Climate Change. Geneva, Switzerland.
- IPCC, Masson-Delmotte, V., P. Zhai, A. Pirani, S.L. Connors, C. Péan, S. Berger, N. Caud, Y. Chen, L. Goldfarb, M.I. Gomis, M. Huang, K. Leitzell, E. Lonnoy, J.B.R. Matthews, T.K. Maycock, T. Waterfield, O. Yelekçi, R. Yu, and B. Zhou, 2021. Climate Change 2021: The Physical Science Basis. Contribution of Working Group I to the Sixth Assessment Report of the Intergovernmental Panel on Climate Change. Cambridge University Press.
- IPCC, Masson-Delmotte, V., P. Zhai, A. Pirani, S.L. Connors, C. Péan, S. Berger, N. Caud, Y. Chen, L. Goldfarb, M.I. Gomis, M. Huang, K. Leitzell, E. Lonnoy, J.B.R. Matthews, T.K. Maycock, T. Waterfield, O. Yelekçi, R. Yu, and B. Zhou, 2012. Managing the Risks of Extreme Events and Disasters to Advance Climate Change Adaptation. A Special Report of Working Groups I and II of the Intergovernmental Panel on Climate Change. Cambridge University Press, Cambridge, UK, and New York, NY, USA.
- IPCC Working Group I Technical Support Unit, 2015. Workshop Report of the Intergovernmental Panel on Climate Change. Presented at the Workshop on Regional Climate, University of Bern, Bern, Switzerland.
- Jägermeyr, J., Müller, C., Ruane, A.C., Elliott, J., Balkovic, J., Castillo, O., Faye, B., Foster, I., Folberth, C., Franke, J.A., Fuchs, K., Guarin, J.R., Heinke, J., Hoogenboom, G., Iizumi, T., Jain, A.K., Kelly, D., Khabarov, N., Lange, S., Lin, T.-S., Liu, W., Mialyk, O., Minoli, S., Moyer, E.J., Okada, M., Phillips, M., Porter, C., Rabin, S.S., Scheer, C., Schneider, J.M., Schyns, J.F., Skalsky, R., Smerald, A., Stella, T., Stephens, H., Webber, H., Zabel, F., Rosenzweig, C., 2021. Climate impacts on global agriculture emerge earlier in new generation of climate and crop models. *Nat. Food* 2, 873–885. <https://doi.org/10.1038/s43016-021-00400-y>
- Jones, Matthew W.A., Betts, R., Canadell, J. G., Prentice, I. C., & Le Quéré, C., 2020. Climate change increases the risk of wildfires. *ScienceBrief Review* v 116, 117.
- Joo, J., Lee, J., Kim, J.H., Jun, H., Jo, D., 2014. Inter-Event Time Definition Setting Procedure for Urban Drainage Systems. *Water* 6, 45–58. <https://doi.org/10.3390/w6010045>
- Kendall, 1948. Rank correlation methods. Griffin.
- Kishtawal, C.M., Jaiswal, N., Singh, R., Niyogi, D., 2012. Tropical cyclone intensification trends during satellite era (1986–2010). *Geophys. Res. Lett.* 39. <https://doi.org/10.1029/2012GL051700>
- Kistler, R., Kalnay, E., Collins, W., Saha, S., White, G., Woollen, J., Chelliah, M., Ebisuzaki, W., Kanamitsu, M., Kousky, V., van den Dool, H., Jenne, R., Fiorino, M., 2001. The NCEP–NCAR 50-Year Reanalysis: Monthly Means CD-ROM and Documentation. *Bull. Am. Meteorol. Soc.* 82, 247–268.
- Knutson, T., Camargo, S.J., Chan, J.C.L., Emanuel, K., Ho, C.-H., Kossin, J., Mohapatra, M., Satoh, M., Sugi, M., Walsh, K., Wu, L., 2020. Tropical Cyclones and Climate Change Assessment: Part II: Projected Response to Anthropogenic Warming. *Bull. Am. Meteorol. Soc.* 101, E303–E322. <https://doi.org/10.1175/BAMS-D-18-0194.1>
- Konrad II, C.E., Meaux, M.F., Meaux, D.A., 2002. Relationships between tropical cyclone attributes and precipitation totals: considerations of scale. *Int. J. Climatol.* 22, 237–247. <https://doi.org/10.1002/joc.721>
- Li, C., Zwiers, F., Zhang, X., Li, G., Sun, Y., Wehner, M., 2021. Changes in Annual Extremes of Daily Temperature and Precipitation in CMIP6 Models. *J. Clim.* 34, 3441–3460. <https://doi.org/10.1175/JCLI-D-19-1013.1>
- Lobell, D.B., Schlenker, W., Costa-Roberts, J., 2011. Climate Trends and Global Crop Production Since 1980. *Science* 333, 616–620. <https://doi.org/10.1126/science.1204531>
- Macamo, C., 2021. After Idai: Insights from Mozambique for Climate Resilient Coastal Infrastructure [WWW Document]. *Afr. Portal*. URL <https://www.africaportal.org/publications/after-idai-insights-mozambique-climate-resilient-coastal-infrastructure/> (accessed 3.4.22).
- Macamo, C.C.F., Massuanganhe, E., Nicolau, D.K., Bandeira, S.O., Adams, J.B., 2016. Mangrove’s response to cyclone Eline (2000): What is happening 14 years later. *Aquat. Bot.* 134, 10–17. <https://doi.org/10.1016/j.aquabot.2016.05.004>
- MacQueen, J., 1967. Some methods for classification and analysis of multivariate observations. In *Proceedings of the fifth Berkeley symposium on mathematical statistics and probability*. pp. 281–297.

- Mahmood, R., Jia, S., 2017. Spatial and temporal hydro-climatic trends in the transboundary Jhelum River basin. *J. Water Clim. Change* 8, 423–440. <https://doi.org/10.2166/wcc.2017.005>
- Malherbe, J., Engelbrecht, F.A., Landman, W.A., 2013. Projected changes in tropical cyclone climatology and landfall in the Southwest Indian Ocean region under enhanced anthropogenic forcing. *Clim. Dyn.* 40, 2867–2886. <https://doi.org/10.1007/s00382-012-1635-2>
- Mann, H.B., 1945. Nonparametric Tests Against Trend. *Econometrica* 13, 245–259. <https://doi.org/10.2307/1907187>
- McGregor, G.R., Bessemoulin, P., Ebi, K.L., Menne, B., World Meteorological Organization, World Health Organization, 2015. Heatwaves and health: guidance on warning-system development.
- Molesworth, A.M., Cuevas, L.E., Connor, S.J., Morse, A.P., Thomson, M.C., 2003. Environmental Risk and Meningitis Epidemics in Africa. *Emerg. Infect. Dis.* 9, 1287–1293. <https://doi.org/10.3201/eid0910.030182>
- Mozambique - Floods and Cyclone Fact Sheet #1, Fiscal Year (FY) 2007 - Mozambique [WWW Document], n.d. . ReliefWeb. URL <https://reliefweb.int/report/mozambique/mozambique-floods-and-cyclone-fact-sheet-1-fiscal-year-fy-2007> (accessed 2.1.22).
- Murray, V., Ebi, K.L., 2012. IPCC Special Report on Managing the Risks of Extreme Events and Disasters to Advance Climate Change Adaptation (SREX). *J Epidemiol Community Health* 66, 759–760. <https://doi.org/10.1136/jech-2012-201045>
- Neria, Y., Nandi, A., Galea, S., 2008. Post-traumatic stress disorder following disasters: a systematic review. *Psychol. Med.* 38, 467–480. <https://doi.org/10.1017/S0033291707001353>
- O'Neill, B.C., Tebaldi, C., van Vuuren, D.P., Eyring, V., Friedlingstein, P., Hurtt, G., Knutti, R., Kriegler, E., Lamarque, J.-F., Lowe, J., Meehl, G.A., Moss, R., Riahi, K., Sanderson, B.M., 2016. The Scenario Model Intercomparison Project (ScenarioMIP) for CMIP6. *Geosci. Model Dev.* 9, 3461–3482. <https://doi.org/10.5194/gmd-9-3461-2016>
- Ongoma, V., Chen, H., Gao, C., Nyongesa, A. M., & Polong, F., 2018. Future changes in climate extremes over Equatorial East Africa based on CMIP5 multimodel ensemble. *Natural Hazards*, 90(2), 901–920.
- Pesce, M., von Hardenberg, J., Viglione, A., 2020. A Correlation Analysis of Extreme Climate Indices and River Flood Events in Northwestern Italy 2020, H172-0001.
- Pohlert, T., 2020. Non-Parametric Trend Tests and Change-Point Detection.
- Pörtner, H.-O., D.C. Roberts, H. Adams, I. Adelekan, C. Adler, R. Adrian, P. Aldunce, E. Ali, R. Ara Begum, B. Bednar-Friedl, R. Bezner Kerr, R. Biesbroek, J. Birkmann, K. Bowen, M.A. Caretta, J. Carnicer, E., Castellanos, T.S. Cheong, W. Chow, G. Cissé, S. Clayton, A. Constable, S. Cooley, M.J. Costello, M. Craig, W. Cramer, R. Dawson, D. Dodman, J. Efitre, M. Garschagen, E.A. Gilmore, B. Glavovic, D. Gutzler, M., Haasnoot, S. Harper, T. Hasegawa, B. Hayward, J.A. Hicke, Y. Hirabayashi, C. Huang, K. Kalaba, W., Kiessling, A. Kitoh, R. Lasco, J. Lawrence, M.F. Lemos, R. Lempert, C. Lennard, D. Ley, T. Lissner, Q. Liu, E. Liwenga, S. Lluch-Cota, S. Löschke, S. Lucatello, Y. Luo, B. Mackey, K. Mintenbeck, A. Mirzabaev, V., Möller, M. Moncassim Vale, M.D. Morecroft, L. Mortsch, A. Mukherji, T. Mustonen, M. Mycoo, J., Nalau, M. New, A. Okem (South Africa), J.P. Ometto, B. O'Neill, R. Pandey, C. Parmesan, M. Pelling, P.F. Pinho, J. Pinnegar, E.S. Poloczanska, A. Prakash, B. Preston, M.-F. Racault, D. Reckien, A. Revi, S.K., Rose, E.L.F. Schipper, D.N. Schmidt, D. Schoeman, R. Shaw, N.P. Simpson, C. Singh, W. Solecki, L., Stringer, E. Totin, C.H. Trisos, Y. Trisurat, M. van Aalst, D. Viner, M. Wairu, R. Warren, P. Wester, D., Wrathall, and Z. Zaiton Ibrahim, 2022. Technical Summary, in: *Climate Change 2022: Impacts, Adaptation, and Vulnerability. Contribution of Working Group II to the Sixth Assessment Report of the Intergovernmental Panel on Climate Change*. [H.-O. Pörtner, D.C. Roberts, E.S. Poloczanska, K. Mintenbeck, M. Tignor, A. Alegría, M. Craig, S. Langsdorf, S. Löschke, V. Möller, A. Okem (eds.)] Cambridge University Press. In Press.
- Probst, P., & Annunziato, A., 2019. Tropical Cyclone IDAI: Analysis of the wind, rainfall and storm surge impact.
- Reason, C.J.C., Keibel, A., 2004. Tropical Cyclone Eline and Its Unusual Penetration and Impacts over the Southern African Mainland. *Weather Forecast.* 19, 789–805. [https://doi.org/10.1175/1520-0434\(2004\)019<0789:TCEAIU>2.0.CO;2](https://doi.org/10.1175/1520-0434(2004)019<0789:TCEAIU>2.0.CO;2)
- Riahi, K., van Vuuren, D.P., Kriegler, E., Edmonds, J., O'Neill, B.C., Fujimori, S., Bauer, N., Calvin, K., Dellink, R., Fricko, O., Lutz, W., Popp, A., Cuarema, J.C., Kc, S., Leimbach, M., Jiang, L.,

- Kram, T., Rao, S., Emmerling, J., Ebi, K., Hasegawa, T., Havlik, P., Humpenöder, F., Da Silva, L.A., Smith, S., Stehfest, E., Bosetti, V., Eom, J., Gernaat, D., Masui, T., Rogelj, J., Strefler, J., Drouet, L., Krey, V., Luderer, G., Harmsen, M., Takahashi, K., Baumstark, L., Doelman, J.C., Kainuma, M., Klimont, Z., Marangoni, G., Lotze-Campen, H., Obersteiner, M., Tabeau, A., Tavoni, M., 2017. The Shared Socioeconomic Pathways and their energy, land use, and greenhouse gas emissions implications: An overview. *Glob. Environ. Change* 42, 153–168. <https://doi.org/10.1016/j.gloenvcha.2016.05.009>
- Rosenblatt, M., 1956. Estimation of a probability density-function and mode. *Ann Math Statist*, pp. 27, 832–7.
- Russo, S., Sterl, A., 2011. Global changes in indices describing moderate temperature extremes from the daily output of a climate model. *J. Geophys. Res. Atmospheres* 116. <https://doi.org/10.1029/2010JD014727>
- Scholes, R.J., Montanarella, L., Brainich, E., Brainich, E., Barger, N., Brink, B. ten, Cantele, M., Erasmus, B., Fisher, J., Gardner, T., Holland, T.G., Kohler, F., Kotiaho, S., Maltitz, G. von, Nangendo, G., Pandit, R., Parrotta, J., Potts, M.D., Prince, S., Sankaran, M., Willemen, L., 2018. IPBES (2018): Summary for policymakers of the assessment report on land degradation and restoration of the Intergovernmental Science- Policy Platform on Biodiversity and Ecosystem Services. Intergovernmental Science-Policy Platform on Biodiversity and Ecosystem Services.
- Sen, P.K., 1968. Estimates of the Regression Coefficient Based on Kendall's Tau. *J. Am. Stat. Assoc.* 63, 1379–1389. <https://doi.org/10.1080/01621459.1968.10480934>
- Seneviratne, S.I., X. Zhang, M. Adnan, W. Badi, C. Dereczynski, A. Di Luca, S. Ghosh, I. Iskandar, J. Kossin, S. Lewis, F. Otto, I. Pinto, M. Satoh, S.M. Vicente-Serrano, M. Wehner, and B. Zhou, 2021. Weather and Climate Extreme Events in a Changing Climate. In *Climate Change 2021: The Physical Science Basis. Contribution of Working Group I to the Sixth Assessment Report of the Intergovernmental Panel on Climate Change*. Cambridge University Press. In Press.
- Seo, S.B., Kim, Y.-O., Kim, Y., Eum, H.-I., 2019. Selecting climate change scenarios for regional hydrologic impact studies based on climate extremes indices. *Clim. Dyn.* 52, 1595–1611. <https://doi.org/10.1007/s00382-018-4210-7>
- Sharmila, S., Walsh, K.J.E., 2018. Recent poleward shift of tropical cyclone formation linked to Hadley cell expansion. *Nat. Clim. Change* 8, 730–736. <https://doi.org/10.1038/s41558-018-0227-5>
- Sillmann, J., Kharin, V. V., Zwiers, F. W., Zhang, X., & Brunaugh, D., 2013. Climate extremes indices in the CMIP5 multimodel ensemble: Part 2. Future climate projections *Journal of Geophysical Research: Atmospheres*, 2473–2493.
- Smirnov, N. V., 1939. On the estimation of the discrepancy between empirical curves of distribution for two independent samples. *Bull. Math. Univ. Moscou*, p. 2(2), 3–14.
- Spearman, C., 1904. The Proof and Measurement of Association between Two Things. *Am. J. Psychol.* 15, 72–101. <https://doi.org/10.2307/1412159>
- Spekker, H., & Heskamp, J., 2017. Flood protection for the City of Beira: an exemplary climate adaptation project in Mozambique. , *Bautechnik*, 872–874.
- Tank, A.M.G.K., Können, G.P., 2003. Trends in Indices of Daily Temperature and Precipitation Extremes in Europe, 1946–99. *J. Clim.* 16, 3665–3680. [https://doi.org/10.1175/1520-0442\(2003\)016<3665:TIHODT>2.0.CO;2](https://doi.org/10.1175/1520-0442(2003)016<3665:TIHODT>2.0.CO;2)
- Tebaldi, C., Knutti, R., 2007. The use of the multi-model ensemble in probabilistic climate projections. *Philos. Transact. A Math. Phys. Eng. Sci.* 365, 2053–2075. <https://doi.org/10.1098/rsta.2007.2076>
- The World Bank, 2012. Mozambique then and now: an atlas of socio-economic statistics-1997-2007. No. 87733.
- Tinley, K.L., 1982. The Influence of Soil Moisture Balance on Ecosystem Patterns in Southern Africa, in: Huntley, B.J., Walker, B.H. (Eds.), *Ecology of Tropical Savannas*, Ecological Studies. Springer, Berlin, Heidelberg, pp. 175–192. [https://doi.org/10.1007/978-3-642-68786-0\\_9](https://doi.org/10.1007/978-3-642-68786-0_9)
- Trisos, C.H., I.O. Adelekan, E. Totin, A. Ayanlade, J. Efitre, A. Gemed, K. Kalaba, C. Lennard, C. Masao, Y. Mgaya, G. Ngaruiya, D. Olago, N.P. Simpson, and S. Zakielde, 2022. Africa, in: *Climate Change 2022: Impacts, Adaptation, and Vulnerability. Contribution of Working Group II to the Sixth Assessment Report of the Intergovernmental Panel on Climate Change*. H.-O. Pörtner, D.C. Roberts, M. Tignor, E.S. Poloczanska, K. Mintenbeck, A. Alegría, M. Craig, S.

- Langsdorf, S. Löschke, V. Möller, A. Okem, B. Rama (eds.)Cambridge University Press. In Press.
- Trujillo, M., 2019. Mozambique Cyclone Idai post-disaster needs assessment (PDNA).
- Vila-Traver, J., González de Molina, M., Infante-Amate, J., Aguilera, E., 2022. Disentangling the effect of climate and cropland changes on the water performance of agroecosystems (Spain, 1922–2016). *J. Clean. Prod.* 130811. <https://doi.org/10.1016/j.jclepro.2022.130811>
- Wang, X.L., Swail, V.R., 2001. Changes of Extreme Wave Heights in Northern Hemisphere Oceans and Related Atmospheric Circulation Regimes. *J. Clim.* 14, 2204–2221. [https://doi.org/10.1175/1520-0442\(2001\)014<2204:COEWHI>2.0.CO;2](https://doi.org/10.1175/1520-0442(2001)014<2204:COEWHI>2.0.CO;2)
- Weather and climate change [WWW Document], n.d. . Met Off. URL <https://www.metoffice.gov.uk/> (accessed 2.11.22).
- Węglarczyk, S., 2018. Kernel density estimation and its application. *ITM Web Conf.* 23, 00037. <https://doi.org/10.1051/itmconf/20182300037>
- Wilhite, D., & Pulwarty, R. S. (Eds.), 2017. *Drought and Water Crises: Integrating Science, Management, and Policy*. CRC Press.
- Xu, L., Chen, N., Zhang, X., 2019. Global drought trends under 1.5 and 2 °C warming. *Int. J. Climatol.* 39, 2375–2385. <https://doi.org/10.1002/joc.5958>
- Xu, Y., Wu, Jie, Shi, Y., Bo-Tao, Z., Rou-Ke, L., Wu, Jia, 2015. Change in Extreme Climate Events over China Based on CMIP5. *Atmospheric Ocean. Sci. Lett.* 8. <http://dx.doi.org/10.3878/AOSL20150006>
- Zhang, P., Ren, G., Xu, Y., Wang, X.L., Qin, Y., Sun, X., Ren, Y., 2019. Observed Changes in Extreme Temperature over the Global Land Based on a Newly Developed Station Daily Dataset. *J. Clim.* 32, 8489–8509. <https://doi.org/10.1175/JCLI-D-18-0733.1>
- Zhang, X., Alexander, L., Hegerl, G.C., Jones, P., Tank, A.K., Peterson, T.C., Trewin, B., Zwiers, F.W., 2011. Indices for monitoring changes in extremes based on daily temperature and precipitation data. *WIREs Clim. Change* 2, 851–870. <https://doi.org/10.1002/wcc.147>
- Zhang, X., Hegerl, G., Zwiers, F.W., Kenyon, J., 2005. Avoiding Inhomogeneity in Percentile-Based Indices of Temperature Extremes. *J. Clim.* 18, 1641–1651. <https://doi.org/10.1175/JCLI3366.1>



## **8. APPENDIX A: destructive past events for Beira**

In this appendix, the most critical rainfall-related events for the city of Beira that have occurred in the recent past are briefly described.

### **1997**

Heavy rains and subsequent floods affected Mozambique and the province of Sofala for over one month (January-February). On the 2<sup>nd</sup> March, Severe Tropical Storm Lisette made landfall just north of the city of Beira. The storm caused a storm surge of about 4m along the coasts of Beira, and dropped heavy rainfall across the region, causing severe flooding. In Mozambique, 17,000 homes were destroyed, and 300,000 people were affected. Across the country, the storm killed 87 people.

### **2000**

In February 2000, Mozambique was ravaged by an equivalent of two years' worth of rainfall in less than two weeks. On the 22<sup>nd</sup> of the same month, the Leon-Eline Tropical Cyclone made landfall about 80 km south of Beira. The subsequent torrential rains and strong winds on the areas that were already flooded left a situation that was considered the country's worst natural disaster in a century<sup>31</sup>. More than 2 million are estimated to have been affected, with over 700 fatalities. Damage and destruction of homes, schools, hospitals, roads, power systems and other infrastructures were extensive. The inundation hit 140,000 hectares of agricultural crops, killed or seriously injured 350,000 cattle, and vastly destroyed fishing equipment, severely affecting key sectors for Mozambique's economy and subsistence. Images of the flooding spread around the world, and the scale of the event prompted extensive documentation of the disaster, including a book entirely devoted to it (Christie et al., 2001).

---

<sup>31</sup> Reason et al., 2004; DisasterRelief <https://reliefweb.int/>



Figure 47: During the flood, residents had to climb trees to save themselves, while waiting for rescue<sup>32</sup>

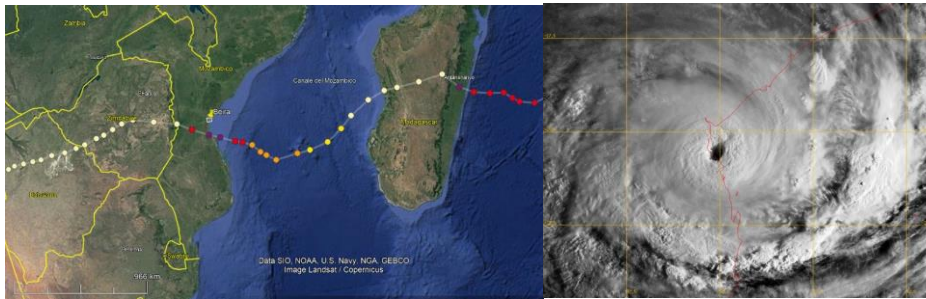


Figure 48: Cyclone Eline-Leon. Right: Track of the cyclone approaching the area of Beira. Colours toward the violet indicate an increasing power of the tropical cyclone (category 4 TC). Source: <http://www.meteofrance.re>  
Right: Cyclone Eline while making landfall close to Beira. The red line is the Mozambique boundary with the ocean. Source: RSMC ARCHIVES<sup>33</sup>

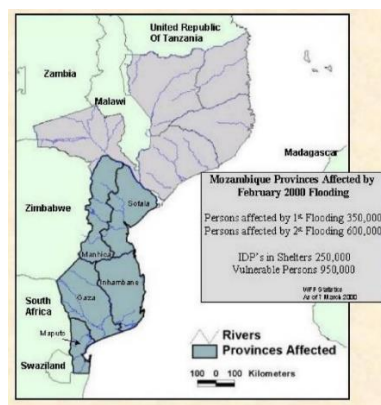


Figure 49: Flooding of Mozambique before and after the cyclone and number of persons affected. Area of Sofala was heavily affected by the event. Source: Reliefweb<sup>34</sup>

<sup>32</sup> <https://chemonics.com/wp-content/uploads/2017/10/Mozambique-Disaster-Preparedness.pdf>

<sup>33</sup> [http://www.meteo.fr/temps/dontom/La\\_Reunion/webcmrs9.0/anglais/archives/index.html](http://www.meteo.fr/temps/dontom/La_Reunion/webcmrs9.0/anglais/archives/index.html)

<sup>34</sup> <https://reliefweb.int/map/mozambique/mozambique-provinces-affected-february-2000-flooding>

## 2001

After the 2000 disaster, the following year's rainy season was not kind to Mozambique. During February, prolonged and heavy rainfall in the central part of the country and increased flows from the Kariba and Cabora Bassa dams in neighboring countries caused extensive flooding. In particular, the flooding occurred in the Sofala province because of the overflow in the Buzi and Pungoe Rivers<sup>35</sup>. 500.000 people were affected and 115 is the estimated number of deaths.

## 2007

Between December 2006 and February 2007, heavy rains across northern and central Mozambique led to flooding in the Sofala province, affecting and estimated of 285,000 people in the whole Mozambique. These rains closely followed earlier flooding from October to December 2006, which affected 46,500 people. On February 22, Tropical Cyclone Favio made landfall in Mozambique, killing 10 people and affecting more than 160,000 people, destroying crops and undermining local food security<sup>36</sup>.

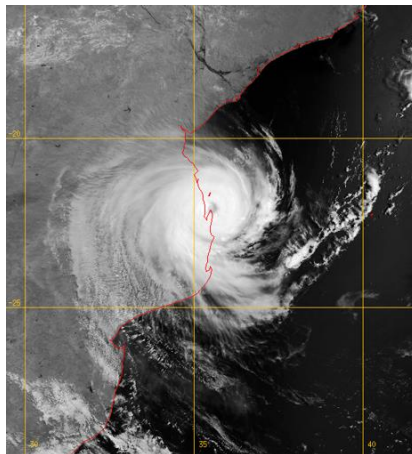


Figure 50: Cyclone Favio while making landfall in the south of Beira. Source: RSMC ARCHIVES<sup>37</sup>

<sup>35</sup>Report: 2001 Floods Lessons Learned Workshop Beira 26 – 27 July. OCHA final report.

<sup>36</sup> <https://reliefweb.int/report/mozambique/fews-mozambique-food-security-warning-cyclone-favio-drought-rack-south-north>

<sup>37</sup> [http://www.meteo.fr/temps/dontom/La\\_Reunion/webcmrs9.0/anglais/archives/index.html](http://www.meteo.fr/temps/dontom/La_Reunion/webcmrs9.0/anglais/archives/index.html)



Figure 51: Cyclone Favio track, area affected by it and by the previous floods. Source: US Agency for International Development<sup>38</sup>

## 2019

In the period between December 2018 and March 2019, heavy precipitation and flooding affected around 10,000 people in the province of Sofala. Tropical Cyclone Idai made landfall during the night of 14 to 15 March causing a destructive combination of torrential rain, high winds and storm surges. The massive flooding resulting from torrential rainfall

<sup>38</sup> <https://reliefweb.int/map/somalia/usaيدofda-programs-mozambique-22-mar-2007>

(more than 200mm in one day), strong winds (215 km/h) and storm surges (4.4m high) left the city of Beira in an inundated state with catastrophic devastation. The unprecedented damages on facilities, infrastructures and the enormous amount of fatalities made it the most destructive and deadliest tropical cyclone in the South-West Indian Ocean of recorded history. The situation was further aggravated by cholera epidemics and the spread of Malaria, due to the precarious hygienic conditions after the catastrophe. The humanitarian disaster has shifted the spotlight on the vulnerability of Mozambique and Beira, raising the question of whether a future for the city is possible under climate change.



*Figure 52: Cyclone Idai approaching Mozambique on 14 March 2019. Image acquired by Nasa's aqua satellite<sup>39</sup>*

---

<sup>39</sup> <https://worldview.earthdata.nasa.gov/>



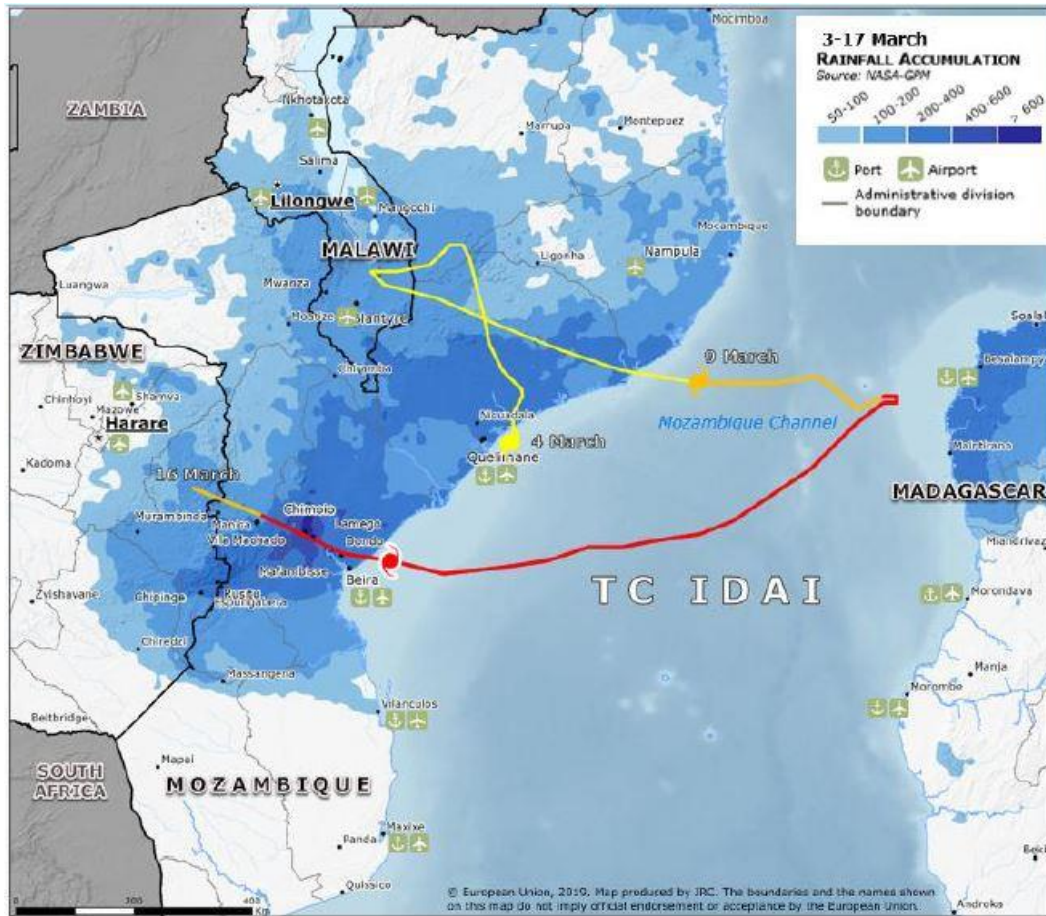
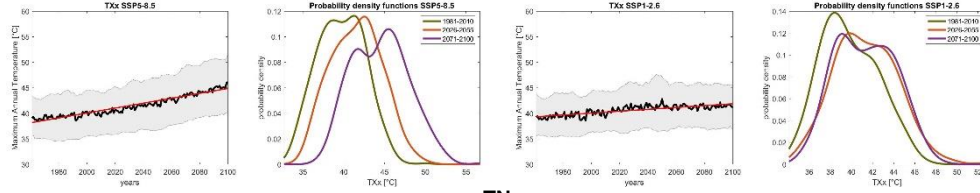


Figure 53: Rainfall accumulation between 3 and 17 March 2019 and storm track of Idai cyclone. Image taken from Probst et al. (2019)

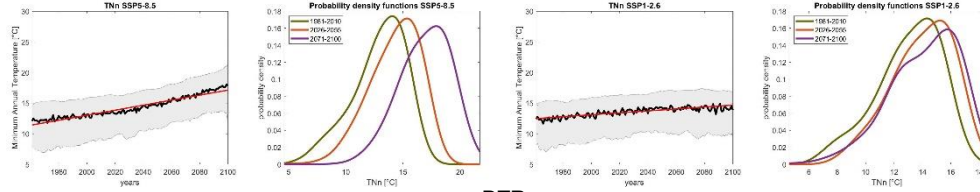
To be noted is the very large spatial scale of these events, visible in the previous figures (48,50,52,53), confirming the choice of having considered a  $3 \times 3$  lonlat area as dataset (section 3.4).

# 9. APPENDIX B: future projections

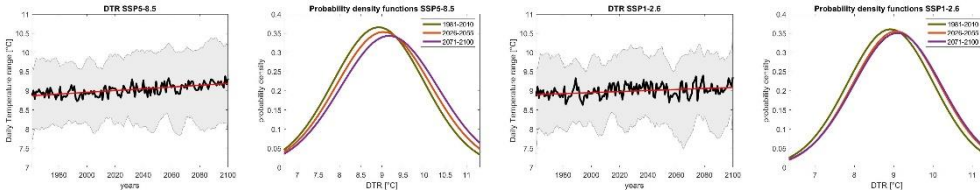
## TXx



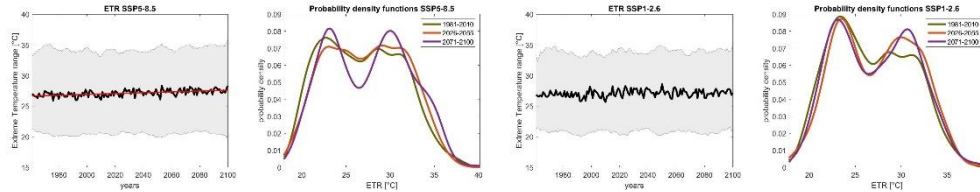
## TNn



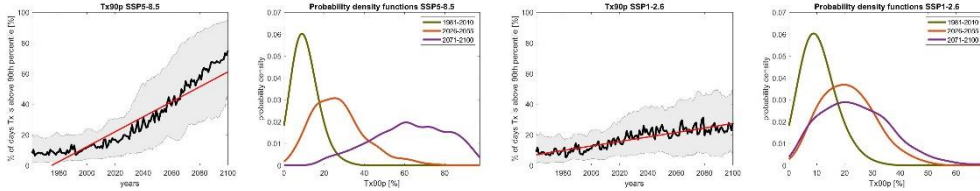
## DTR



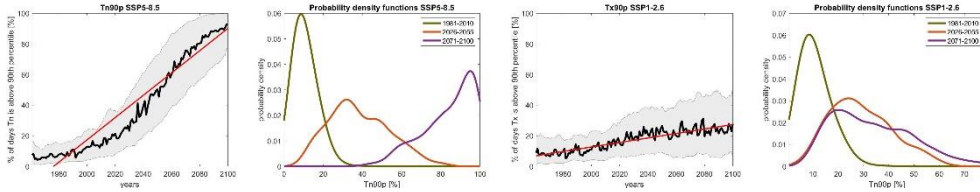
## ETR



## Tx90p



## Tn90p



## Tx10p

